



University Transportation Research Center - Region 2

Final Report



Pavement Deicing Using Hydronic Heat Exchange Loops in the Base Layer: Experimental and Modeling Feasibility Study

Performing Organization: State University of New York (SUNY)



April 2018



Sponsor:
University Transportation Research Center - Region 2

University Transportation Research Center - Region 2

The Region 2 University Transportation Research Center (UTRC) is one of ten original University Transportation Centers established in 1987 by the U.S. Congress. These Centers were established with the recognition that transportation plays a key role in the nation's economy and the quality of life of its citizens. University faculty members provide a critical link in resolving our national and regional transportation problems while training the professionals who address our transportation systems and their customers on a daily basis.

The UTRC was established in order to support research, education and the transfer of technology in the field of transportation. The theme of the Center is "Planning and Managing Regional Transportation Systems in a Changing World." Presently, under the direction of Dr. Camille Kamga, the UTRC represents USDOT Region II, including New York, New Jersey, Puerto Rico and the U.S. Virgin Islands. Functioning as a consortium of twelve major Universities throughout the region, UTRC is located at the CUNY Institute for Transportation Systems at The City College of New York, the lead institution of the consortium. The Center, through its consortium, an Agency-Industry Council and its Director and Staff, supports research, education, and technology transfer under its theme. UTRC's three main goals are:

Research

The research program objectives are (1) to develop a theme based transportation research program that is responsive to the needs of regional transportation organizations and stakeholders, and (2) to conduct that program in cooperation with the partners. The program includes both studies that are identified with research partners of projects targeted to the theme, and targeted, short-term projects. The program develops competitive proposals, which are evaluated to insure the most responsive UTRC team conducts the work. The research program is responsive to the UTRC theme: "Planning and Managing Regional Transportation Systems in a Changing World." The complex transportation system of transit and infrastructure, and the rapidly changing environment impacts the nation's largest city and metropolitan area. The New York/New Jersey Metropolitan has over 19 million people, 600,000 businesses and 9 million workers. The Region's intermodal and multimodal systems must serve all customers and stakeholders within the region and globally. Under the current grant, the new research projects and the ongoing research projects concentrate the program efforts on the categories of Transportation Systems Performance and Information Infrastructure to provide needed services to the New Jersey Department of Transportation, New York City Department of Transportation, New York Metropolitan Transportation Council, New York State Department of Transportation, and the New York State Energy and Research Development Authority and others, all while enhancing the center's theme.

Education and Workforce Development

The modern professional must combine the technical skills of engineering and planning with knowledge of economics, environmental science, management, finance, and law as well as negotiation skills, psychology and sociology. And, she/he must be computer literate, wired to the web, and knowledgeable about advances in information technology. UTRC's education and training efforts provide a multidisciplinary program of course work and experiential learning to train students and provide advanced training or retraining of practitioners to plan and manage regional transportation systems. UTRC must meet the need to educate the undergraduate and graduate student with a foundation of transportation fundamentals that allows for solving complex problems in a world much more dynamic than even a decade ago. Simultaneously, the demand for continuing education is growing – either because of professional license requirements or because the workplace demands it – and provides the opportunity to combine State of Practice education with tailored ways of delivering content.

Technology Transfer

UTRC's Technology Transfer Program goes beyond what might be considered "traditional" technology transfer activities. Its main objectives are (1) to increase the awareness and level of information concerning transportation issues facing Region 2; (2) to improve the knowledge base and approach to problem solving of the region's transportation workforce, from those operating the systems to those at the most senior level of managing the system; and by doing so, to improve the overall professional capability of the transportation workforce; (3) to stimulate discussion and debate concerning the integration of new technologies into our culture, our work and our transportation systems; (4) to provide the more traditional but extremely important job of disseminating research and project reports, studies, analysis and use of tools to the education, research and practicing community both nationally and internationally; and (5) to provide unbiased information and testimony to decision-makers concerning regional transportation issues consistent with the UTRC theme.

Project No(s):

UTRC/RF Grant No: 49198-30-27

Project Date: April 2018

Project Title: Self-Heated Pavements

Project's Website:

<http://www.utrc2.org/research/projects/self-heated-pavements>

Principal Investigator(s):

Sherif L. Abdelaziz

Assistant Professor
Department of Civil Engineering
Stony Brook University
Stony Brook, NY 11794
Tel: (631) 632-9341
Email: Sherif.Abdelaziz@stonybrook.edu

Co Principal Investigator(s):

Jon P. Longtin

Professor
Department of Mechanical Engineering
Stony Brook University
Email: jon.longtin@stonybrook.edu

Huiming Yin

Associate Professor
Department of Civil Engineering and Engineering Mechanics
Columbia University
New York, NY 10027
Email: hy2251@columbia.edu

David Orr

Director
Cornell Local Roads Program
Cornell University
Ithaca, NY 14853
Email: dpo3@cornell.edu

Soji P. Abraham

Research Assistant
Department of Mechanical Engineering
Stony Brook University

Xin He

Research Assistant
Department of Civil Engineering and Engineering Mechanics
Columbia University

Performing Organization(s):

Stony Brook University

Sponsor(s):

University Transportation Research Center (UTRC)

To request a hard copy of our final reports, please send us an email at utrc@utrc2.org

Mailing Address:

University Transportation Research Center
The City College of New York
Marshak Hall, Suite 910
160 Convent Avenue
New York, NY 10031
Tel: 212-650-8051
Fax: 212-650-8374
Web: www.utrc2.org

Board of Directors

The UTRC Board of Directors consists of one or two members from each Consortium school (each school receives two votes regardless of the number of representatives on the board). The Center Director is an ex-officio member of the Board and The Center management team serves as staff to the Board.

City University of New York

Dr. Robert E. Paaswell - Director Emeritus of NY
Dr. Hongmian Gong - Geography/Hunter College

Clarkson University

Dr. Kerop D. Janoyan - Civil Engineering

Columbia University

Dr. Raimondo Betti - Civil Engineering
Dr. Elliott Sclar - Urban and Regional Planning

Cornell University

Dr. Huaizhu (Oliver) Gao - Civil Engineering
Dr. Richard Geddes - Cornell Program in Infrastructure Policy

Hofstra University

Dr. Jean-Paul Rodrigue - Global Studies and Geography

Manhattan College

Dr. Anirban De - Civil & Environmental Engineering
Dr. Matthew Volovski - Civil & Environmental Engineering

New Jersey Institute of Technology

Dr. Steven I-Jy Chien - Civil Engineering
Dr. Joyoung Lee - Civil & Environmental Engineering

New York Institute of Technology

Dr. Nada Marie Anid - Engineering & Computing Sciences
Dr. Marta Panero - Engineering & Computing Sciences

New York University

Dr. Mitchell L. Moss - Urban Policy and Planning
Dr. Rae Zimmerman - Planning and Public Administration

(NYU Tandon School of Engineering)

Dr. John C. Falocchio - Civil Engineering
Dr. Kaan Ozbay - Civil Engineering
Dr. Elena Prassas - Civil Engineering

Rensselaer Polytechnic Institute

Dr. José Holguín-Veras - Civil Engineering
Dr. William "Al" Wallace - Systems Engineering

Rochester Institute of Technology

Dr. James Winebrake - Science, Technology and Society/Public Policy
Dr. J. Scott Hawker - Software Engineering

Rowan University

Dr. Yusuf Mehta - Civil Engineering
Dr. Beena Sukumaran - Civil Engineering

State University of New York

Michael M. Fancher - Nanoscience
Dr. Catherine T. Lawson - City & Regional Planning
Dr. Adel W. Sadek - Transportation Systems Engineering
Dr. Shmuel Yahalom - Economics

Stevens Institute of Technology

Dr. Sophia Hassiotis - Civil Engineering
Dr. Thomas H. Wakeman III - Civil Engineering

Syracuse University

Dr. Baris Salman - Civil Engineering
Dr. O. Sam Salem - Construction Engineering and Management

The College of New Jersey

Dr. Thomas M. Brennan Jr - Civil Engineering

University of Puerto Rico - Mayagüez

Dr. Ismael Pagán-Trinidad - Civil Engineering
Dr. Didier M. Valdés-Díaz - Civil Engineering

UTRC Consortium Universities

The following universities/colleges are members of the UTRC consortium under MAP-21 ACT.

City University of New York (CUNY)
Clarkson University (Clarkson)
Columbia University (Columbia)
Cornell University (Cornell)
Hofstra University (Hofstra)
Manhattan College (MC)
New Jersey Institute of Technology (NJIT)
New York Institute of Technology (NYIT)
New York University (NYU)
Rensselaer Polytechnic Institute (RPI)
Rochester Institute of Technology (RIT)
Rowan University (Rowan)
State University of New York (SUNY)
Stevens Institute of Technology (Stevens)
Syracuse University (SU)
The College of New Jersey (TCNJ)
University of Puerto Rico - Mayagüez (UPRM)

UTRC Key Staff

Dr. Camille Kamga: *Director, Associate Professor of Civil Engineering*

Dr. Robert E. Paaswell: *Director Emeritus of UTRC and Distinguished Professor of Civil Engineering, The City College of New York*

Dr. Ellen Thorson: *Senior Research Fellow*

Penny Eickemeyer: *Associate Director for Research, UTRC*

Dr. Alison Conway: *Associate Director for Education/Associate Professor of Civil Engineering*

Nadia Aslam: *Assistant Director for Technology Transfer*

Nathalie Martinez: *Research Associate/Budget Analyst*

Andriy Blagay: *Graphic Intern*

Tierra Fisher: *Office Manager*

Dr. Sandeep Mudigonda, *Research Associate*

Dr. Rodrigue Tchamna, *Research Associate*

Dr. Dan Wan, *Research Assistant*

Bahman Moghimi: *Research Assistant;*
Ph.D. Student, Transportation Program

Sabiheh Fagigh: *Research Assistant;*
Ph.D. Student, Transportation Program

Patricio Vicuna: *Research Assistant*
Ph.D. Candidate, Transportation Program

DISCLAIMER

The contents of this report reflect the views of the authors, who are responsible for the facts and the accuracy of the information presented herein. The contents do not necessarily reflect the official views or policies of the UTRC or the Federal Highway Administration. This report does not constitute a standard, specification or regulation. This document is disseminated under the sponsorship of the Department of Transportation, University Transportation Centers Program, in the interest of information exchange. The U.S. Government assumes no liability for the contents or use thereof.

1. Report No.	2. Government Accession No.	3. Recipient's Catalog No.	
4. Title and Subtitle Pavement Deicing Using Hydronic Heat Exchange Loops in The Base Layer: Experimental and Modeling Feasibility Study		5. Report Date April 2018	6. Performing Organization Code
7. Author(s) Sherif Abdelaziz, PI, Jon Longtin, Co-PI Huiming Yin, Co-PI David Orr, Co-PI		8. Performing Organization Report No.	
9. Performing Organization Name and Address SUNY Stonybrook 100 Nicolls Road, Stony Brook, NY 11794		10. Work Unit No.	11. Contract or Grant No. 49198-30-27
12. Sponsoring Agency Name and Address UTRC The City College of New York, Marshak Hall 910 West 137 th Street and Convent Avenue New York, NY 10031		13. Type of Report and Period Covered Final, June 1, 2015-April 30, 2018	14. Sponsoring Agency Code
15. Supplementary Notes			
<p>16. Abstract</p> <p>Extreme weather conditions play a vital factor in the deterioration of the national transportation infrastructure including pavements. Freezing and thawing of the pavement sections is one of the most critical processes resulting from these extreme weather conditions. In addition to negatively impacting the structural integrity of the pavement layers, frozen pavement surfaces increase highway risks and decrease mobility of people, goods, and first responders. It is, thus, recognized that reducing and potentially eliminating pavement freezing is crucial to increase the resiliency level of the national infrastructure and reduce highway risks.</p> <p>This report presents a feasibility study investigating the use of a hydronic heat exchange loops installed in the aggregate base layer to de-ice pavement surfaces. The concept of using similar heat exchange loops was previously investigated and the thermal effectiveness was confirmed for loops installed in the surface layer, either asphalt or concrete. However, construction difficulties and performance challenges resulted from the installation of these loops in the surface layers including compaction difficulties, concentrated stresses and strains, and pavement surface cracks. Therefore, this study considered relocating the heat exchange loops in the base layer, beneath the surface layer, to avoid such construction and performance challenges.</p> <p>This study consisted of experimental and modeling components. First, the thermal performance of the proposed technique was validated experimentally. In this experimental work, a pavement section provided with heat exchange loops in the aggregate base layer was constructed inside a freeze chamber where the ambient air temperature was precisely controlled. Two experiments were performed: the first one considered low ambient air temperature without snow or ice on the pavement surface, while the second had initial icy pavement surface. Heated fluid was circulated inside the loops in the two experiments with temperature measurements recorded at various locations within the pavement section and at the surface. The results of this experimental program confirm that burying the heat exchangers in the base layer provides enough heat to the pavement surface that keeps it ice free, despite the significant downward-propagating heat losses.</p>			
17. Key Words hydronic heat exchange loops, deicing, self-heated pavements		18. Distribution Statement	
19. Security Classif (of this report) Unclassified	20. Security Classif. (of this page)	21. No of Pages 73	22. Price

Table of Contents

List of Figures	vi
List of Tables	ix
Project Summary	x
1 Introduction	1
1.1 Current pavements de-icing techniques	1
1.2 Proposed self-heated pavement technology	3
1.3 Research goals	4
2 Background for the Surface Energy Balance of Pavements	5
2.1 Energy Balance Relation at Pavement Surface.....	5
2.2 Energy Balance for the Proposed Pavement De-icing System.....	7
3 System Thermal Performance: Proof of Concept Using a Laboratory Experiment.....	8
3.1 Pavement Section and Experimental Setup.....	8
3.1.1 Instrumented Pavement Section	8
3.1.2 Climate Change (Freeze-Thaw) Chamber	10
3.1.3 Fluid Heating Unit	10
3.1.4 Data Acquisition System.....	10
3.2 Experimental Procedure.....	11
3.3 Experiment Results and Discussion	12
3.3.1 Experimental Set 1: Cold Pavement Surface without Ice	12
3.3.2 Experimental Set 2: Ice Cubes on Pavement Surface	18
3.4 Conclusions of the experimental work	20

4	System Thermal Performance: Numerical Modeling	21
4.1	Model Development, Validation, and Possible Simplification.....	21
4.1.1	3-D Finite element model of the experiments	21
4.1.2	3-D FE Boundary Conditions, initial values, meshing, and numerical solver	26
4.1.3	3-D Model Validation	27
4.1.4	3-D Model Results and Discussions	29
4.2	Predicting System Behavior for Actual Weather Conditions	30
4.2.1	2-D Model Simplification	31
4.2.2	Effectiveness of Proposed Heat Exchangers.....	33
4.3	Conclusions.....	37
5	Pavement Mechanical Performance	38
5.1	Background	38
5.2	Mechanical performance of the proposed self-heated pavement	40
5.2.1	Static tire load on a pavement with elastic HMA layer	40
5.2.2	Static tire load on a pavement with viscoelastic HMA layer	44
5.2.3	Moving tire load of a pavement with viscoelastic HMA layer.....	46
5.3	Parametric analysis	48
5.3.1	Effect of loop space	49
5.3.2	Effect of loop depth.....	52
5.4	Simplified 1-D analytical approximation.....	54
5.4.1	Mechanistic-Empirical Review of Base Pavement Section.....	56
5.4.2	Updated Design.....	58
5.4.3	Probabilistic Analysis of Updated Pavement Design	63
6	Conclusions.....	65

References 67

List of Figures

Fig. 1 Sketches of (a) the Dutch heated pavement, and (b) the proposed technology.	3
Fig. 2 Different components of the proposed self-heated pavement technology.	4
Fig. 3 Pavement section used in the experiment: (a) half-width 3-D view, (b) mid-plane cross-section X-X, and (c) the used heat exchange loop at tube plane (section Y-Y).....	8
Fig. 4 Pavement surface temperature for first experimental set (i.e., -10 °C air temperature and 31.5 °C inlet fluid temperature).....	13
Fig. 5 Temperature change in different pavement layers for -10 °C air temperature and 31.5 °C inlet fluid temperature.	15
Fig. 6 Inlet and outlet fluid temperatures and heating rate applied to the pavement section for -10 °C air temperature and 31.5 °C inlet fluid temperature.	16
Fig. 7 Heat supplied to various pavement layers for -10 °C air temperature and 31.5 °C inlet fluid temperature.....	17
Fig. 8 Pavement surface temperature for -10 °C air temperature and 31.5 °C inlet fluid temperature with and without ice on pavement surface.	19
Fig. 9 Air temperature inside the chamber when ice is placed on the pavement surface.	19
Fig. 10 Three-dimensional (3-D) COMSOL finite element model for the laboratory experiments.	22
Fig. 11 Discretization of the 3-D finite element model for the experiments.	27
Fig. 12 Comparison between the observed (Qin and Hiller 2014) and the simulated pavement temperature at 38.1 mm in the asphalt layer.....	28
Fig. 13 Validation of numerical model against the experimental results for -10 °C chamber temperature and 31.5 °C inlet fluid temperature.	29
Fig. 14 Surface temperature contour lines after 30 hours.	30
Fig. 15 Pavement temperature at different cross-sections along the length of the heat exchange loop after 30 hours; (a) at center of the loop, (b) at solid end of the wooden box, and (c) at the wooden side for the inlet and outlet loops entrances.....	30
Fig. 16 Pavement section with proposed loops installed in the base layer.....	31

Fig. 17 Domain discretization mesh and assigned boundary conditions for the 2-D finite element models.	33
Fig. 18 Surface temperature for conventional pavement (without loops) over winter months in New York City.....	34
Fig. 19 Surface temperature for conventional pavement (without loops) over winter months in Washington, D.C.....	35
Fig. 20 Surface temperature for conventional pavement (without loops) over winter months in Buffalo.....	35
Fig. 21 Effect of burying heat exchange loops in the base layer on the pavement surface temperature over winter months in New York City.....	36
Fig. 22 Pavement surface temperatures for the three considered cities over winter months with 100 W/m applied to the surface.....	37
Fig. 23 ABAQUS FE model geometry (a) General view and, (b) Loops in the base layer.	41
Fig. 24 Tire Load and boundary conditions of the pavement.....	42
Fig. 25 Discretization mesh used for the model.....	42
Fig. 26 Model results (a) Field of displacement along thickness direction (m), and (b) Stress field (Pa).	43
Fig. 27 Lateral profiles for (a) surface displacements at the center of the modeled pavement, and (b) Stress distribution on the top of the center loop.....	44
Fig. 28 (a) Field of displacement along thickness direction (m); (b) Stress field (Pa).	45
Fig. 29 History of displacement along thickness direction at center point of pavement surface.	46
Fig. 30 Comparison of (a) Distribution of displacement along thickness direction at the center line of pavement surface; (b) Stress distribution along the center tube between elastic HMA layer and viscoelastic HMA layer cases.....	46
Fig. 31 Denote of how loading is applied through a rigid cylinder part.	47
Fig. 32 History of displacement along thickness direction at the center point of pavement surface	48
Fig. 33 Deformation of self-heated pavement.....	48

Fig. 34 (a) Change of surface deformation with different HDPE loop spacing; (b) Change of surface deformation with different aluminum loop spacing.....	51
Fig. 35 Effect of tube material on surface deformation when the load is applied (a) on tube; and (b) between tubes.	51
Fig. 36 (a) Change of surface deformation with different HDPE loop depth; (b) Change of surface deformation with different aluminum loop depth.	54
Fig. 37 Effect of tube material on surface deformation when the load is applied (a) on tube; and (b) between tubes.	54
Fig. 38. Generic Pavement Cross Section.....	55
Fig. 39. Base Pavement Section.....	56
Fig. 40. Loop spacing and distance nomenclature.	58
Fig. 41. Asphalt Horizontal Tensile Strain Criteria (Irwin 2002).....	61
Fig. 42. Subgrade Vertical Compressive Strain Criteria (Irwin 2002).....	62
Fig. 43. Design with 25-year expected lifespan.....	62
Fig. 44. Typical variation curve for moduli and thickness.....	63
Fig. 45. Histogram of Design Life for Updated Pavement in Probabilistic Study.	64

List of Tables

Table 1 Thermal Properties of Materials used in the validation analysis.	10
Table 2 Thermal properties of various materials used in the 2-D numerical model.	32
Table 3. Summary of model geometry and material properties.	41
Table 4 Details of discretization mesh.	43
Table 5 Prony Series Coefficients for HMA Layer (Liao 2007).	44
Table 6 Surface deformation of pavement with HDPE loops at different loop spacing.	49
Table 7 Surface deformation of pavement with HDPE loops at different loop spacing.	50
Table 8 Surface deformation of pavement with HDPE loops at different loop depths.	52
Table 9 Surface deformation of pavement with aluminum loops at different loop depths.	53
Table 10. Base model with pipe layer setup.	57
Table 11. Comparison of CHEVLAY and FEM analysis.	60

Project Summary

Extreme weather conditions play a vital factor in the deterioration of the national transportation infrastructure including pavements. Freezing and thawing of the pavement sections is one of the most critical processes resulting from these extreme weather conditions. In addition to negatively impacting the structural integrity of the pavement layers, frozen pavement surfaces increase highway risks and decrease mobility of people, goods, and first responders. It is, thus, recognized that reducing and potentially eliminating pavement freezing is crucial to increase the resiliency level of the national infrastructure and reduce highway risks.

This report presents a feasibility study investigating the use of a hydronic heat exchange loops installed in the aggregate base layer to de-ice pavement surfaces. The concept of using similar heat exchange loops was previously investigated and the thermal effectiveness was confirmed for loops installed in the surface layer, either asphalt or concrete. However, construction difficulties and performance challenges resulted from the installation of these loops in the surface layers including compaction difficulties, concentrated stresses and strains, and pavement surface cracks. Therefore, this study considered relocating the heat exchange loops in the base layer, beneath the surface layer, to avoid such construction and performance challenges.

This study consisted of experimental and modeling components. First, the thermal performance of the proposed technique was validated experimentally. In this experimental work, a pavement section provided with heat exchange loops in the aggregate base layer was constructed inside a freeze chamber where the ambient air temperature was precisely controlled. Two experiments were performed: the first one considered low ambient air temperature without snow or ice on the pavement surface, while the second had initial icy pavement surface. Heated fluid was circulated inside the loops in the two experiments with temperature measurements recorded at various locations within the pavement section and at the surface. The results of this experimental program confirm that burying the heat exchangers in the base layer provides enough heat to the pavement surface that keeps it ice free, despite the significant downward-propagating heat losses.

The results of the experiments were then used to predict the thermal performance of pavements provided with heat exchange loops in the base layer at different weather conditions using numerical models. Energy balance at the pavement surface was implemented in these models to consider the various weather conditions at each location. First, three-dimensional (3-D) finite element models were developed mimicking the experiments; these models were used as a validation of the ability of the finite element method to accurately predict the performance of the pavements. Along with the validation, these preliminary models showed that the heat propagation in the pavement section used in the experiment occurred mainly in the vertical dimension suggesting that 2-D finite element models can be adequately used. Thus, 2-D models were used to consider three U.S. locations: Buffalo, NY; New York City, NY; and Washington D.C. The weather conditions for each of these locations were obtained from the TMY3 database and were implemented in the respective model. The results of these models suggest that the proposed technique to bury the heat exchange loops in the base layer will potentially be able to deice typical pavement surfaces at all the considered locations.

Additionally, finite element models were developed to predict the effect of the heat exchange loops on the stresses and strains within the pavement section and at the pavement surface. The complexity of these mechanical models was increased gradually. Firstly, the displacement and stress fields in the pavement with an elastic HMA layer subjected to a static tire load was considered. Then, viscoelasticity was introduced to the HMA layer and the displacements and stress fields were analyzed. Compared with the elastic HMA layer, the pavement with viscoelastic HMA layer developed less stresses and displacements indicating that the design of self-heated pavements (e.g. loop geometry and material) can be accurately performed considering an elastic HMA layer. After that, the response of pavement under moving load was modeled. For simplicity, the contact between the tire and the pavement was simulated using a uniformly distributed stress over a circular loaded area mimicking the tire on the pavement surface. No explicit relationship was found between the surface deformations and the loop depth for pavements with HDPE tubes, while for pavements with aluminum loops the differential surface deformations above and between the loops decrease and converge to zero with increasing the loop depth.

At the end and based on the results of the experimental and numerical models performed in this project, burying heat exchange loops in the pavement base layer appears to be a feasible technique to de-ice pavement surfaces from both the thermal and mechanical perspectives. This finding, however, needs to be validated using an actual full-scale pavement with potentially a thicker asphalt layer compared to that considered in this study.

1 Introduction

During winter, pavements in New York State and other northern states freeze forming icy surfaces that: (1) reduce highway capacity due to slow moving vehicles or lane closures as a result of snow accumulations or accidents. Depending on the snow falling rate, up to 30% reduction in highway capacity may occur (U.S. Department of Transportation, 2018) due to icy surfaces. (2) Crack asphalts and loosen aggregate layers due to the thermal expansion of water upon freezing. (3) Increase the fuel consumption of vehicles due to the slow moving or blocked traffic, and the high tires/cracked-pavement frictional resistance. In fact, a 10% increase in pavement roughness (due to cracks) increases vehicles' fuel consumption by 2% wasting, on an annual basis in NY State, about 30 million fuel gallons and introduces 8 million tons of carbon dioxide (CO₂) to the atmosphere (Calwell 2002, Evans et al. 2009, Friedrich 2002). Moreover, (4) increase the number of transportation-related fatalities and injuries due to losing vehicle's control. At the national level, over 150,000 crashes occur annually due to icy pavements with about 45,000 injuries, and 600 fatalities—averaging four times the fatalities from natural disasters (U.S. Department of Transportation, 2018).

Attempting to reduce these negative impacts of icy pavements, NY State spends \$1.6 billion annually for roadway de-icing (Henry 1991) by spraying various types of deicing salts on pavement surfaces to keep these surfaces ice-free. The impact of the deicing salts extends for a limited time. Moreover, these deicing salts deteriorate pavement materials (Balbay and Esen 2010, Shi 2008) and increase the chloride concentration in NY fresh water streams to about 25% of the concentration in seawater (Jackson and Jobbagy 2005, Kaushal et al. 2005, Novotny et al. 2008). Therefore, there is an urgent need to develop sustainable and clean techniques to de-ice pavements, or even better prevent freezing.

1.1 Current pavements de-icing techniques

Initially, asphalts resisting ice formation were thought to be the way to overcome the hazards associated with icy pavement surfaces. Highly-permeable asphalt mixtures, for example, assure faster drainage of surface water reducing the potential to form ice in winter. However, the high asphalt porosity decreases the asphalt effective thermal conductivity leading to a significant

increase in the pavement temperature in summer. Such high asphalt temperatures in summer increase the potential for plastic flow of the asphalt under vehicles tires — an asphalt deficiency known as rutting. Further, in addition to their relatively expensive costs, highly-permeable asphalts lose their ability for quick water drainage as fine particles block the porous structure over time. Therefore, these asphalts form icy-roads at a delayed time during their lifespan.

Recently, various techniques to heat pavements were developed including the use of resistive heat from the flow of an electrical current through metallic cables embedded in the pavement (Havens et al. 1978, Hoppe 2001, Kumagai and Nohara 1988, Liu et al. 2006a, Liu et al. 2006b, Minsk 1999, Spitler and Ramamoorthy 2000). Despite the feasibility of these techniques to keep pavement surfaces ice-free, their practical applications were very limited due to the high associated operational costs (Liu et al. 2006b). Additionally, the use of hydronic systems that circulate a heated fluid within a pipe network in the roadway or bridge was proven to be efficient for pavement de-icing (Ramsey et al. 1999, Rees et al. 2002, Hamada et al. 2007, Lund 1999). In the original hydronic systems, the fluid was heated using gas-fired or electric boilers, which had significant heat losses that constrained the widespread of these techniques.

As an effort to reducing the reliance on external heating sources for heated pavements, the Netherlands has proposed the use of geothermal energy stored in the shallow ground layers (<500 ft.) to heat pavements (Spitler and Ramamoorthy 2000, de Bondt et al. 2003, 2006). This technology was implemented in a field experiment by circulating a geothermal fluid between loops installed in the asphalt layer and geothermal wells drilled at the sides of the highway. Based on the experimental results, this technique was successfully able to keep pavement surfaces ice-free throughout the winter (de Bondt 2003, de Bondt and Jansen 2006, Loomans et al. 2003, Sullivan et al. 2007, Van Bijsterveld and de Bondt 2002).

The Dutch system, however, required the use of a specially formulated, expensive high-crack-resisting asphalt mix and a three-dimensional polypropylene geogrid to limit asphalt cracks from severe stress concentrations around the loops (de Bondt 2003, de Bondt and Jansen 2006, Loomans et al. 2003, Sullivan et al. 2007, Van Bijsterveld and de Bondt 2002). These modifications to the asphalt mix increase the materials' costs significantly. Further, installing the loops in the asphalt layer necessitates implementing special construction techniques to limit the

asphalt temperature at paving time to the maximum allowed by the loop manufacturer and achieve proper asphalt compaction around the loops (Van Bijsterveld and de Bondt 2002). These construction challenges coupled with the excessive material costs severely limited the adoption of the Dutch technology in the U.S.

1.2 Proposed self-heated pavement technology

To overcome the high material costs and construction challenges associated with the Dutch system, this study investigates the potential to bury the heating loops in the base layer beneath the asphalt, rather than to embed the loops directly within the thin asphalt layer as shown in Fig. 1. Placing the heating loops in the base layer allows the use of standard, inexpensive thin asphalt layers without special construction precautions or geogrids to limit asphalt cracks.

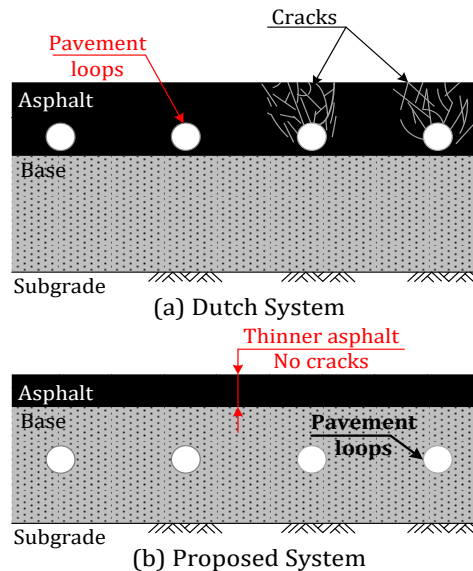


Fig. 1 Sketches of (a) the Dutch heated pavement, and (b) the proposed technology.

The overall proposed technique consists of, as shown in Fig. 2: (1) a pavement loop installed in the pavement base layer, (2) geothermal ground loops installed at the sides of the highway (Abdelaziz et al. 2015, Olgun et al. 2012), (3) circulation pumps to circulate a geothermal fluid between the pavement loop and the ground loops, and (4) a solar system to power the circulation pumps. This solar system includes photovoltaic solar panels, converters, batteries to store the electricity generated during the day for use at night, and controllers to manage the system operation. The use of a solar system to operate the circulation pumps extends the applicability of the technology to U.S. highways in remote areas away far from electrical sources.

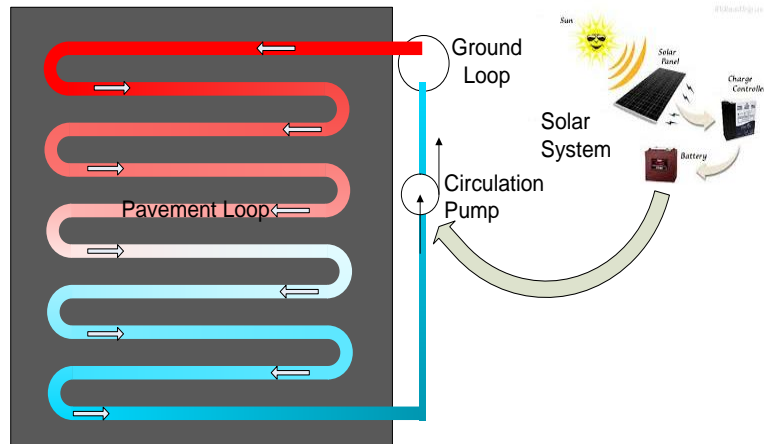


Fig. 2 Different components of the proposed self-heated pavement technology.

1.3 Research goals

The overall goals of this study are to

1. Experimentally investigate the feasibility of using heat exchange loops buried in the base layer to de-ice pavement surfaces.
2. Determine the viability of the proposed system (i.e., heating loops buried in the base layer) to de-ice pavements at different weather conditions.
3. Determine the effect of the buried loops on the stresses and the strains in the pavement section.

Aiming to address these goals, Chapter 2 of this report provides the background underlying the different components of the research, Chapter 3 discusses the performed laboratory experiment, Chapter 4 generalizes the results of the laboratory experiment at various weather conditions, Chapter 5 discuss the effects of the pavement loop on the stresses and the strains within the pavement section, and Chapter 6 summarizes the findings of the research and outlines future directions.

2 Background for the Surface Energy Balance of Pavements

Since the focus of this study is to keep pavement surfaces ice-free throughout winter times, it is important to understand the thermal energy balance at a pavement surface. Thus, this chapter focuses on surface energy balance relations for pavement surfaces. The background needed to analyze the loop-induced stresses and strains in the pavement section is presented at the beginning of Chapter 5.

2.1 Energy Balance Relation at Pavement Surface

Pavement surfaces are subjected to diurnal temperature variations that depend on a number of weather-related factors such as solar radiation, wind velocity, air temperature, groundwater and others. Out of the total amount of the instantaneous incident solar radiation (I), in W/m^2 , that fall on a pavement surface, and depending on the surface albedo (ρ), a significant amount of this radiation is reflected at the surface back to the atmosphere. The un-reflected solar radiation is, then, divided into four different thermal fluxes (W/m^2): conduction (G), convection (H), long-wave emission (L), and evaporation (E). The former two heat fluxes (i.e., conduction and convection) are well known. The long-wave emission represents the heat due to absorbing the incoming short-wave radiations and emitting long-wave radiations; while the evaporation heat flux is the flux required to evaporate a fluid mainly due to evapotranspiration. Unlike grassland and trees, pavement surfaces have almost no evapotranspiration; thus, the effect of the evaporation (E) can be neglected. Therefore, the relationship between these various heat fluxes and the amount of the un-reflected solar radiation can be developed, using the law of energy conservation, as given by the energy balance equation shown in Eq. (1).

$$(1 - \rho) \cdot I - G - H - L = 0 \quad 1$$

The progress of the conduction heat flux into the ground (G) depends on the thermal conductivity of the ground (k) and the thermal gradient (dT/dz). Solving the heat conduction relation in Eq. (2) at the pavement surface (i.e., $z = 0$) will, therefore, allow estimating the conduction heat flux (G).

$$G = -k \frac{dT}{dz} (z = 0) \quad 2$$

Moreover, the convection heat flux at the pavement surface (H) depends on the wind velocity (v) and the difference between the temperature of the pavement surface (T_s) and the air temperature (T_a) as given in Eq. (3).

$$H = h_c \cdot (T_s - T_a) \quad 3$$

where T_s and T_a are in K ; and h_c is the heat convection coefficient, in $W/m^2 \cdot K$, that varies with the wind velocity (v) as given by Eq. (4) (Bentz 2000). Since Eq. (4) is an empirical relation, the wind velocity in Eq. (4) should be in (m/s) and the resulting heat convection coefficient is in ($W/m^2 \cdot K$).

$$h_c = \begin{cases} 5.6 + 4 \cdot v & \text{for } v < 5 \text{ m/s} \\ 7.2 v^{0.7} & \text{for } v \geq 5 \text{ m/s} \end{cases} \quad 4$$

Finally, the long-wave emission (L) can be approximated from Eq. (5).

$$L = h_r \cdot (T_s - T_{sky}) \quad 5$$

where T_{sky} is the sky temperature in K ; and h_r is the irradiative coefficient in $W/m^2 \cdot K$.

The sky temperature (T_{sky}) can be approximated by factoring the air temperature (T_a), as per Eq. (6). The relating factor (ε_{sky}) is the sky emissivity, which is defined as a function of the dew point temperature (T_d) in Eq. (7).

$$T_{sky} = \varepsilon_{sky}^{0.25} \cdot T_a \quad 6$$

$$\varepsilon_{sky} = 0.574 + 0.0044 T_d \quad 7$$

The dew point temperature (T_d) in $^{\circ}C$ can be estimated using Eq. (8) and Eq. (9).

$$T_d = \frac{237.7 \cdot \gamma}{17.3 - \gamma} \quad 8$$

$$\gamma = \frac{17.3 \cdot T_a}{237.7 + T_a} + \ln\left(\frac{RH}{100}\right) \quad 9$$

where RH is the relative humidity and T_a is given in $^{\circ}C$.

The irradiative coefficient (h_r) in Eq. (5) is typically estimated using Eq. (10).

$$h_r = \varepsilon \cdot \sigma \cdot (T_s^2 + T_{sky}^2) \cdot (T_s + T_{sky}) \quad 10$$

where ε is the surface emissivity, and σ is the Stefan-Boltzmann constant ($5.67 \times 10^{-8} \text{ W/ m}^2 \cdot \text{K}^4$).

2.2 Energy Balance for the Proposed Pavement De-icing System

The energy balance relation, shown in Eq. (1), accounts for various effects of the atmosphere on the pavement temperature; it does not consider any heat source within the pavement itself. Therefore, the pavement surface temperature varies with the weather condition causing freezing in winter time. Since the proposed system relies on providing a heat source within the pavement section using the hydronic pavement loops in the base layer, the energy balance equation for the pavement should account for this additional heat (q_{loop}) as shown in Eq. (11).

$$(1 - \rho) \cdot I - G - H - L + q_{loop} = 0 \quad 11$$

The magnitude of the heat provided by the pavement loop (q_{loop}) determines the ability of the proposed system to keep pavement surface ice-free during winter time. It should be noticed that the system performance also depends on the ambient conditions; the loop heat increases to de-ice pavements at colder weathers. Therefore, this study focuses on determining the feasibility of the proposed pavement loop system to de-ice pavement surfaces by validating finite element models using the results of controlled laboratory experiments, then utilizing the validated models to consider the system performance at different weather conditions.

3 System Thermal Performance: Proof of Concept Using a Laboratory Experiment

This chapter aims to assure that installing heat exchangers in the base layer of pavements can deice the pavement surface. The proof-of-concept in this chapter was performed using a laboratory experiment in which a pavement section, with pre-installed loops in the base layer, was constructed inside a freeze-thaw chamber. The pavement surface was subjected to freezing temperatures, while a heated fluid was circulated in the loops. The temperature of the pavement surface as well as at different depths were monitored throughout the experiment. The equipment, the experimental setup and procedure, and the results are presented in this chapter.

3.1 Pavement Section and Experimental Setup

This section presents the different components incorporated in the laboratory setup used for the experiment. As shown in Fig. 3, the experiment was performed on an instrumented pavement section with pre-installed heat exchange loops. The following sections describe the materials and geometry of the used pavement section, climate control (freeze-thaw) chamber, fluid temperature control system, and instrumentations.

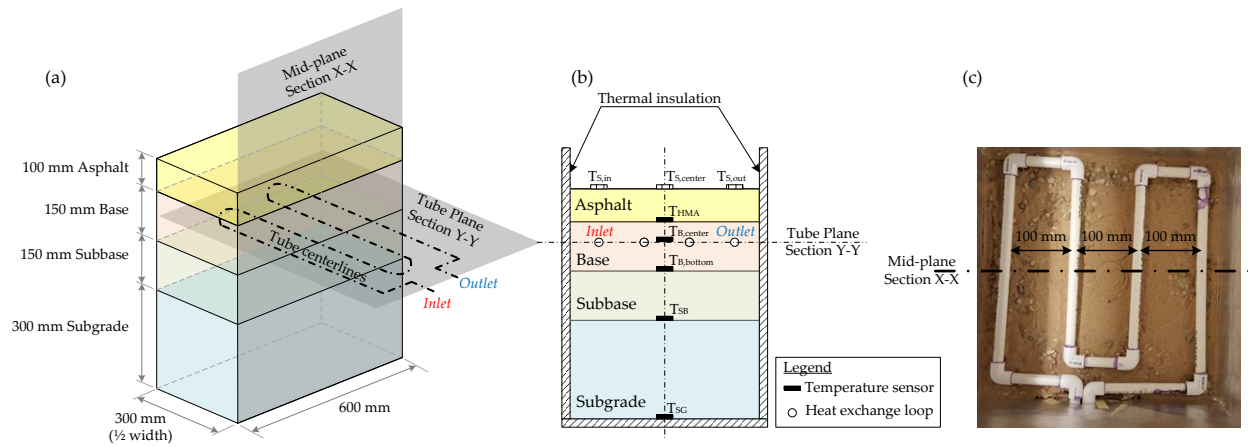


Fig. 3 Pavement section used in the experiment: (a) half-width 3-D view, (b) mid-plane cross-section X-X, and (c) the used heat exchange loop at tube plane (section Y-Y).

3.1.1 Instrumented Pavement Section

Referring to Fig. 3, the pavement section was constructed inside a 600 mm square wooden box with inner dimensions of 560 mm. This size was the maximum that can fit inside the freeze-thaw

chamber. The bottom and the sides of the box were insulated using 25 mm (1 inch) foam insulation panels on the inside. The used foam insulation was a Super TUFF-R polyisocyanurate with an R-value of 6.5. A 50 mm (~ 2 inch) hole was drilled through one side of the wooden box and the insulation 0.56 m (~ 22 inch) from the bottom. This hole was used to pass the inlet and outlet loops and the instrumentation cables.

The box was placed inside the freeze-thaw chamber where the various pavement layers were compacted. The compaction was performed using a 10-kg hammer free-falling from a 100-mm (~ 4 inches) a total of 100 times. As shown in Fig. 3(a), the pavement section consisted of a 300 mm (~12 inches) subgrade layer, a 150 mm (~6 inches) sub-base layer, a 150 mm (~6 inches) base layer, and a 100 mm (~4 inches) asphalt layer. The asphalt layer was a cold asphalt mix (Latexite Super Patch) purchased from a local store; the other aggregate layers were made of gravel and sand mixtures in accordance with NYSDOT Type 1 Subbase (NYSDOT 2000).

Prior to the compaction of the pavement section, several temperature sensors were installed at the center point of the pavement section at the bottom of asphalt (T_{HMA}), half-depth of the base layer ($T_{B,center}$), the bottom of the base layer ($T_{B,bottom}$), the bottom of the subbase layer (T_{SB}), and bottom of subgrade layer (T_{SG}) as shown in Fig. 3(b). Additionally, a 12-mm (~0.5 inch) heat exchange W-shaped loop (Fig. 3(c)) was installed at the mid-plane of the base layer, i.e., the centerline of the loop was 175 mm deep from the pavement surface, as shown in Fig. 3. The spacing between the W-shaped legs of the loop was 165 mm (~6.5 inch) as shown in Fig. 3(c). It is worth noting that while the pavement loop used in the experiment was manufactured from PVC tubes, PVC is not recommended in actual pavements due to the high rigidity of PVC, which may reduce the tube life under vehicle dynamic loads. Rather, high-density polyethylene (HDPE) or metal-based tubes are recommended for actual pavements due to their higher resistance to dynamic loads. The thermal properties and wall thickness of the PVC tubes and HDPE are comparable.

The thermal properties of all materials used in the experiment were measured using a portable thermal properties analyzer (KD2 Pro). A total of ten measurements were recorded for each layer at different locations and depths; while three measurements were taken for the pipe material and

working fluid. Overall, the variability in the thermal properties was less than 2%. The average thermal properties for the different materials are summarized in Table 1.

Table 1 Thermal Properties of Materials used in the validation analysis.

Thermal Property	Asphalt	Base	Subbase	PVC pipe	Working Fluid
Density, kg/m ³	1500	1920	1920	1040	1037
Thermal conductivity, W/m · K	1.00	1.30	1.30	0.16	0.35
Specific heat, J/kg · K	700	1700	1700	1050	3570

3.1.2 Climate Change (Freeze-Thaw) Chamber

To control the environment surrounding the experimental setup, the wooden box was housed inside a Caron 6241 freeze-thaw chamber. This chamber has a temperature range between -25°C and 70°C with $\pm 0.1^{\circ}\text{C}$ temperature step-size. A 3-wire RTD temperature sensor was used to measure the chamber temperature. Two pre-manufactured access ports in the chamber walls were used to pass the instrumentation wires and tubing to the chamber inner space. The chamber was also provided with a drain to remove water that condenses on the chamber inner surfaces.

3.1.3 Fluid Heating Unit

A Polyscience 6000-Series temperature control unit was used to heat and pump a mixture of 50% water and 50% propylene glycol in the pavement loops. This temperature control unit has a 2.9 kW capacity and a fluid temperature setpoint between -20°C and 70°C . The unit has a magnetic centrifugal pump with a maximum flow rate of 4.1 gpm.

3.1.4 Data Acquisition System

A Campbell Scientific CR10-XPB0 data logger was used to record the pavement surface temperature, the temperature within the pavement section at various locations, the ambient temperature and relative humidity inside the freeze-thaw chamber, and the inlet and outlet fluid temperatures. Data were collected in 15-minute intervals. The air temperature and relative humidity above the pavement were also recorded. The various sensors used in this experiment were:

Embedded Temperature Sensors: The temperature sensors embedded within the pavement section were RioRand type DS18B20 that have a measuring range of -55°C to 125°C with $\pm 0.5^{\circ}\text{C}$

accuracy. These sensors were used to measure the temperature at various locations within the pavement layers as well as the inlet and the outlet fluid temperatures. As shown in Fig. 3(b) for the temperatures within the pavement layers, the sensors were installed during the compaction of the pavement section at the bottom of the asphalt layer (T_{HMA}), at the center ($T_{B,center}$) and at the bottom ($T_{B,bottom}$) of the base layer, at the bottom of the subbase layer (T_{SB}), and at the bottom of the subgrade layer (T_{SG}).

To measure the fluid temperature four RioRand DS18B20 temperature sensors were attached to the external wall of the pipe at both the inlet and the outlet using a silicon adhesive paste. After installation on the tubes, the sensors were insulated to minimize heat loss to the ambient. The maximum difference between the four fluid temperatures at the inlet and the outlet of the tube was less than ± 0.5 °C; thus, the average temperature of each four sensors were used to determine the inlet and the outlet fluid temperatures which is considered acceptable.

Temperature and Relative Humidity Sensor: A Campbell Scientific CS-215 sensor was used to measure temperature and relative humidity in the ambient air in the environmental chamber. The sensor measures the relative humidity, with 0.03% resolution and $\pm 2\%$ accuracy over a temperature range from -20 °C to 60 °C, while temperature is measured with 0.01 °C resolution and ± 0.3 °C accuracy.

Surface Temperature Probes: manufactured by Campbell Scientific 110PV with a range of -40 °C to 135 °C and ± 0.2 °C accuracy. Three probes were used as shown in Fig. 3(b): one attached to the pavement surface above the inlet leg of the pavement loop ($T_{S,in}$), the second was attached above the center ($T_{S,center}$), and the third probe was attached above the outlet leg of the pavement loop ($T_{S,out}$). These locations were chosen to investigate the uniformity of the pavement surface temperature at different locations with respect to the pavement loop length. These probes were attached to the pavement surface using Kapton tape with Silicone adhesive paste.

3.2 Experimental Procedure

Two sets of experiments were performed in this study. The first represents the condition of freezing conditions in which no ice or snow on the pavement surface was initially placed on the pavement surface. The second condition includes a layer of ice on the pavement when the heating

system was turned on. The testing procedure for these two experimental cases was the same, except that a 25-mm (~1 inch) layer of ice cubes was placed on top of the pavement surface for the second set before circulating the heated fluid in the pavement loops.

The procedure followed in the experiments started with setting the air temperature inside the freeze-thaw chamber to $-10\text{ }^{\circ}\text{C}$ for 48 hrs, which is the time required for the system to reach steady state. After this time, the pavement surface was found to have stabilized at about $-7.0 \pm 0.2\text{ }^{\circ}\text{C}$. During this period the tubes were filled with fluid, however no fluid circulation in the pavement loop took place. After the pavement temperature profile reached steady state, the circulation of the heated fluid inside the pavement loop was initiated with the inlet fluid temperature set to $31.5\text{ }^{\circ}\text{C}$ ($88.7\text{ }^{\circ}\text{F}$). The fluid circulation was initiated immediately after the stabilization of the pavement temperature for the case without ice on the pavement. The fluid was started after placing the ice layer for the second experimental set, i.e. without reaching steady state condition between the placed ice and the pavement surface. While this step complicates the data processing of the experimental results, it is believed to better replicate the actual conditions of snow falling on the pavement surface. The fluid circulation was continued until the measured temperatures at the considered locations on the pavement surface and within the pavement section stabilized.

3.3 Experiment Results and Discussion

3.3.1 Experimental Set 1: Cold Pavement Surface without Ice

The evolutions of the temperature of the pavement surface at the three considered locations, i.e. $T_{S,in}$, $T_{S,center}$, $T_{S,out}$ in Fig. 3(b), in the first experiment are presented in Fig. 4. The pavement surface temperature before starting the circulation of the $31.5\text{ }^{\circ}\text{C}$ fluid in the pavement loops was $-7\text{ }^{\circ}\text{C}$ at all locations as shown in Fig. 4 at time = 0 hr. Over the first two hours of the circulation of the heated fluid, the pavement surface temperature at all locations decreased to about $-8\text{ }^{\circ}\text{C}$. This initial reduction in the pavement surface temperature is believed to be independent of the heated fluid; it was rather caused by the heat exchange between the pavement surface and the $-10\text{ }^{\circ}\text{C}$ cold air inside the freeze-thaw chamber. Moreover, this reduction in temperature could also be a result of the initially cold fluid since, as stated earlier, the tube was filled with the fluid during

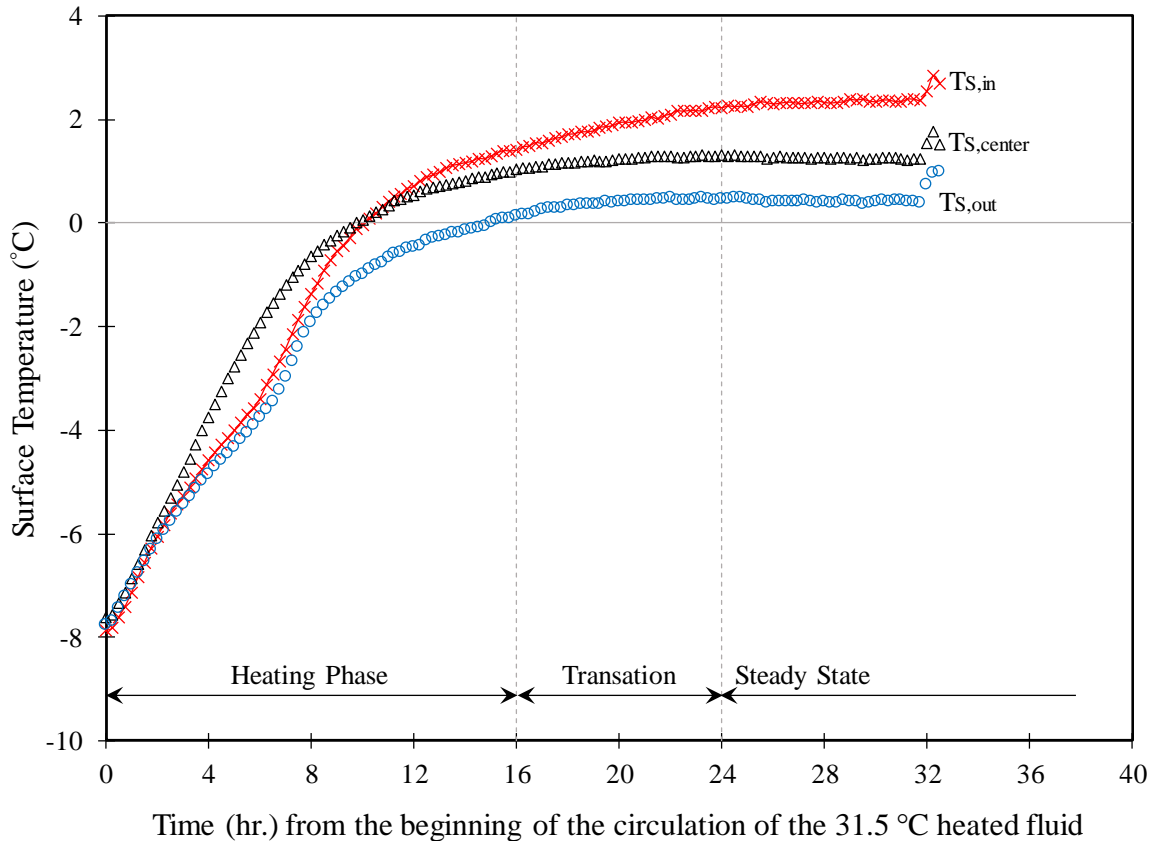


Fig. 4 Pavement surface temperature for first experimental set: $-10\text{ }^{\circ}\text{C}$ air temperature and $31.5\text{ }^{\circ}\text{C}$ inlet fluid temperature

the initial thermal stabilization time. After that, the pavement surface temperature continued to increase as the heated fluid injected heat into the pavement section.

While it was expected that the temperature sensor placed above the inlet tube ($T_{S,in}$) should experience a higher rate of temperature increase compare to the other two sensors due to the higher inlet fluid temperature, Fig. 4 shows that the initial temperature increase rate for the temperature sensor at the center ($T_{S,center}$) is the highest, while the temperature sensors above the inlet ($T_{S,in}$) and the outlet ($T_{S,out}$) loops experienced the same temperature change rate over the first 10 hours. This unexpected behavior may have occurred due to potential shifts in locating the sensors right above the respective loop leg, which is supported by the observed increase in the temperature change rate for $T_{S,in}$ after 10 hours.

At about 11 hours, the two temperature sensors above the inlet loop and at the center exceeded the freezing point, while the sensor above the outlet loop exceeded the freezing point after 16 hours. This period defines the *mandatory heating phase*, which is required to bring the pavement

above freezing. Heating was continued after the pavement temperature exceeded the freezing temperature, with a minor increase in the pavement surface temperature observed at all locations over next eight hours. The expected temperature distribution from hot-side to cold-side ($T_{S,in} > T_{S,center} > T_{S,out}$) was observed during this period. After approximately 24 hrs a steady-state temperature distribution was achieved and no further changes in the recorded pavement surface temperatures were observed.

In Fig. 3, it is noted that the surface temperature above the fluid inlet to the heating loop stabilized at a higher temperature (~ 2.5 °C) compared to that achieved at the center (~ 1 °C) and above the outlet loop (~ 0.5 °C). This variation in the pavement surface temperature implies that the critical location along the pavement is closer to the exit loop as the circulating fluid gets colder. Thus, a reliable design of the pavement loops requires confirming that the minimum surface temperature at the exit loop always remains above freezing. Moreover, the results of this experiment confirm that installing heat exchange loops in the base layer will facilitate maintaining the pavement surface above freezing, thus providing excess heat to melt snow and ice, while avoiding freezing of any surface water on the pavement.

While the pavement surface temperatures shown in Fig. 4 are promising, a critical aspect of the proposed concept is to minimize heat conduction down into the soil, as this represents a loss of heat that could otherwise be made available to the pavement surface. Fig. 5 shows that the heat injected to the pavement section via the heat exchange loops also increased the temperature at the interface between the base and the subbase layers ($T_{B,bottom}$), which indicates that heat propagates in all directions. The temperature increase at the bottom of the asphalt layer (ΔT_{HMA}) is about 22.5 °C, which is higher than the 11 °C temperature increase observed at the bottom of the base layer ($\Delta T_{B,bottom}$) suggesting that more heat propagated upward towards the pavement surface. This suggestion is supported by the fact that the temperature change at the pavement surface is much higher than those observed at the bottom of the subbase (T_{SB}) and the subgrade (T_{SG}) as shown in Fig. 5.

The fact that the temperature change at the bottom of the base layer is almost half of that at the top of the layer suggests a considerable heat flow downward. To quantify the magnitude of this downward heat losses, the amount of heat delivered to the top and to the bottom of the base

layer are calculated and compared to the heat provided from the pavement loops. The fluid heating is calculated from Eq. (12) using the measured inlet and outlet fluid temperatures and the thermal properties of the fluid presented in Table 1:

$$q = \dot{m}C_{pf}(T_{f,in} - T_{f,out}) \quad 12$$

where \dot{m} is the mass flow rate of the fluid in kg/s , C_{pf} is the heat capacity of the fluid in $J/kg \cdot K$, $T_{f,in}$ is the inlet temperature in $^{\circ}C$, and $T_{f,out}$ is the outlet temperature in $^{\circ}C$.

Fig. 6 shows the estimated heating over the duration of the experiment, and indicates presents that the total calorimetric power applied to the pavement section stabilizes at about 2,300 W.

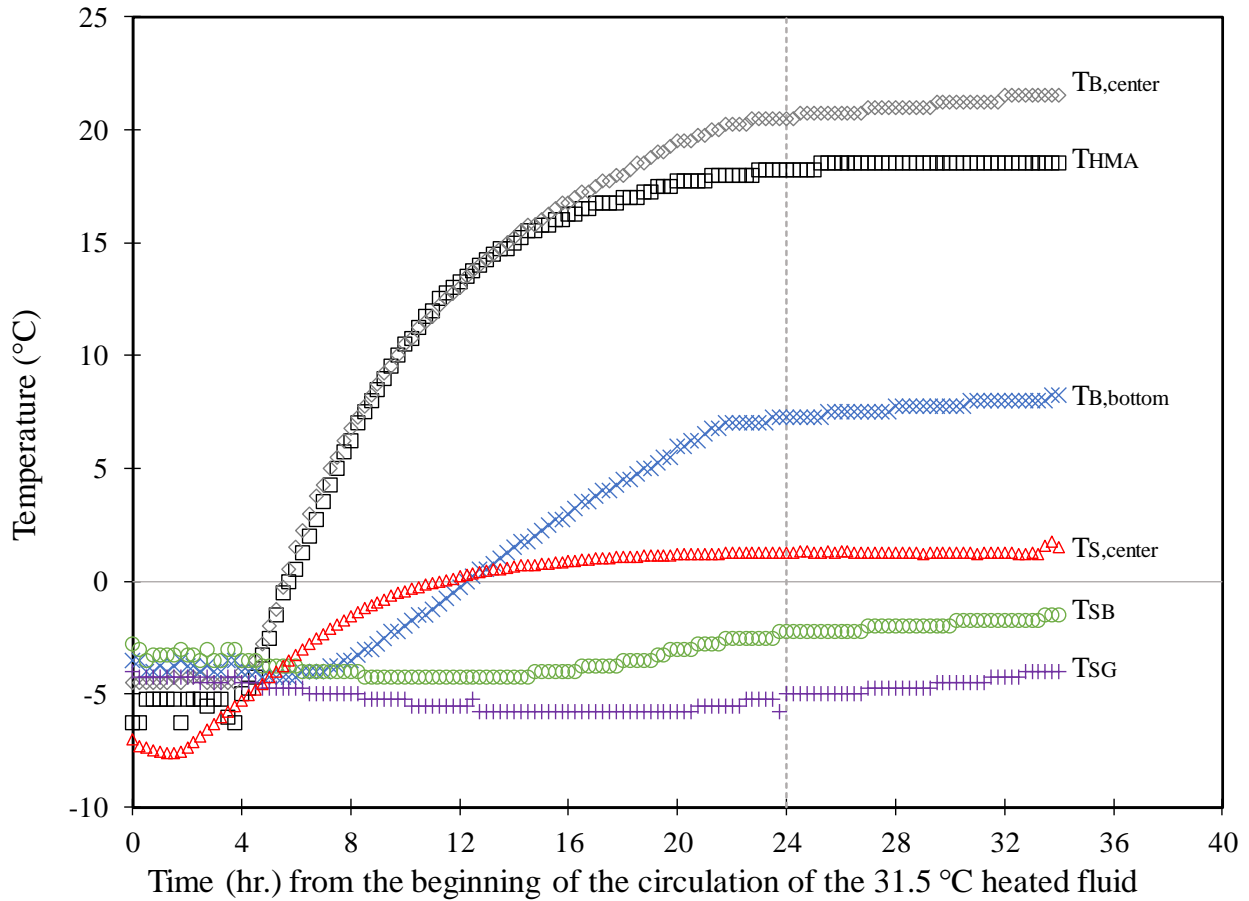


Fig. 5 Temperature change in different pavement layers for $-10^{\circ}C$ air temperature and $31.5^{\circ}C$ inlet fluid temperature.

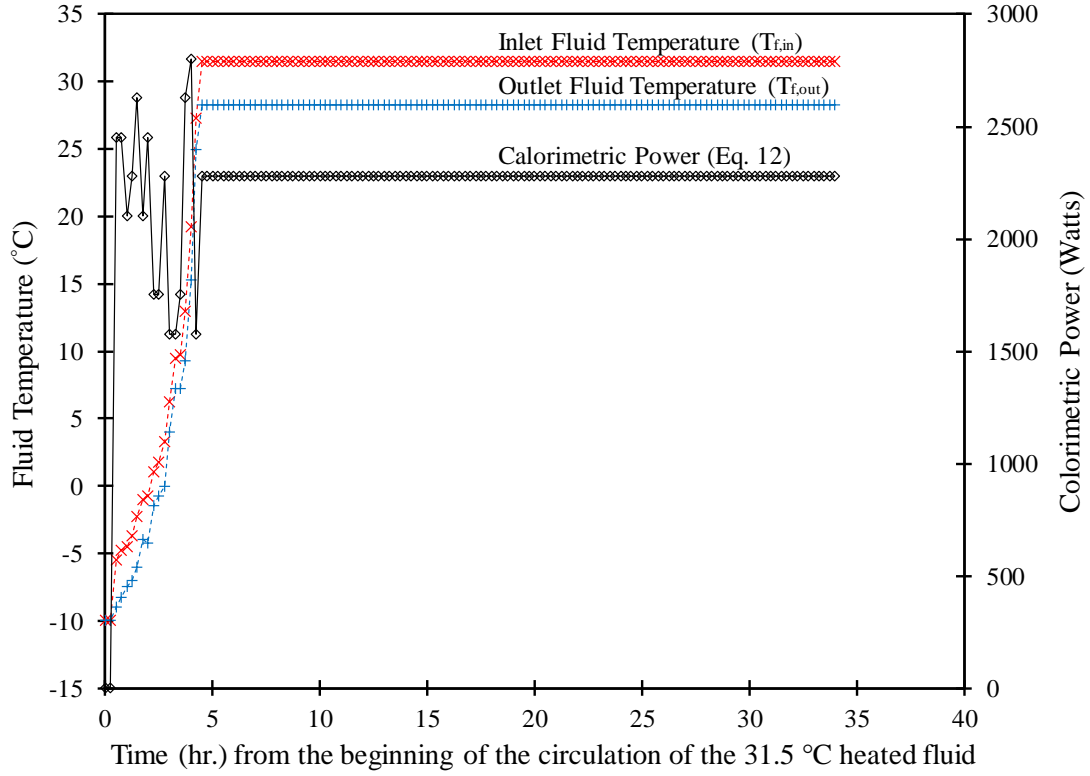


Fig. 6 Inlet and outlet fluid temperatures and heating rate applied to the pavement section for -10 °C air temperature and 31.5 °C inlet fluid temperature.

The amount of heat required to raise the temperature at the top and at the bottom of the base layer, i.e., T_{HMA} and $T_{B,bottom}$, were estimated using Eq. (13) for all time increments, assuming one-dimensional heat propagation.

$$Q_j = A\rho_{base}C_{p,base}\Delta x \sum_{i=1}^N \frac{\Delta T_{avg,j,i}}{\Delta t_i} \quad 13$$

where Q_j is the heat required to heat layer j , which is either the top half or the bottom half of the base layer, A is the cross-sectional area of the pavement section (i.e., 0.56 x 0.56 m), ρ_{base} and $C_{p,base}$ are the density and the specific heat capacity of the base layer, respectively (Table 1), Δx is half the thickness of the base layer, $\Delta T_{avg,j,i}$ is the average temperature change in layer j for time increment i , Δt_i is the duration of time increment i , and N is the total number of time increments.

Fig. 7 shows the evolution of the heat required to raise the temperature of the top and the bottom halves of the base layer based on Eq. (13), and the heat supplied from the pavement loops from Eq. (12). As shown in this figure, the total heat absorbed by the two halves of the base layer

converged to the heat power estimated from the fluid temperatures using Eq. (13), confirming the accuracy of the calculations.

More importantly, Fig. 7 shows that about 58% of the fluid injected heat propagated upward ($Q_{B,top}$), while 42% of the total heat propagated downward. This considerable downward heat propagation indicates that significant losses are expected to occur despite the promising use of heat exchangers installed in the base layer to de-ice pavement surfaces. Therefore, it is recommended to install an insulation layer below the heat exchange loops to minimize these heat losses. Minimizing the downward heat losses will allow reducing the total heat required to deice pavement surfaces and will facilitate increasing the loop spacing resulting in a reduction in cost. However, the mechanical performance of the pavement with the recommended insulation layer needs to be assessed.

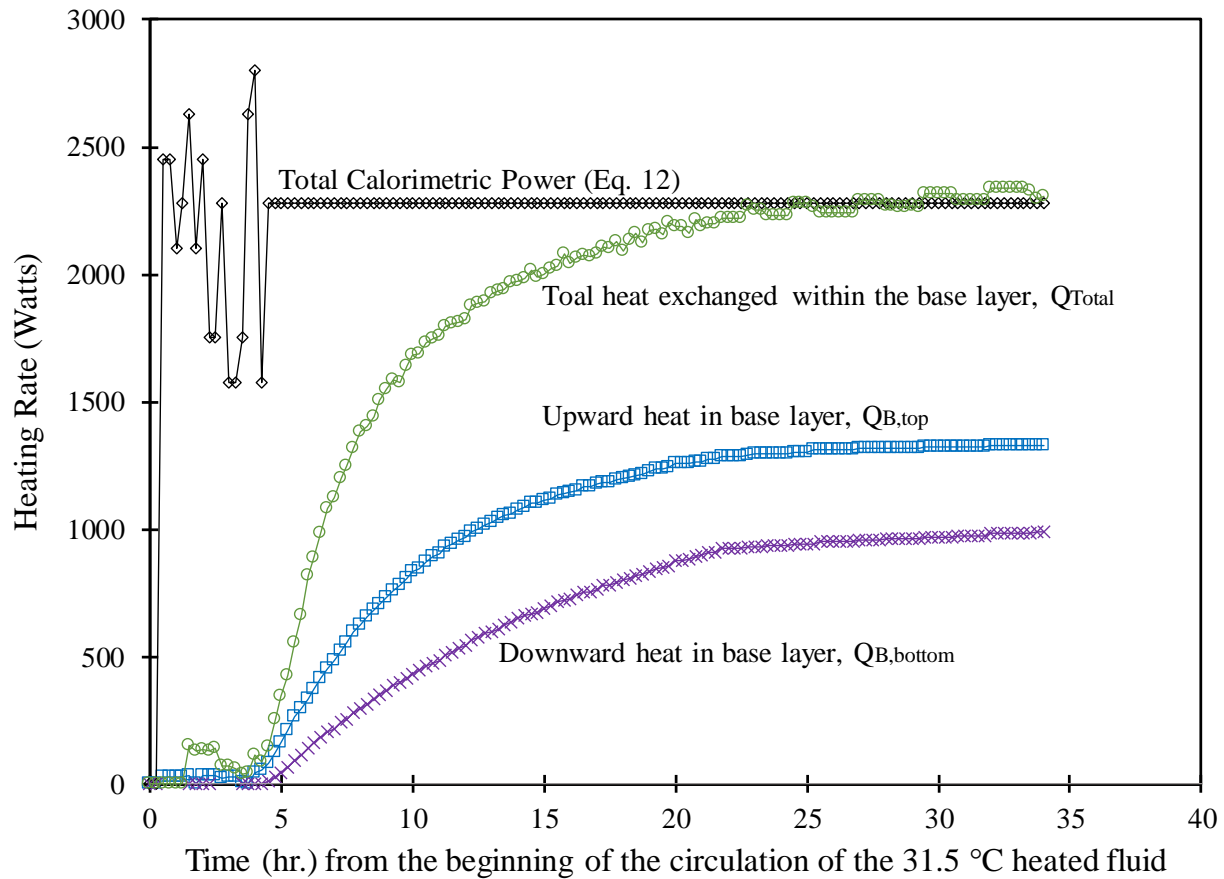


Fig. 7 Heat supplied to various pavement layers for $-10\text{ }^{\circ}\text{C}$ air temperature and $31.5\text{ }^{\circ}\text{C}$ inlet fluid temperature.

3.3.2 Experimental Set 2: Ice Cubes on Pavement Surface

While the results of the first experiment demonstrated the ability of a heating loop installed in the pavement base layer to maintain the pavement surface temperature above freezing, it did not consider the latent heat of fusion required to melt snow and ice already present on the pavement. The latent heat of fusion is the heat required to change frozen ice/snow into liquid water. To include the heat of fusion in the experimental program, a second experiment was performed following the same procedure as the first experiment, except that a 25 mm (~ 1 inch) ice layer was placed on top of the pavement surface before the circulation of the heated fluid.

Fig. 8 shows the pavement surface temperature measured at $T_{s,center}$ in Fig. 3 with ice placed on the pavement surface. For comparison, the pavement surface temperature at the same location from the experiment with no ice on the pavement surface is also plotted. Fig. 8 shows that the heat injected into the icy pavement was sufficient to raise the pavement surface temperature above freezing in about 10 hours; this observation proves that installing heat exchange loops in the pavement base layer provides adequate heat to deice any icy pavement surfaces.

Interestingly, Fig. 8 shows that the temperature of the icy pavement surface is higher than that of a cold pavement surface without ice from the first experiment, even though the same amount of heat was supplied to the pavement in the two experiments. The observed higher pavement surface temperature in the icy pavement experiment is believed to be due to the system attempt to reach thermal stability. The ice layer begins to melt as it adsorbs heat from the heat exchange loops producing water at a temperature higher than the preset air temperature ($-10\text{ }^{\circ}\text{C}$). The temperature difference between the resulting water and the surrounding air initiates an evaporative cooling process, i.e. water evaporation in attempt to reduce the temperature of the liquid water to stabilize with the surrounding temperature. As the evaporative cooling process continues the heat of fusion (phase change from liquid to vapor) is released to the surrounding raising the temperature of the air, which is shown in Fig. 9. This increase in the air temperature, in comparison to the constant $-10\text{ }^{\circ}\text{C}$ air temperature in the first experiment, is believed to cause higher overall pavement surface temperatures in the icy pavement experiment. Despite this effect, the experimental results confirm that the proposed installation of heat exchange loops

inside the base layer provides enough heat to the pavement section used in the experiments, which needs to be confirmed with field experiments in the future.

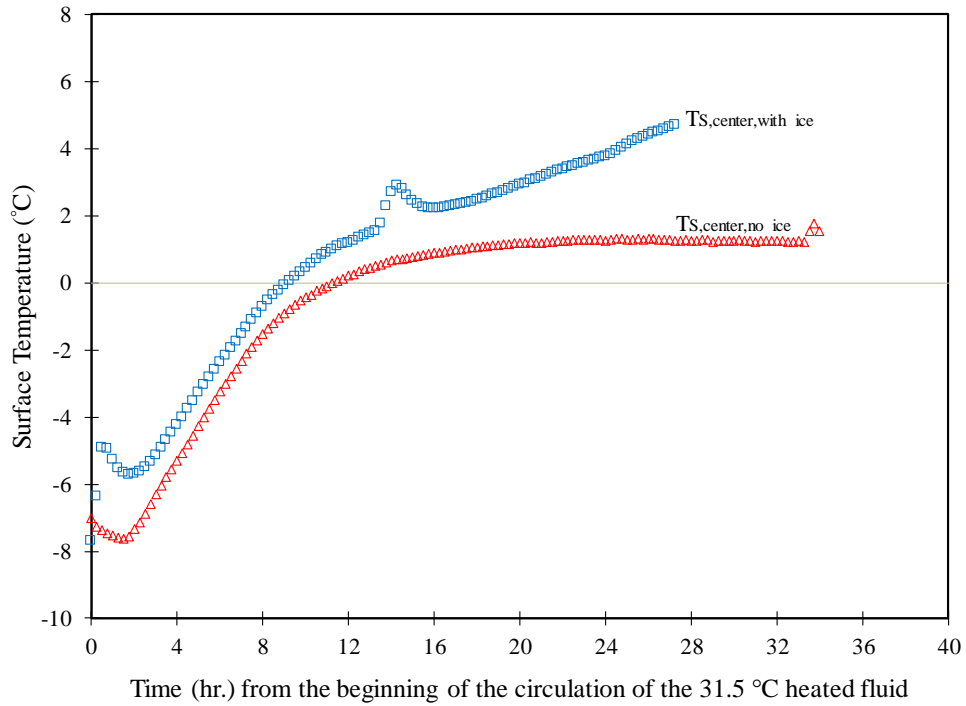


Fig. 8 Pavement surface temperature for -10°C air temperature and 31.5°C inlet fluid temperature with and without ice on pavement surface.

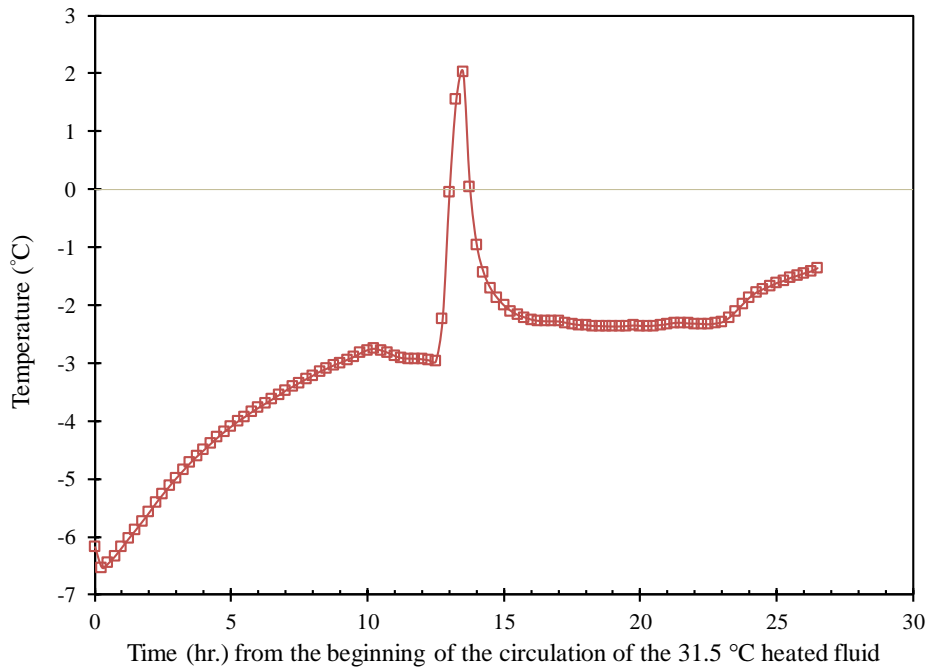


Fig. 9 Air temperature inside the chamber when ice is placed on the pavement surface.

3.4 Conclusions of the experimental work

The results of the laboratory experiments presented in this chapter show that:

1. Installing the pavement loops in the base layer beneath the asphalt layer is a feasible technique to de-ice pavement surfaces.
2. A significant percentage of the heat applied in the heat exchange loops is lost downward since heat transfer occurs in all directions around the pavement loops. While not included in the experiments, these energy losses can be minimized by installing an insulation layer underneath the pavement loops. The insulation layer will facilitate more heat transfer in the upward direction. However, the effect of this insulation layer on the mechanical behavior of the pavement needs to be investigated.
3. Since the experiments were performed in controlled laboratory environment, the behavior of the proposed self-heated pavements under actual weather conditions should be investigated.

4 System Thermal Performance: Numerical Modeling

While the experimental results presented in Chapter 3 proved that installing heat exchange loops in the aggregate base layer underneath the asphalt layer is sufficient to de-ice pavement surfaces, these results were obtained for a unique pavement section under fully controlled lab environment. Therefore, we need to explore the validity of the proposed technique for actual weather conditions applied on different pavement sections. Thus, the main objectives of this chapter are to (1) develop and validate numerical models using the experimental results presented in Chapter 3, and (2) use the validated numerical models to investigate the efficiency of the proposed pavement de-icing technique subjected to different weather conditions.

4.1 Model Development, Validation, and Possible Simplification

The aim of this section is to develop and validate a finite element numerical model capable of predicting the response of the proposed self-heated pavement technology. Therefore, we start this modeling task by developing a three-dimensional (3-D) finite element model mimicking the laboratory experiments discussed earlier in Chapter 3. The experimental results are thus used to validate the finite element model.

4.1.1 3-D Finite element model of the experiments

COMSOL Multiphysics (COMSOL 2014) is used to perform all finite element (FE) models performed in this Chapter. Fig. 10 presents the developed COMSOL model with the heat exchange loop highlighted. In this model, the dimensions of each layer and the heat exchange loops were taken from the experiments as shown in Fig. 3. Furthermore, the thermal properties assigned to each material are the same as those presented in Table 1.

Moreover, three distinct heat exchange processes were incorporated in the FE model. These processes are:

- (1) Fluid/pipe convective heat exchange: This represents the heat exchange between the circulating fluid and the inner surface of the pavement loops.
- (2) Conductive heat exchange within various materials: This heat exchange represents the heat transfer through the walls for the pavement loops and through the various pavement layers.

(3) *Air/pavement heat exchange*: This heat exchange occurs at the pavement surface and it represents the heat exchange between the ambient air and the pavement section.

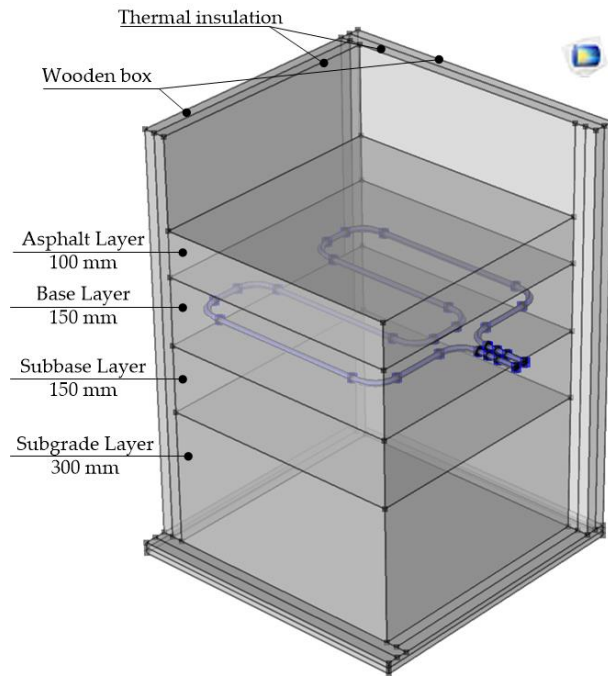


Fig. 10 Three-dimensional (3-D) COMSOL finite element model for the laboratory experiments. *Note: front and side wooden box and insulation are hidden to show pavement layers and the loop.*

The technique adopted to incorporate each of these heat exchange processes in the developed FE model is presented in the following sections.

a. Fluid/Pipe convective heat exchange

The convective heat transfer between the fluid flowing in the loops and the inner surface of the loops was modeled following the procedure developed by Ozudogru et al. (2014). In this procedure, the 3-D pipe and fluid flow inside are simplified using 1-D linear elements accounting for the heat exchange between these 1-D elements and the surroundings. This simplification allows reducing the computational time significantly, while maintaining high accuracy of the heat exchange results.

The simplification adopted by Ozudogru et al. (2014) relies on solving two sets of differential equations simultaneously: the equations for the fluid flow inside the pipe and the heat transfer equations along the pipe and between the fluid and the surroundings. It should be noticed that while the fluid flow equations are not directly related to the considered heat transfer process,

considering the fluid flow is critical to obtain accurate heat transfer results since the velocity vector of the fluid along the pipe is used in the heat transfer equation to determine (i) the heat dissipation due to viscous shearing of the fluid and (ii) distribution of the fluid temperature along the pipe, as discussed later.

To explain the importance of the fluid flow velocity vector on the heat transfer analysis along the pipe, the differential equation for the analysis of the heat transfer in the pipes is considered. This heat transfer equation relies on the energy equation for an incompressible fluid flowing in a pipe as given in Eq. (14).

$$\rho_f A_{pi} c_{pf} \frac{\partial T}{\partial t} + \rho_f A_{pi} c_{pf} \mathbf{u} \cdot \nabla T = \nabla \cdot A_{pi} k_f \nabla T + f_D \cdot \frac{\rho_f A_{pi}}{2d_h} |\mathbf{u}|^3 + q'_{wall} \quad 14$$

where ρ_f , c_{pf} , and k_f are the density, specific heat capacity, and the thermal conductivity of the flowing fluid, respectively; A_{pi} is the inner cross-sectional area of pipe, T is the temperature, t is the time, f_D is Darcy friction factor, d_h is the hydraulic diameter of the pipe, \mathbf{u} is the velocity field along the pipe, and q'_{wall} is the heat transfer through the pipe walls.

As shown in governing heat exchange Eq. (14), the velocity field of the fluid appears in the second term on the left-hand side as well as the second term on the right-hand side. The former term provides the fluid temperature distribution along the length of the pipe, while the latter term corresponds to the friction heat dissipated due to viscous shear. Thus, solving the fluid flow momentum and continuity equations, Eq. (15) and Eq. (16), is necessary to model the fluid heat transfer in the pipe adequately.

$$\rho_f \frac{\partial \mathbf{u}}{\partial t} = -\nabla p - f_D \frac{\rho_f}{2d_h} \mathbf{u} |\mathbf{u}| \quad 15$$

$$\frac{\partial A_{pi} \rho_f}{\partial t} + \nabla \cdot (A_{pi} \rho_f \mathbf{u}) = 0 \quad 16$$

Darcy friction factor, f_D in Eq. (14) and Eq. (15), can be estimated using the Churchill (1997) equation, which is valid for any flow condition, i.e. laminar or turbulent, as given in Eq. (17).

$$f_D = 8 \cdot \left[\left(\frac{8}{Re} \right)^{12} + (c_a + c_b)^{-1.5} \right]^{1/12} \quad 17$$

where c_a and c_b are given by Eq. (18) and Eq. (19), respectively.

$$c_a = \left[-2.457 \ln \left(\left(\frac{7}{Re} \right)^{0.9} + 0.27 \frac{e}{d_h} \right) \right]^{16} \quad 18$$

$$c_b = \left(\frac{37530}{Re} \right)^{16} \quad 19$$

where e is the absolute surface roughness of the pipe which is 0.0015 mm for plastic pipes, and Re is Reynolds number that can be calculated using Eq. (20).

$$Re = \frac{\rho_f u d_h}{\mu} \quad 20$$

where μ is the dynamic viscosity of the fluid.

Using Eqs. (18) through (23), the fluid velocity field is first estimated then used in Eq. (17) to calculate the fluid temperature and the heat exchanged with the surroundings. This heat exchanged with the surroundings is incorporated in Eq. (17) using the q'_{wall} term, which is given by Eq. (21).

$$q'_{wall} = (hZ)_{eff} \cdot (T_{ext} - T) \quad 21$$

where T_{ext} is the temperature of the pipe surrounding, i.e. the base layer, that is estimated using the heat conduction model, and $(hZ)_{eff}$ is the overall heat transfer coefficient per unit length of the pipe, which is given by Eq. (22).

$$(hZ)_{eff} = \frac{2\pi}{\frac{2}{d_{pi} h_{int}} + \frac{\log(\frac{d_e}{d_i})}{k_p}} \quad 22$$

The first term in the denominator represents the heat resistance due to the internal film between the fluid and the inner pipe surface through the internal film resistance heat transfer coefficient (h_{int}) which is estimated using Eq. (23) and Eq. (24). The second term in the denominator accounts for the thermal resistance due to the heat conduction through the pipe wall that has an inner diameter of d_i , an outer diameter of d_e , and a thermal conductivity of k_p .

$$h_{int} = N_u \frac{k_f}{d_h} \quad 23$$

$$N_u = \frac{(f_D/8)(Re-1000)Pr}{1+12.7(f_D/8)^{1/2}(Pr^{(2/3)}-1)} \quad 24$$

Therefore, solving the fluid flow and the fluid heat transfer equations at the same time allows the estimation of the heat rate applied from the pipe to the base layer in the model. To solve these coupled fluid/pipe heat transfer and flow equations, the inlet fluid temperature used in the experiments, i.e. 31.5 °C, was assigned at the pipe inlet in the model. The pipe inlet in the model was also assigned the mass flow rate used in the experiment, i.e. 4.1 gpm, which is used to calculate the inlet fluid velocity. Further, the pipe heat transfer model was coupled with the conductive heat exchange model (the following section) using T_{ext} in Eq. (24).

b. Conductive heat exchange with various materials

The heat propagation in the solid domains including the pseudo tube walls (Ozudogru et al., 2014), the base layer, the asphalt layer, the subbase and subgrade layers is expected to be conductive in nature. Any convection heat transfer in these layers due to potential groundwater flow is ignored. Thus, the heat conduction in the solid layers is governed by Eq. (25).

$$\rho C_p \frac{\partial T}{\partial t} + \nabla \cdot (-k \cdot \nabla T) = 0 \quad 25$$

where ρ , C_p , and k are the density, the specific heat capacity, and the thermal conductivity of each of the respective materials.

The conduction heat transfer equation, Eq. (25), is solved for the temperature (T). This conduction heat transfer model is coupled with the fluid convective heat transfer (previous section) by assigning the temperature outside the pipe from this model as T_{ext} in Eq. (24). It must be noticed that while generating the model geometry, the internal pavement loops were constructed as separate domains so that the pipes' external surfaces can be assigned appropriate boundary conditions.

c. Air/pavement heat exchange

The interaction between the pavement section and the cold air in the freeze-thaw chamber is performed by applying the various heat fluxes typically present in the energy balance relation as presented earlier in Chapter 2. The considered heat fluxes include irradiation (I), convection (H), long-wave emission (L), and conduction (G). The latter heat flux, i.e. conduction, is calculated using the heat conduction Eq. (25), while the former three fluxes are signed as boundary conditions on the pavement surface.

4.1.2 3-D FE Boundary Conditions, initial values, meshing, and numerical solver

As discussed in the previous section, the top surface of the pavement was assigned the three heat fluxes representing the energy balance equation of the pavement surface, i.e. convection, long-wave emission, and irradiation, as estimated using the mathematical formula in Chapter 2. To mimic the experiments, the modeled irradiation was set to zero throughout the model since the pavement section was housed inside the freeze-thaw chamber away from the sun. Furthermore, the air velocity in Eq. (4) was also set to zero throughout the model. Thus, the convective heat transfer coefficient for the model was constant at $5.6 \text{ W/ m}^2\text{K}$ which was used to calculate the convection heat transfer using Eq. (3). Moreover, the long-wave emission heat flux was calculated using Eq. (5) through Eq. (10) based on the measured relative humidity and air temperatures inside the freeze-thaw chamber throughout the experiments. Additionally, the sides of the wooden box were assigned an insulation (no heat flux or Neumann) boundary conditions since the presence of the thermal insulation prevented any heat exchange to take place through these walls. Finally, the inlet fluid temperature measured during the experiments (Fig. 6) was assigned at the inlet of the modeled pipe.

The initial temperature assigned for each layer mimicked the average temperature recorded in the considered layer before the beginning of the fluid circulation. The assigned initial temperatures for the asphalt layer, the base layer, the subbase layer, and the subgrade layer were $-7.1 \text{ }^\circ\text{C}$, $-4.5 \text{ }^\circ\text{C}$, $-3.5 \text{ }^\circ\text{C}$ and $-3.5 \text{ }^\circ\text{C}$, respectively. These values match those shown in Fig. 5 at time = 0 for each layer. Furthermore, the assigned initial fluid temperature was $-6 \text{ }^\circ\text{C}$ mimicking the measured temperature as shown in Fig. 6 at time = 0.

The mesh selected for the analysis was varied in preliminary models to ensure that the results are mesh-independent. Based on these preliminary models, it was found that adequate mesh is made of triangular elements with minimum and maximum element sizes of 3.7 mm and 51.7 mm, respectively, with an element growth rate of 1.4 and 0.7 refinement in narrow regions. Therefore, these mesh properties were used in the analysis reported here. Fig. 11 shows the selected mesh.

Finally, a time dependent analysis was performed to predict the temperature within the pavement section and the fluid temperature throughout the modeled experiment. This analysis

was performed for a total of 150 hour with results stored every 15 minutes. The analysis was performed using the COMSOL built-in GMRES iterative solver.

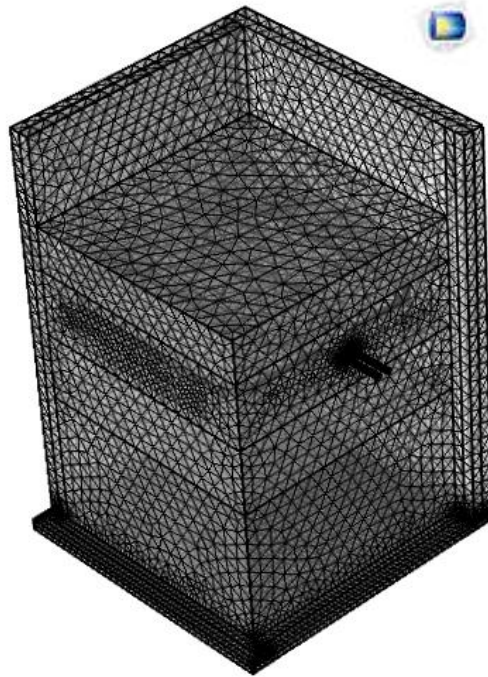


Fig. 11 Discretization of the 3-D finite element model for the experiments.

4.1.3 3-D Model Validation

The validation of the developed model was two-fold: the first is validating the implemented energy balance equations at the pavement surface, while the second is validating that the developed model is capable or mimicking the experimental results. This section presents the details of the two validation steps.

a. Validation of the surface energy balance model

The results of the experiment reported by Qin and Hiller (2014) were used for this validation of the energy balance equations implemented in the model. In this experiment, Qin and Hiller (2014) reported temperature changes at three different depths (12.7, 38.1, and 63.5 mm) in an asphalt layer of a conventional pavement (i.e. without heat exchange loops) in Davis, CA over a 10-days period extending from July 1st to July 11th, 2012. The solar radiation, wind speed, relative humidity, and ambient temperature were recorded over this period. Therefore, the validation

model considered for this step did not include heat exchange loops and it used the recorded weather conditions and the thermal properties reported in Qin and Hiller (2014). Fig. 12 presents a comparison between the measured pavement temperature at 38.1 mm and this approximated using the adopted surface energy balance equations. As can be seen from this figure, the pavement temperatures approximated using the finite element model are in good agreement with the measured temperatures with a relative error of about $\pm 7.5\%$. Similar results were found for the temperatures at other depths (i.e. 12.7 and 63.5 mm), suggesting that the adopted surface energy balance equations provide a robust technique to mimic reality.

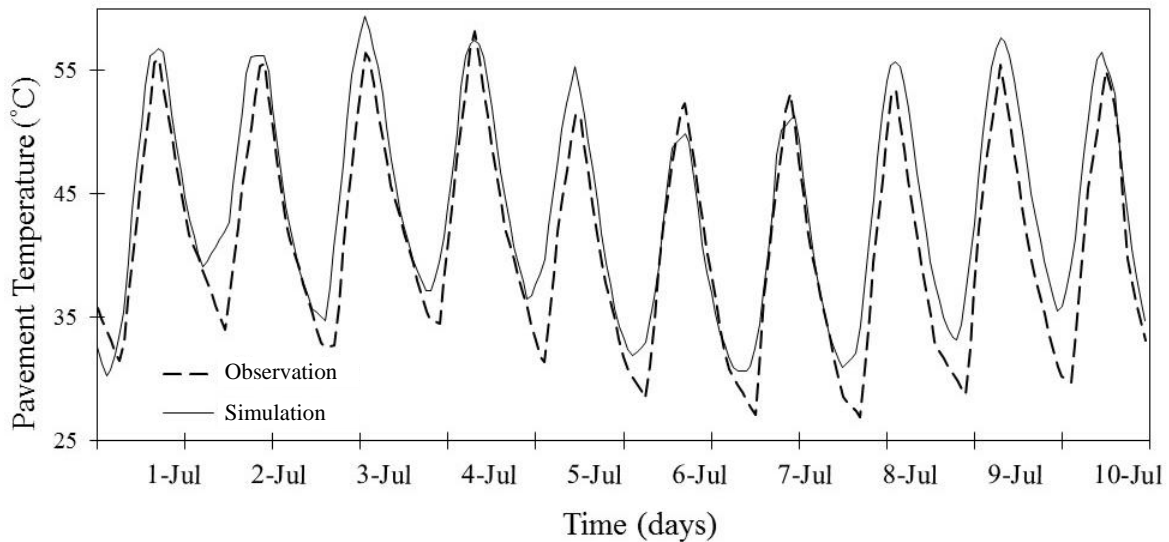


Fig. 12 Comparison between the observed (Qin and Hiller 2014) and the simulated pavement temperature at 38.1 mm in the asphalt layer.

b. Validation of 3-D model

The developed finite element model was validated against the temperatures measured in the experiment. Fig. 13 shows the results of the 3-D numerical model compared to the experimental results when the freeze-thaw chamber was set to temperature $-10\text{ }^{\circ}\text{C}$ and a fluid inlet temperature at $31.5\text{ }^{\circ}\text{C}$. The thermal properties for the various materials used in this model were the same as those shown in Table 1. As shown in Fig. 13, the results of the 3-D model not only captured the overall response of the surface temperature change, but also replicated the heating, transition and steady state stages.

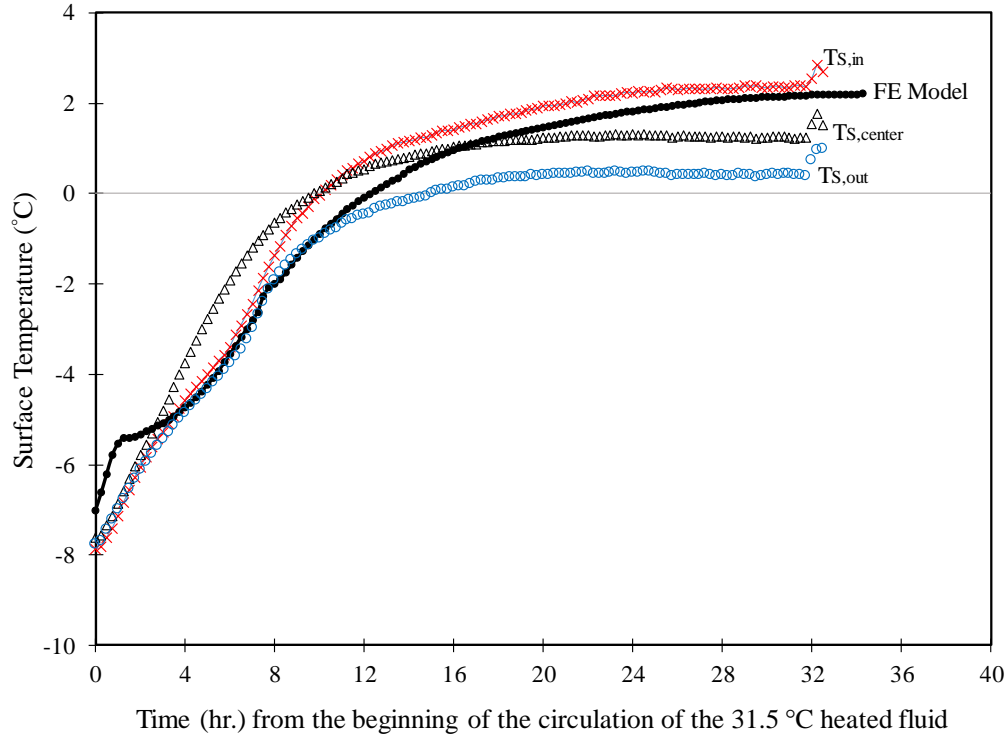


Fig. 13 Validation of numerical model against the experimental results for -10 °C chamber temperature and 31.5 °C inlet fluid temperature.

4.1.4 3-D Model Results and Discussions

As shown in Fig. 13, the developed 3-D finite element model was able to replicate the trend and average values for the pavement surface temperature changes as observed in the experiment validating the accuracy of the model. This validated model is, thus, used to understand the propagation of the thermal energy in the pavement section.

More importantly, the results of this 3-D finite element model suggest that the use of 2-D models is adequate to model the proposed de-icing system. As shown in Fig. 14, the contour lines for the pavement surface temperature appear to be consistent along the length of the pavement loop. Furthermore, the Fig. 15 shows that the temperatures distribution within the various pavement layers along the length of the pavement loop are independent of the considered cross-section. Therefore, 2-D finite element models are recommended for analyzing the effectiveness of the proposed de-icing technique under different weather conditions. The use of 2-D models will significantly reduce the computational costs and time compared to 3-D models.

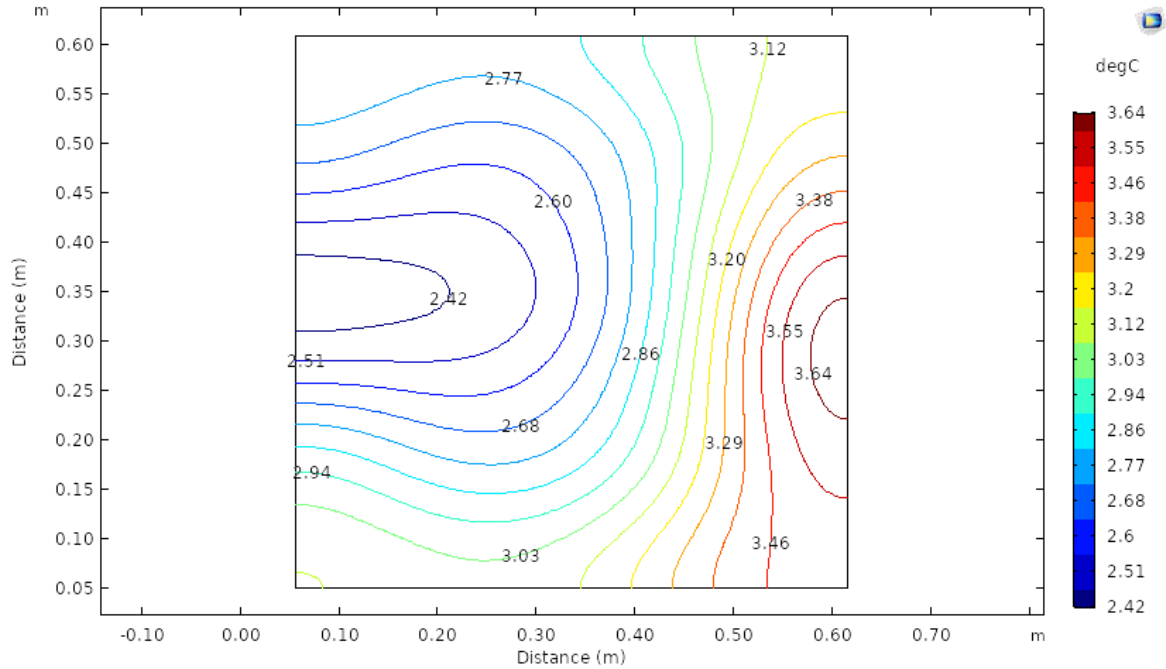


Fig. 14 Surface temperature contour lines after 30 hours.

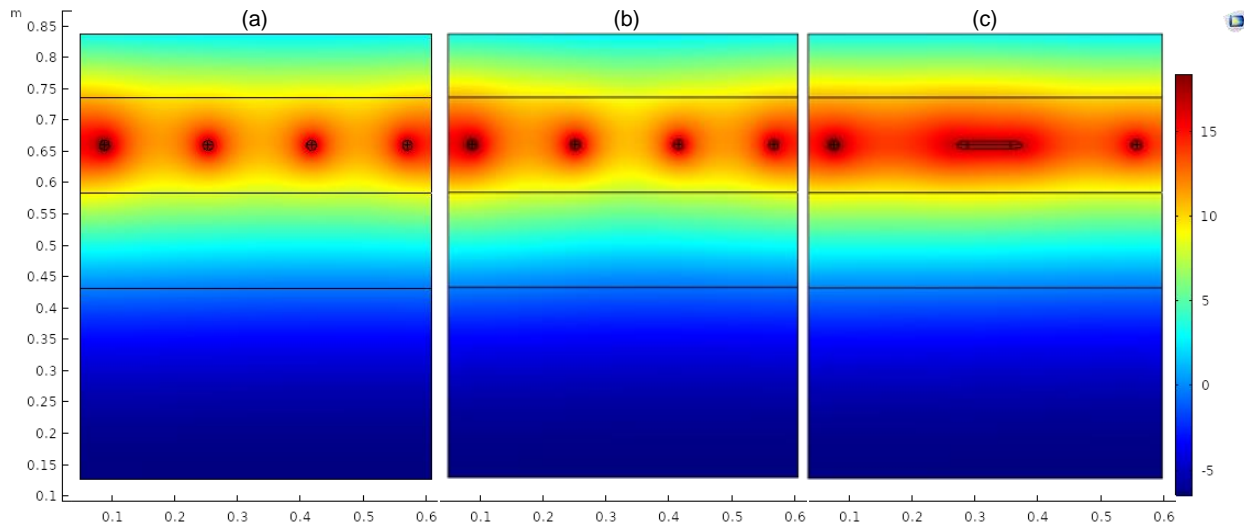


Fig. 15 Pavement temperature at different cross-sections along the length of the heat exchange loop after 30 hours; (a) at center of the loop, (b) at solid end of the wooden box, and (c) at the wooden side for the inlet and outlet loops entrances.

4.2 Predicting System Behavior for Actual Weather Conditions

This section presents the adopted simplification of the 3-D finite element models to 2-D models based on the previously discussed results of the 3-D models. Then, the weather conditions of

three locations in the U.S. are incorporated in the model to determine the effectiveness of burying heat exchange loops in the base layer to de-ice pavement surfaces.

4.2.1 2-D Model Simplification

To convert the 3-D physics of the fluid into 2-D, the method developed by Lazzari et al. (2010) was adopted. In this method, the fluid was replaced by an equivalent solid that has the same heat capacity and density as the fluid, but with a very high thermal conductivity; a thermal conductivity of 1000 W/m·K was used in this study.

The pavement section used in the 2-D models for this study represent a conventional cross-section in an actual pavement with heat exchange loops in the base layer. The considered pavement section consists of 125-mm asphalt layer on top of a 300-mm aggregate base layer and a 6-m sub-grade layer as shown in Fig. 16. Pavement loops are placed in the base layer at 75-mm below the bottom of the asphalt layer with a center-to-center spacing of 230-mm. Finally, the modeled loops have inner and outer diameters of 25-mm and 28-mm, respectively.

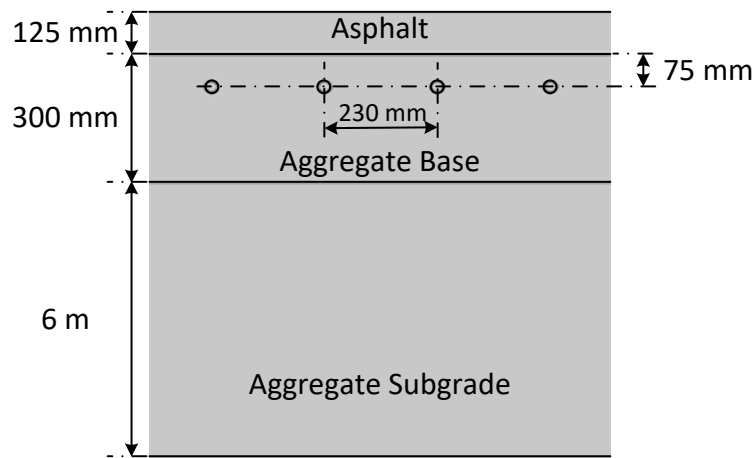


Fig. 16 Pavement section with proposed loops installed in the base layer.

The thermal properties of the various layers in the pavement section being used in the 2-D models are given in Table 2. While the values in Table 2 differ from those measure in the experiments performed in this study and shown in Table 1, these values were selected to represent the average values expected for various materials typically used in actual pavement construction. The sides of the model were assigned symmetrical boundary conditions, while the

bottom of the model was assigned a no-heat flux boundary condition as shown in Fig. 17. Moreover, the impact of the weather condition at each of the considered locations was implemented in the model via incorporating the solar radiation, wind speed, humidity, and ambient temperature as boundary conditions at the pavement surface using the surface energy balance equations discussed in Chapter 2.

Table 2 Thermal properties of various materials used in the 2-D numerical model.

Thermal Property	Asphalt	Base	Subgrade	Loops	Working fluid
Density (kg/m ³)	2350	2000	1750	960	1000
Thermal Conductivity (W/m·K)	1.80	2.0	2.0	0.39	0.594
Specific Heat Capacity (J/kg·K)	900	800	1500	2300	4187

The weather data for each of the considered locations were obtained from the typical meteorological year (TMY) database that provides the critical hourly weather data for the last 30 years (Wilcox and Marion, 2008). The hourly variation of ambient air temperature, relative humidity, solar intensity, and wind velocity for three cities were considered (1) New York City, NY, (2) Buffalo, NY, and (3) Washington D.C. These cities were selected to determine the effectiveness of the proposed de-icing technique under different weather conditions; Buffalo, NY representing an extreme winter conditions, while Washington D.C. represents a mild winter, and New York City being a moderate weather condition.

The pavement section was meshed using a hierarchical discretization approach. The fluid domains within the loops were meshed first using quadrilateral elements followed by the loop wall domains which were meshed using quadrilateral elements. Pavement layers were then meshed using triangular elements. The first pavement layer that was meshed was the asphalt layer, then the base layer, and finally the sub-grade layer with an increase in the mesh size with depth. The final adopted mesh for the modeled pavement section is shown in Fig. 17 .

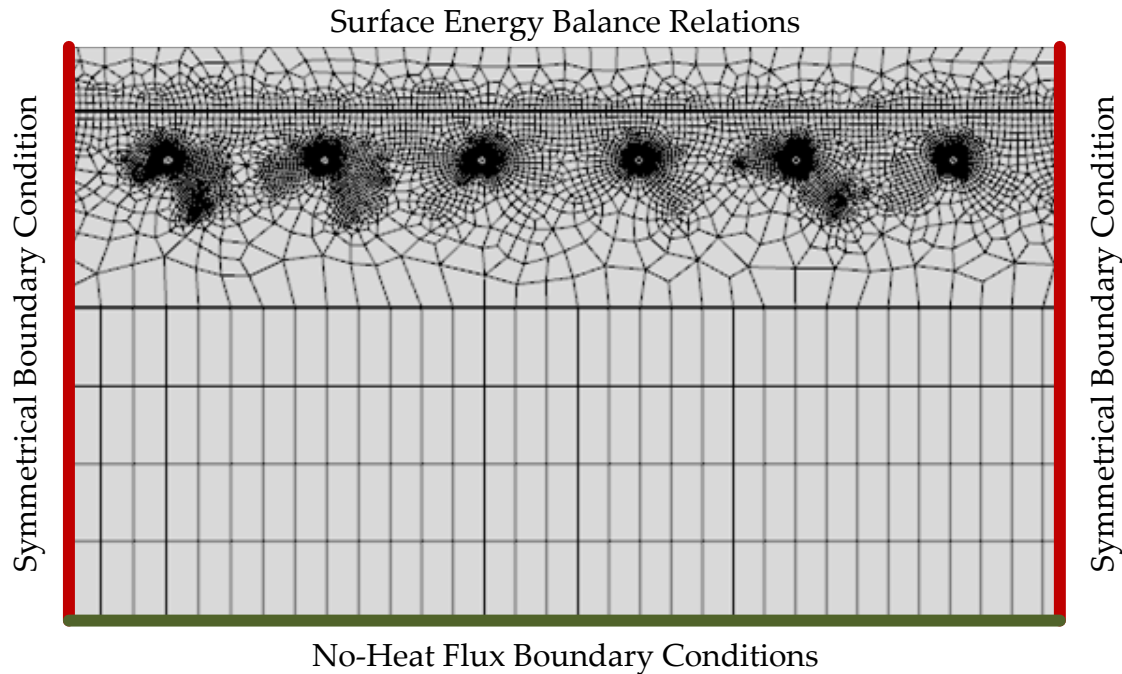


Fig. 17 Domain discretization mesh and assigned boundary conditions for the 2-D finite element models.

To provide a realistic initial ground temperature for each of the considered locations, a one-year transient model was performed for each city with the pavement surface subjected to the respective weather conditions at the considered city and without operating the heat exchange loops. The average temperatures at the end of this modeled year were then assigned as the initial uniform ground temperatures at each city for the model with operational heat exchange loops. These uniform ground temperatures were found to be 9 °C, 7.5 °C, and 12.5 °C for NYC, Buffalo, and Washington D.C., respectively.

4.2.2 Effectiveness of Proposed Heat Exchangers

To determine the ability and effectiveness of heat exchange loops buried in the base layer to de-ice pavement surfaces under different conditions, predicting pavement surface temperatures under normal conditions, i.e. without these loops, is needed. Therefore, the developed 2-D finite element models for the three considered locations were analyzed for one-year (after the one-year analysis used to determine the initial ground conditions as discussed in the previous section) without the heat exchange loops. Figs. 18, 19, and 20 present the predicted pavement surface temperatures for New York City, Washington D.C., and Buffalo, respectively over winter months

without the heat exchange loops. As shown in Fig. 18, the pavement surface temperature for New York City fall below freezing between November and March with $-12.5\text{ }^{\circ}\text{C}$ being the minimum temperature recorded in January. The pavement surface temperatures for Washington D.C. and buffalo fall below freezing between October and March as shown in Fig. 20 and Fig. 19, respectively. Furthermore, the minimum pavement surface temperatures for Buffalo and Washington D.C. occurred in February and were $-13.5\text{ }^{\circ}\text{C}$ and $-10\text{ }^{\circ}\text{C}$, respectively.

Following these initial models, the heat flux applied by the fluid inside the heat exchange loops was increased systematically until the pavement surface for each of the considered cities was raised above freezing. For each heat flux, the models were analyzed for one-year. The heat flux required to ensure that the considered New York City pavement section with pavement loop geometry shown in Fig. 16 will experience no freezing events was found to be 170 W/m as shown in Fig. 21. Similarly, the heat fluxes needed to ensure no freezing events for Washington D.C. and Buffalo were found to be 105 W/m and 130 W/m , respectively.

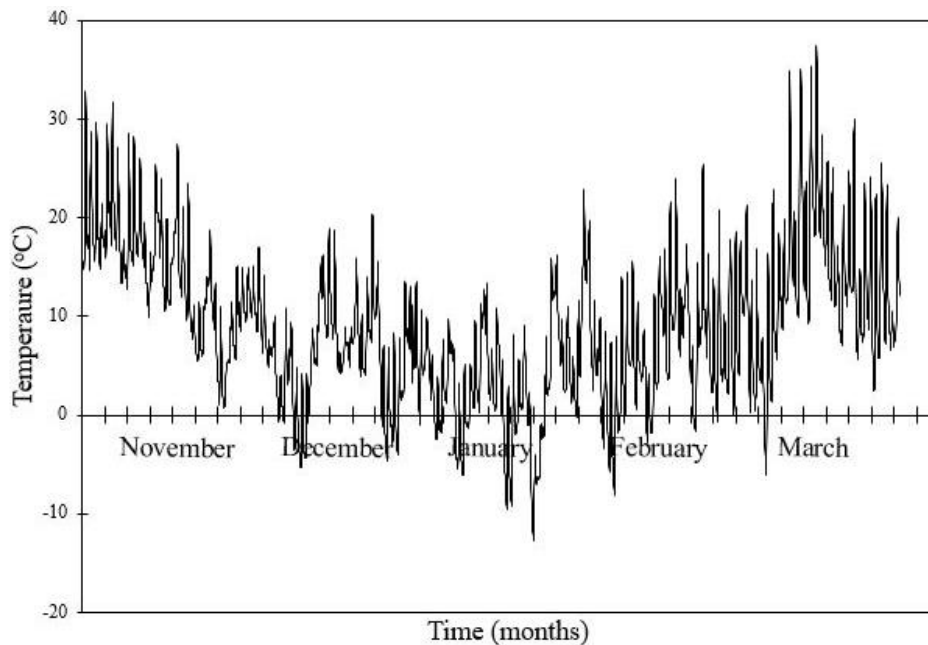


Fig. 18 Surface temperature for conventional pavement (without loops) over winter months in New York City.

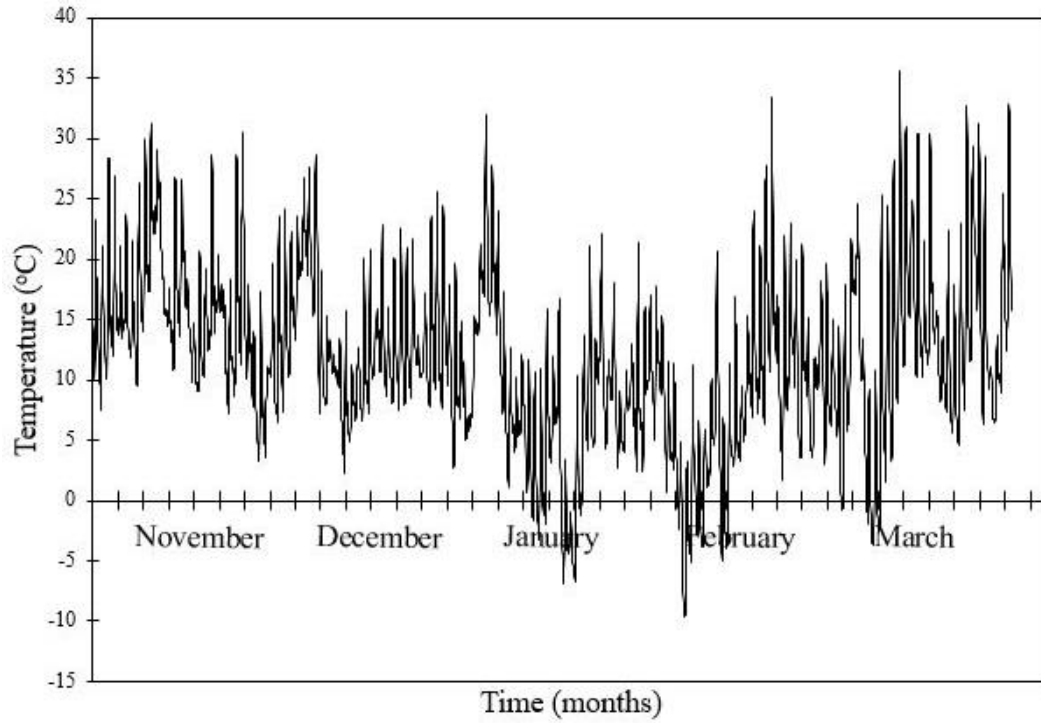


Fig. 19 Surface temperature for conventional pavement (without loops) over winter months in Washington, D.C.

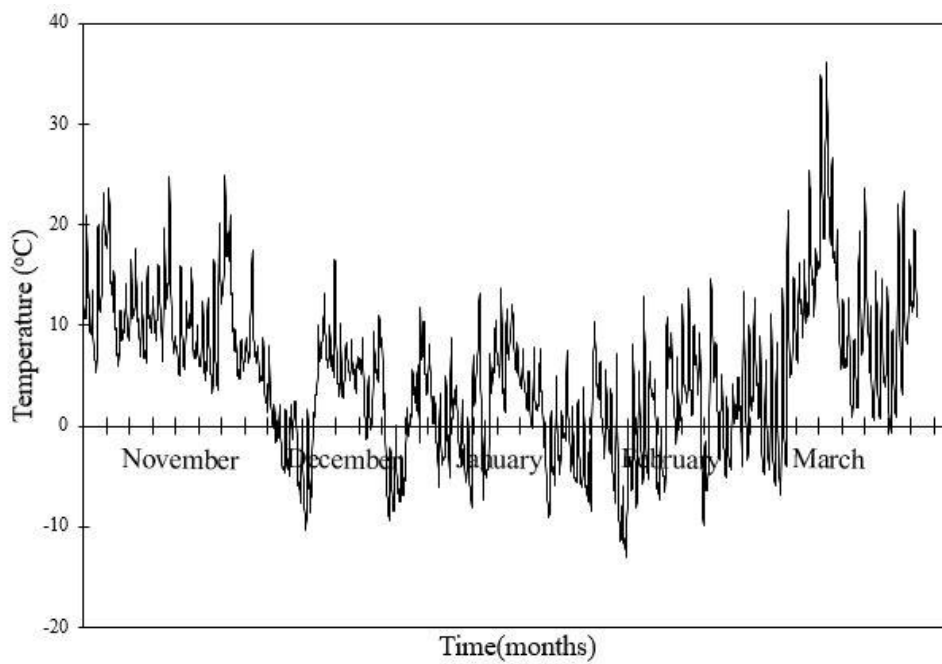


Fig. 20 Surface temperature for conventional pavement (without loops) over winter months in Buffalo.

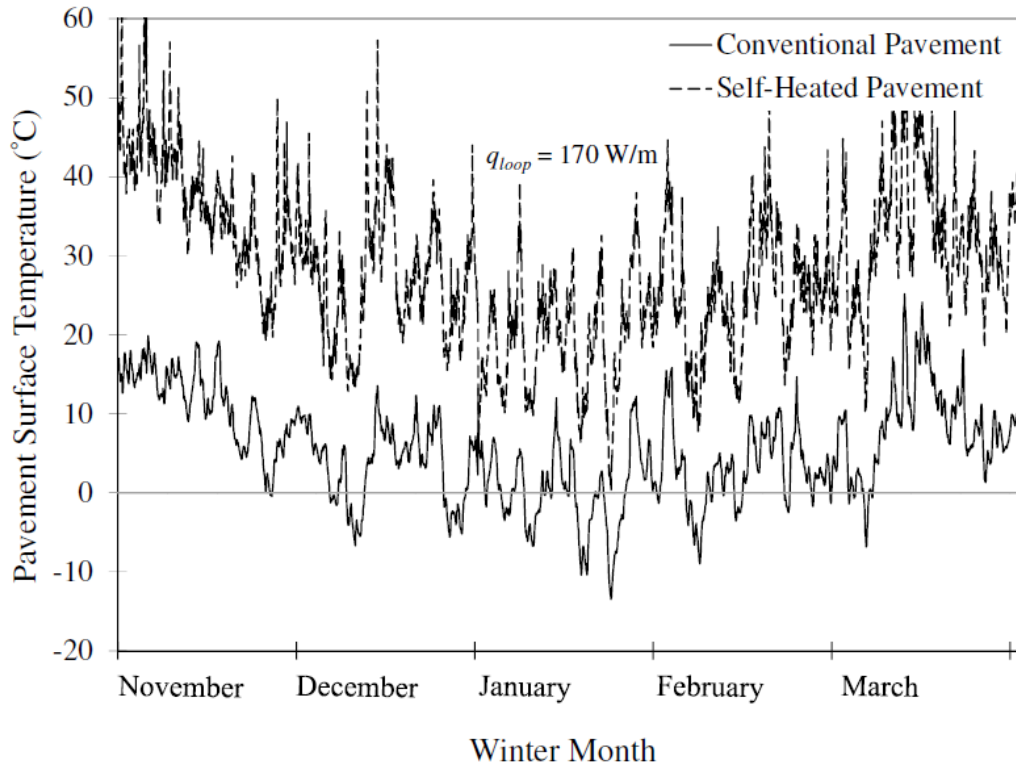


Fig. 21 Effect of burying heat exchange loops in the base layer on the pavement surface temperature over winter months in New York City.

Since the energy applied to the loops will need to be provided by an external system which could be external heaters, ground-coupled heat exchangers, or solar heat exchangers, it is recommended to limit the heat flux in the loops to an acceptable value. In this study, we recommend using 100 W/m because this heat flux will require, on average, a 1:1 pavement loop length to ground-coupled heat exchanger length, which is the recommended technique in this study. Since this selected heat flux is less than that required to ensure no freezing events for each of the three cities, the number of expected freezing events at each location needs to be predicted. Thus, the 2-D model for each of the cities was analyzed using 100 W/m as the applied heat flux in the loops. As shown in Fig. 22, the number of expected pavement surface freezing events for the three locations is considerably smaller than that for conventional pavement (see Figs. 18 through 20) with minimum pavement surface temperatures of $-6 \text{ }^\circ\text{C}$ for New York City, $-0.1 \text{ }^\circ\text{C}$ for Washington D.C, and $-4 \text{ }^\circ\text{C}$ for Buffalo. Thus, the recommended 100 W/m can be used for actual applications.

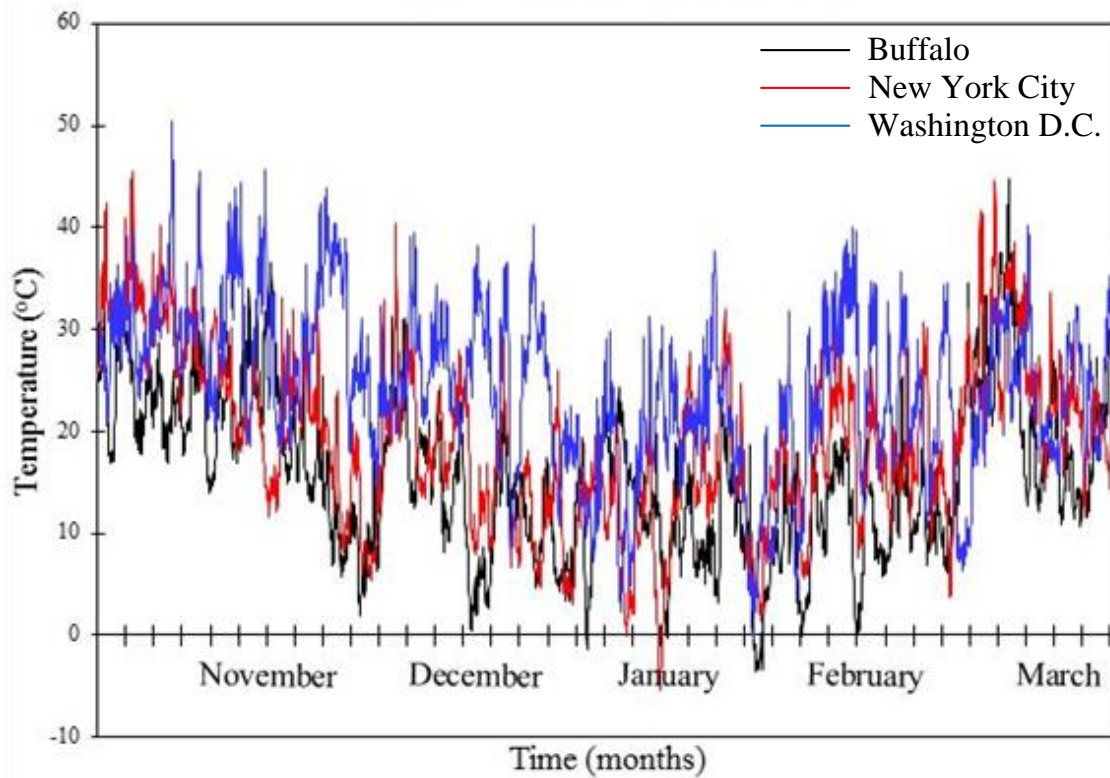


Fig. 22 Pavement surface temperatures for the three considered cities over winter months with 100 W/m applied to the surface.

4.3 Conclusions

Based on the validated numerical models performed in this chapter, the following conclusions are drawn:

- 1) The temperature distribution within the various layers of the pavement section is symmetrical around the heat exchange loops. Thus, the use of simplified 2-D finite element models is acceptable and recommended over the time consuming 3-D models.
- 2) Installing heat exchange loops in the aggregate base layer has the potential to de-ice pavement surfaces across northern U.S. states. However, the amount of heat required to ensure no pavement surface freezing events may compromise the system overall cost. Thus, it is recommended to limit the average heat flux in the loop to a value that correspond to a 1:1 pavement loop length to ground-coupled heat exchanger length. Lower heat fluxes should also be considered for unsaturated grounds to reduce the overall cost of the system.

5 Pavement Mechanical Performance

The experimental and numerical models presented in the previous chapters prove that the proposed self-heated pavement technique will facilitate maintaining the pavement surface ice-free through winter months for different weather conditions. This chapter aims to investigate the effect of the pavement loops buried in the base layer on the mechanical behavior of the pavement, i.e. strains and stresses. This chapter starts with simplified finite element models considering a static tire load with an elastic asphalt layer. Then, more realistic models considering moving tire load and visco-elastic asphalt constitutive relation were performed. Finally, a simple analytical model is considered to obtain quick preliminary design of the proposed self-heated pavement technique.

5.1 Background

To optimize the pavement loop geometry and material for acceptable pavement mechanical and thermal performance, it is essential to know the displacement and stress distribution in the self-heated pavement under both static and dynamic loads. Numerous studies investigated the contact stress distributions between vehicles' tires and pavement surface under different loading conditions, which have significant effects on the prediction of pavement response and performance (Wang and Al-Qadi 2010, De Beer et al. 2000, Al-Qadi et al. 2008). The exact distributions of contact stresses are complex and depend on many factors, such as tire type (bias-ply or radial-ply, dual tires or single wide-base tire), tire structure (geometry, tread pattern, rubber and reinforcement), pavement surface condition (texture and roughness), loading condition (wheel load and inflation pressure) and tire rolling condition (free rolling, acceleration, braking and cornering) (Wang et al. 2012).

The impact of dynamic loads on pavement was studied in the middle of 20th century based on analytic theories restrained. Cole and Huth (1956) proposed the analytic solution for pavement dynamic elastic responses under a steadily moving load in a symmetric half-space. Kenney (1954) simplified pavement as a beam in a steady-state vibration on elastic foundation. Hanazato et al. (1991) studied the traffic-induced ground vibration decreasing phenomenon due to damping force based on elastic theory. Jones et al. (1998) utilized Fourier transform to solve pavement dynamic responses in time history and developed analytical solutions for pavement responses under moving loads with rectangular shapes. Since then, Fourier transform was utilized to describe the

viscoelastic characteristics of asphalt layers, and to analyze pavement dynamic and vibration behaviors (Krylov 1996, Huang et al. 2001). However, these analytical solutions were based on the elastic or viscoelastic assumptions for asphalts and only for specific shapes of load contact areas making these oversimplified models highly different from field conditions (Hao and Ang 1998). Additionally, the ignorance of vehicle inertia, the vehicle-pavement coupling effect, and/or the shell model for pavement structure makes analytical solutions inaccurate (Lu and Xuejun 1998).

With the development of computational mechanics, the finite element method and the boundary element method broke the limitations of boundary conditions and load types in analytical methods. Zaghoul and White (1993) used ABAQUS, a three-dimensional, dynamic finite element program (3D-DFEM), to analyze flexible pavements subjected to moving loads at various speeds. A number of material models were used to represent actual material characteristics based on viscoelasticity and elastoplasticity concepts. The simulation results were then validated with test results which indicated that the 3D-DFEM can be used with confidence to predict actual pavement response from moving loads. Alabi (1992) studied dynamic responses of pavement structure under moving concentrated force through numerical integration and conducted sensitivity analysis on load speed.

Tielking and Roberts (1987) developed a FE model of bias-ply tire for analyzing the effect of inflation pressure and load on tire-pavement contact stresses. In their model, the pavement was modelled as a rigid flat surface, and the tire was modelled as an assembly of axisymmetric shell elements positioned along the carcass mid-ply surface. The simulation results showed that the inflation pressure is magnified about twice in localized areas of the footprint when the tire contacts the road surface because of truck tire stiffness and these high contact pressures produce high strains in thin pavements, which may lead to pre-mature cracking. Shoop (2001) simulated the coupled tire-terrain interaction and analyzed the plastic deformation of soft soil/snow using an Adaptive Lagrangian-Eulerian (ALE) mesh formulation. He suggested that the assumption of a rigid tire might be suitable for soft terrain analysis. Roque et al. (2000) used a simple strip model to simulate the cross section of a tire and concluded that the measurement of contact stresses using devices with rigid foundation was suitable for the prediction of pavement responses. Wang et al. (2012) developed a 3D tire - pavement interaction model to predict the tire - pavement contact stress distributions at both static and rolling conditions. The tire was modelled as a composite structure (rubber and reinforcement) and the pavement was modelled as a non-deformable flat surface to

achieve better computation efficiency. The analysis results showed that the non-uniformity of vertical contact stresses decreases as the load increases, but increases as the inflation pressure increases. However, vehicle maneuverings behavior significantly affects the tire – pavement contact stress distributions. For example, tire braking/acceleration induces significant longitudinal contact stresses, while tire cornering causes the peak contact stresses shifting towards one side of the contact patch.

Compared with the studies mentioned earlier, the goal of this study is to analyze the response of pavement under different loading conditions and investigate the effect of loop geometry and material property on the mechanical and thermal performance of the pavement, for simplicity, the tire is not included in the simulations and the load is applied onto the pavement directly through a circular contact area similarly as that in Wang et al. (2012).

5.2 Mechanical performance of the proposed self-heated pavement

In this section, 3-D self-heated pavement model is constructed, and the response of pavement with different material properties under different loading conditions are studied. The detail of the ABAQUS simulation and the result analysis are discussed below.

5.2.1 Static tire load on a pavement with elastic HMA layer

The considered pavement section consists of three layers namely the subgrade, a base layer and a hot mix asphalt (HMA) layer as shown in Fig. 23. The lateral extension of the model (3.3 m x 3.3 m) was selected to ensure that the results are not impacted significantly by boundaries. It is assumed that the outer surfaces of the loops are tied together with the base material, i.e. no slippage is allowed between the loops and the base layer. Table 3 summarizes the dimensions of different pavement layers and the loops used in this model. It should be noticed that the loop spacing in Table 3 refers to the center-to-center distance between two adjacent loops, while the loop cover is the distance from the bottom of the HMA layer to the top of the loop.

The considered tire load and boundary conditions of the pavement are shown in Fig. 24. The bottom of the pavement is fixed. Only vertical deformations are allowed to occur at the side boundaries of all pavement layers, i.e. the side boundaries are simply supported. Furthermore, a 150 mm contact between the tire and the pavement surface is considered in this model (Wang et al., 2012). Since this model considers a static tire load with no tire rolling, the expected shear stress applied on the pavement surface as the tire rolls is neglected. For simplicity, it is further assumed

that the contact normal stress between the tire and the pavement is uniformly distributed cross the contact area with magnitude of 550 kPa as shown in Fig. 24.

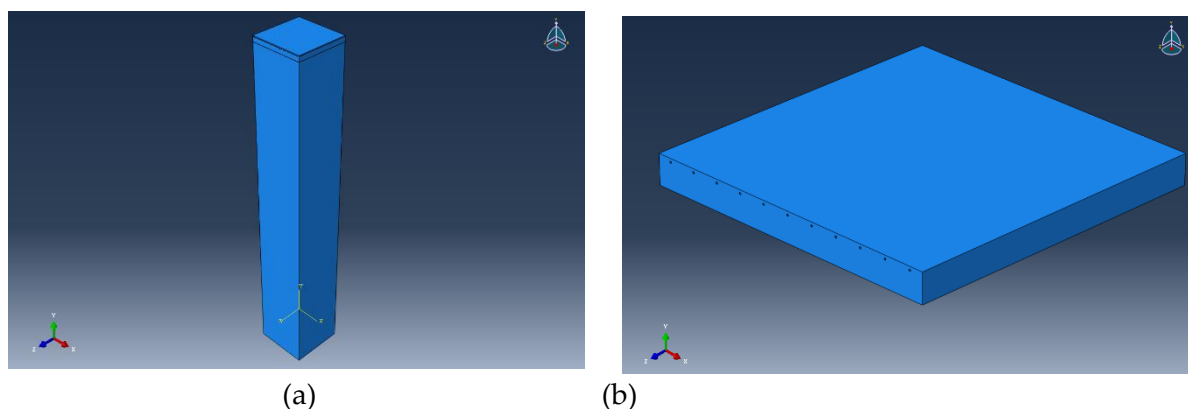


Fig. 23 ABAQUS FE model geometry (a) General view and, (b) Loops in the base layer.

Table 3. Summary of model geometry and material properties.

Property	HMA	Base	Subgrade	HDPE Loop
Thickness (m)	0.05	0.3	20.65	-
Density (kg/m ³)	2300	1700	2000	963
Young's Modulus (MPa)	700	100	20	800
Poisson's Ratio	0.35	0.4	0.45	0.45
Outer Diameter (mm)	-	-	-	10.7
Inner Diameter (mm)	-	-	-	7.9
Loop Spacing (mm)			300	
Loop Cover (mm)			25	

Fig. 25 shows the finite element mesh used for this model with the details of the discretization mesh presented in Table 4. A total of 129,670 elements are used to discretize all model domains. As the load is applied at the center of the HMA surface, small elements (0.025 m) are used for the HMA layer in order to get a more accurate result. Since the thickness of the subgrade is larger than its length and width and the limited effect of tire load as depth increases, as suggested by saint-venant

principle, gradual increase in the size of the elements is applied along the depth of the subgrade to reduce the total number of elements and computational costs.

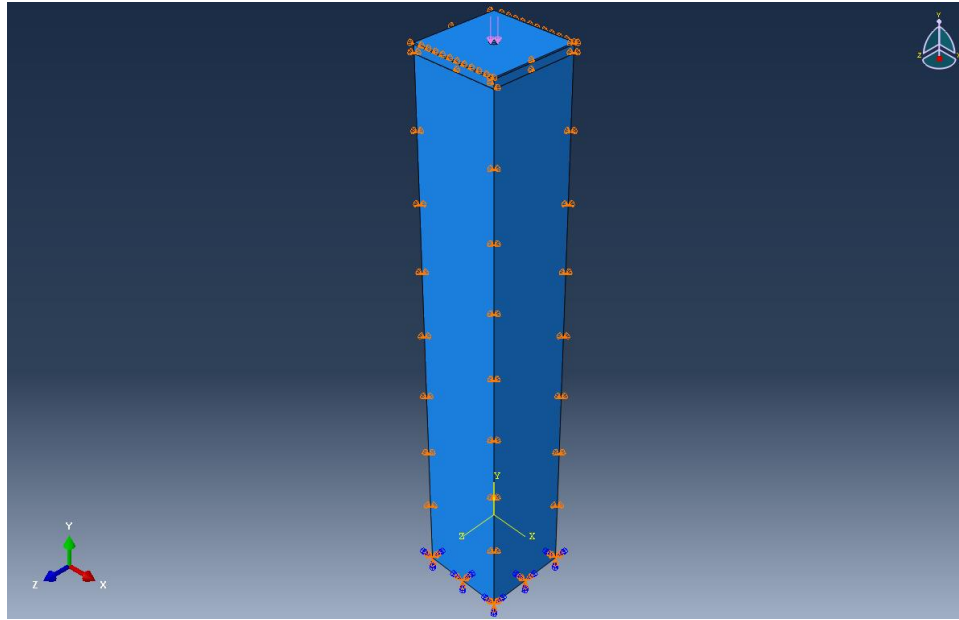


Fig. 24 Tire Load and boundary conditions of the pavement.

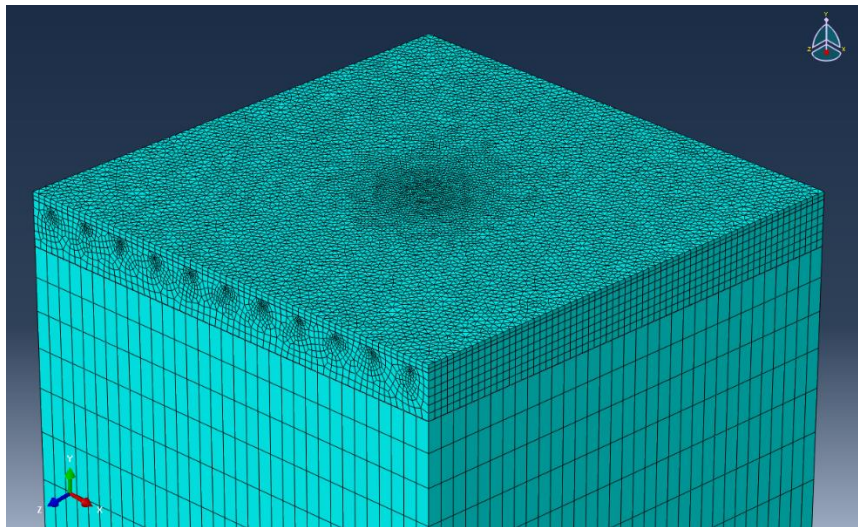


Fig. 25 Discretization mesh used for the model.

The results of the considered model are presented in Fig. 26. with the displacement and the 75% average Von-Mises stress fields over pavement depth are shown in Fig. 26(a) and Fig. 26(b), respectively. As shown in Fig. 26, the displacements and stresses in the pavement are concentrated over a very limited area around the applied circular tire pressure.

Table 4 Details of discretization mesh.

Layer	Element Type	Element Size (m)	Number of Elements
HMA	6-noded, linear, triangular prisms	0.05 × 0.025	22156
Base	8-noded, linear, brick	0.05×0.05×0.05	73392
Subgrade	8-noded, linear, brick	0.1×0.1×0.2~2	28314
HDPE Loop	8-noded, linear, brick	0.0028×0.0082×0.05	528

Lateral profiles for the surface displacements along the model centerline and stresses at the top of the center loop are presented in Fig. 27(a) and Fig. 27(b) which also be compared with the results from pavement without tubes, respectively. As shown in Fig. 27, the maximum observed displacement (-2.63 mm) occurs at the center applied tire pressure as initially anticipated. Similarly, the stress at the center of this tube is largest (0.9 MPa) and there are stress concentrations at two ends of the center tube.

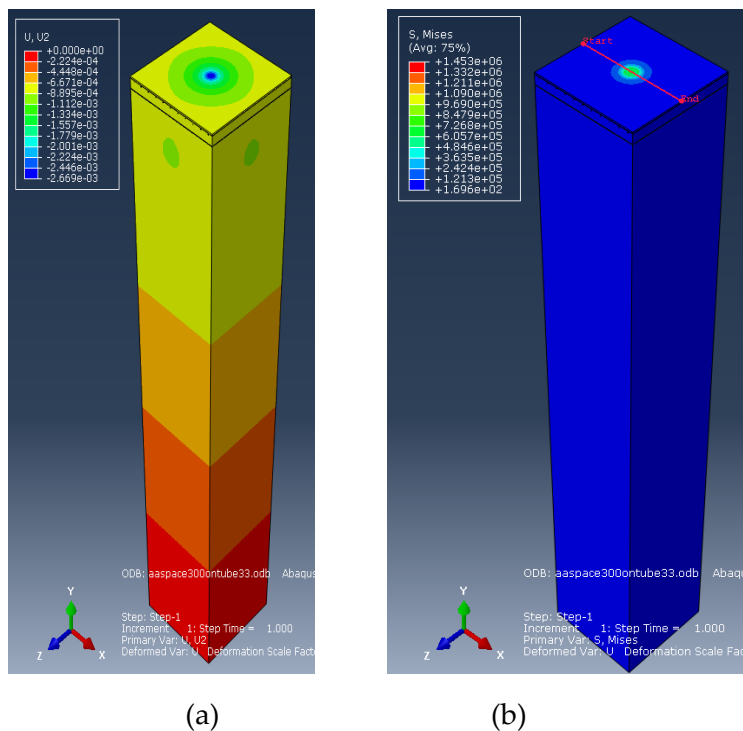


Fig. 26 Model results (a) Field of displacement along thickness direction (m), and (b) Stress field (Pa).

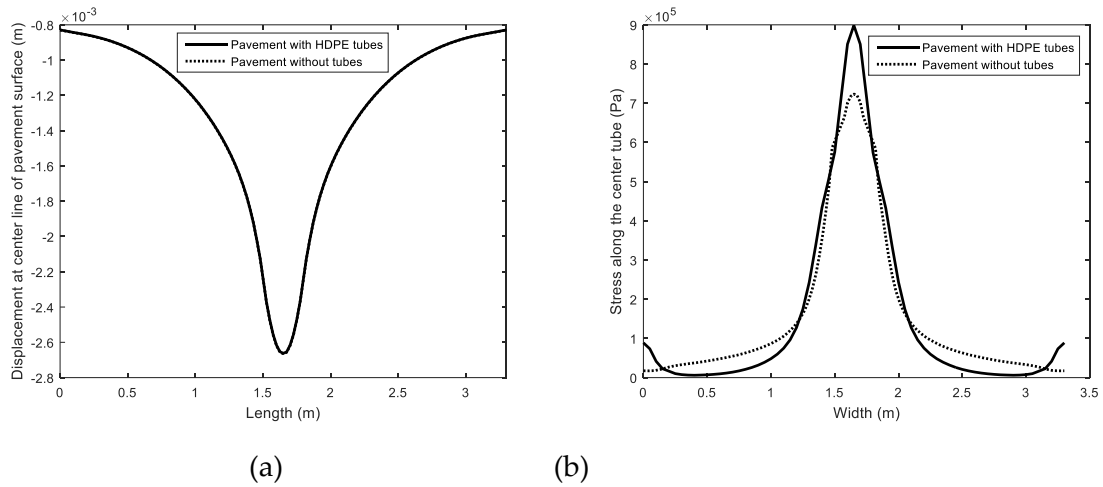


Fig. 27 Lateral profiles for (a) surface displacements at the center of the modeled pavement, and (b) Stress distribution on the top of the center loop.

In addition, the effect of loop on the displacement and stress distribution in pavement are investigated in Fig. 27 which shows that the effect of loops on deformation of pavement surface can be ignored as the displacement curves for pavement with HDPE loops overlap with that for pavement without loops. However, the stress in pavement without loops is smaller than that in pavement with HDPE loops because HDPE is much stiffer than the base layer.

5.2.2 Static tire load on a pavement with viscoelastic HMA layer

In this section, a more realistic model for the HMA is used, namely the viscoelastic model since HMA is a viscoelastic material especially at elevated temperature. Following [37], the viscoelastic material properties of HMA can be expressed using Prony series with the Prony's coefficients shown in Table 5. The same HMA elastic properties used in the elastic model (*Section 5.2.1*) are used for the elastic response of the viscoelastic model. Moreover, the model geometry, discretization mesh, and properties of the loops, base and subgrade layers are identical to those used in the elastic HMA model and summarized in Table 3 and Table 4.

Table 5 Prony Series Coefficients for HMA Layer (Liao 2007).

g_1	0.2301	g_3	0.2432	g_5	7.03E-2	τ_2	2.37E-3	τ_4	8.479
g_2	0.2847	g_4	0.1566	τ_1	9.66E-6	τ_3	1.58E-1	τ_5	470.5

The creep time in the adopted viscoelastic model is set to be 5 second. The displacement and the 75% Von-Mises stress fields over the depth of the pavement at the end of this creep time are shown

in Fig. 28(a) and Fig. 28(b), respectively. As for the case of elastic HMA, the displacements and stresses are limited to the area around the applied tire pressure. To show the history of the creep step, Fig. 29 shows the history of displacement along thickness direction at the center point of pavement surface. Since the tire load there is applied using a static step over 0.01 second before the beginning of the creep, the displacement increases rapidly during the initial static step, as shown in Fig. 29, followed by a slower rate of displacement increase due to the assumed viscosity of the HMA layer.

A comparison between the lateral profiles for the surface displacements along the model centerline and stresses at the top of the center loop from the elastic HMA model and the viscoelastic HMA model are presented in Fig. 30(a) and Fig. 30(b), respectively. While the general distributions of the displacements and stresses appears to be independent of the assumed material model for the HMA layer, the maximum displacement and stress estimated using the viscoelastic HMA are lower than those estimated from the elastic HMA. This behavior is expected due to time-dependent of the viscoelastic model results. Therefore, the viscoelasticity of the HMA layer decreases the displacement and stress in the self-heated pavement. Meanwhile, the design of loop geometry and the selection of material to be used in the self-heated pavement can be based on the simulation with elastic HMA layer. Similarly, as in Fig. 27, for pavement with viscoelastic HMA layer, the deformation of pavement with tube overlap with that in pavement without tubes as the size of tube is very small; the stress at the same location in pavement without loops is smaller compared with that in pavement with HDPE tube because the HDPE is much stiffer than base layer.

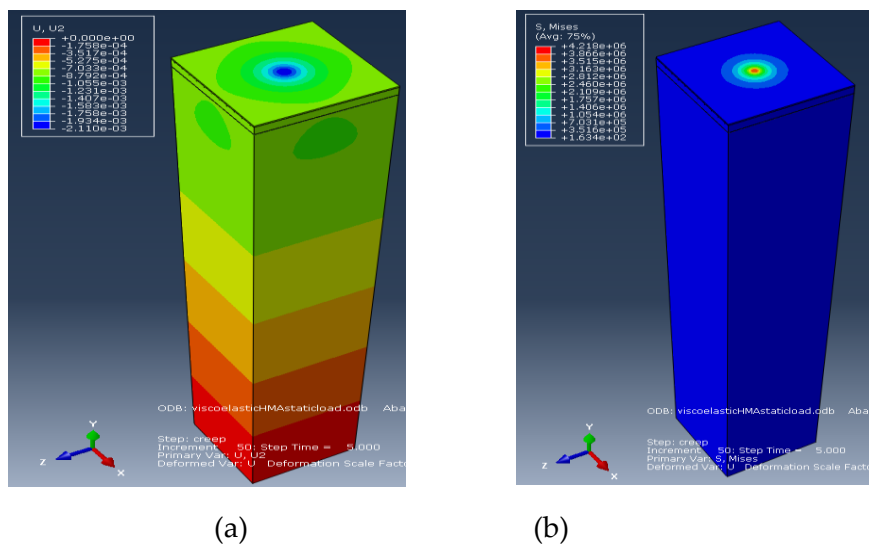


Fig. 28 (a) Field of displacement along thickness direction (m); (b) Stress field (Pa).

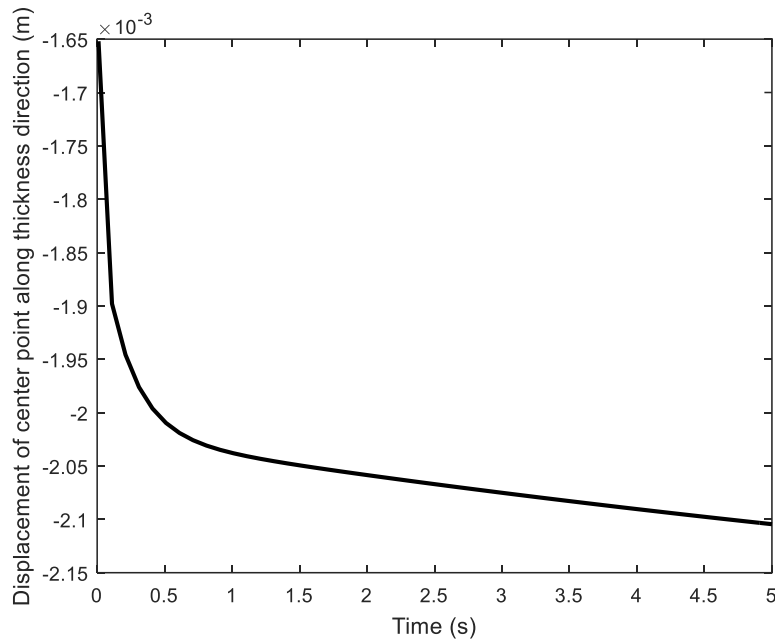


Fig. 29 History of displacement along thickness direction at center point of pavement surface.

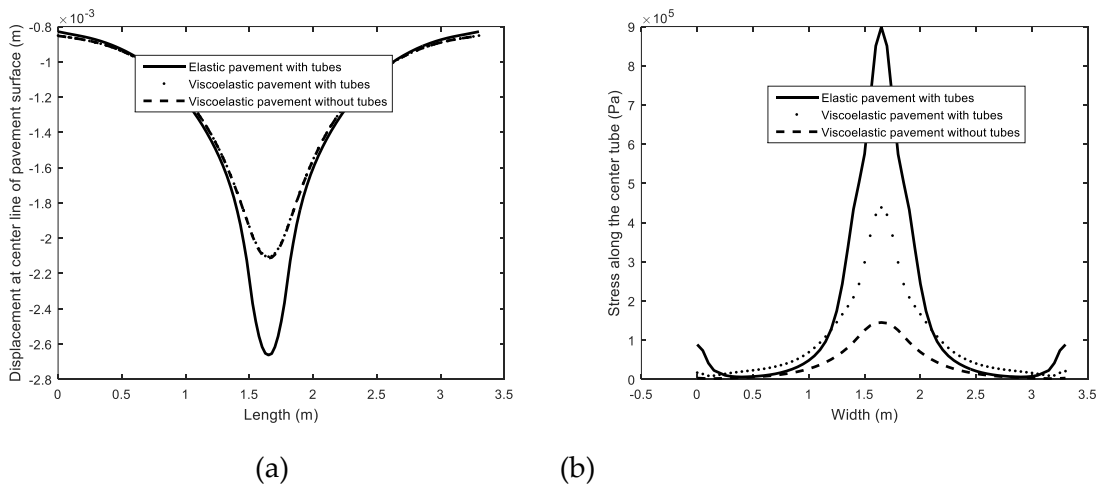


Fig. 30 Comparison of (a) Distribution of displacement along thickness direction at the center line of pavement surface; (b) Stress distribution along the center tube between elastic HMA layer and viscoelastic HMA layer cases.

5.2.3 Moving tire load of a pavement with viscoelastic HMA layer

In this section, the finite element model of the self-heated pavement with viscoelastic HMA layer, from Section 5.2.2., is used to investigate the effect of the pavement loops on the displacement and stresses in the pavement under moving tire load. The loop geometry, material properties, and boundary conditions adopted in Section 5.2.2 are used for the model reported in this section.

Since the stress distribution at the contact between the tire and pavement is not the focus of this study, the adopted moving tire is simulated as a uniformly distributed normal stress applied over a rigid cylinder with a radius equals to the radius of the circular contact area as shown in Fig. 31. The contact between the bottom surface of the rigid cylinder and the pavement surface is simulated using (1) a normal hard contact, and (2) a 0.2 friction coefficient for the tangential behavior. As the rigid cylinder moves along the model, normal and friction stresses are applied to the pavement surface. A tire speed of 3.6 km/hr is adopted in this model.

The history of displacement along thickness direction at the center point of pavement surface is presented in Fig. 32. This figure shows that the displacement increases fast at the beginning because of the static step over which the tire load is applied. When the applied load starts to move, the displacement increases further. However, when the tire moves far away from the center point, which is the focus of Fig. 32, the displacement at the center point decreases the elastic deformations recover. Compared with the result presented in Fig. 30(a), the maximum displacement at the center point of the viscoelastic HMA layer under moving load is smaller than that considering a static tire load. These results confirm that the design of pavement loops and the material selection can reasonably be based on the assumption that the HMA layer is elastic and the tire load is static, which reduces the computational cost and time significantly.

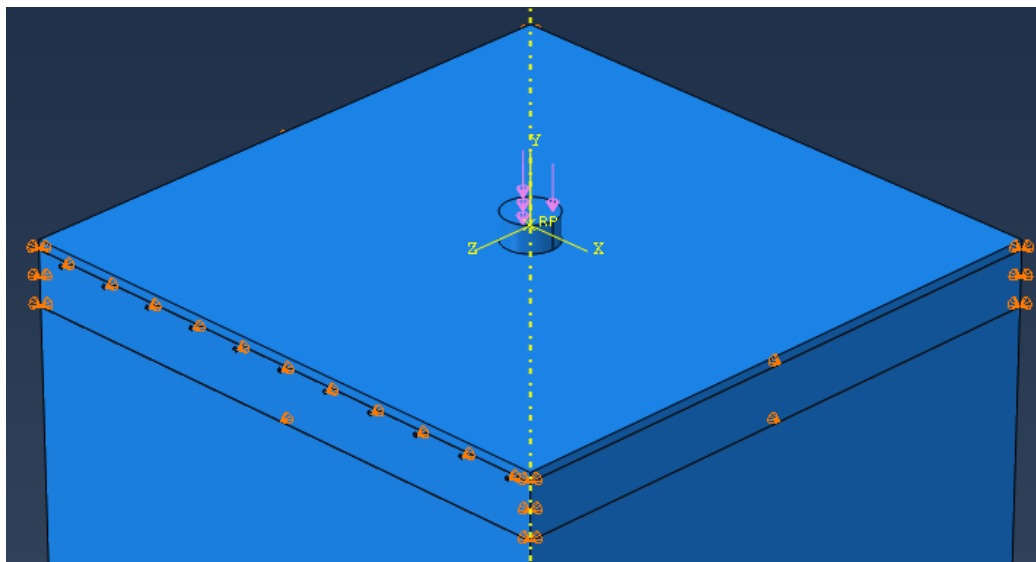


Fig. 31 Denote of how loading is applied through a rigid cylinder part.

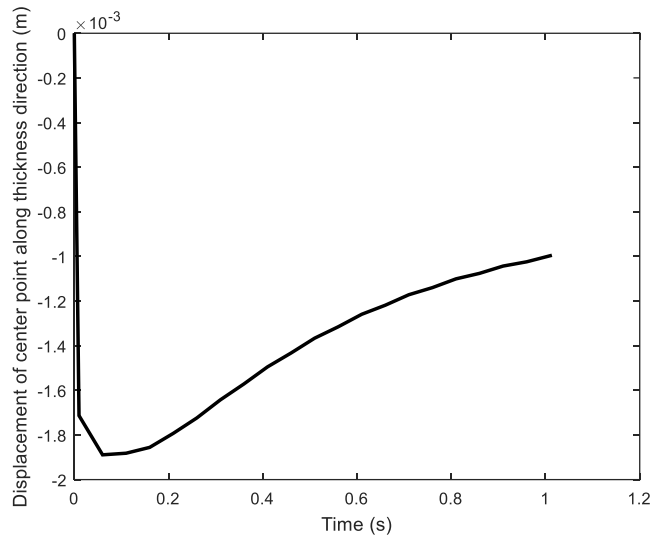


Fig. 32 History of displacement along thickness direction at the center point of pavement surface

5.3 Parametric analysis

A parametric analysis is performed to optimize the loop geometry and provide guidelines for the selection of the loop material for the proposed self-heated pavement. The deformation of the pavement when vehicle tires move above the pavement loops is expected to be less than the deformations when the tires move between the loops, as shown in Fig. 33. Depending on the loop spacing, and depth, as well as the stiffness of various materials, the difference between pavement deformations above and between the loops can be catastrophic causing rough drives. This task aims to define the pavement loop geometrical limits to limit the differential surface deformations above and between the loops to a maximum of 0.05 inch.

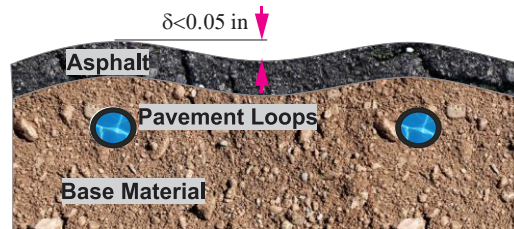


Fig. 33 Deformation of self-heated pavement.

Based on the simulation recommendations of Section 5.2, a pavement section with elastic HMA layer under static load is adequate for the purpose of this parametric study. Therefore, the parametric analysis presented in this section is based on the models of pavements with elastic HMA layer under static load similar to Section 5.2.1.

5.3.1 Effect of loop space

First, the effects of loop space, i.e. the center-to-center distance between two adjacent tubes, are investigated considering HDPE loops and aluminum loops. Seven (7) different loop spacing, from 300 mm to 900 mm with an increment 100 mm, are considered in this parametric analysis. The material properties, FE mesh, and loop geometry —except the loop spacing— are similar to those shown in Table 3 and Table 4. The Young’s modulus of the aluminum tube is 690 GPa and the Poisson’ ratio is 0.33.

The deformation at the center point of loaded tire area with the load applied on or between tubes and the differential surface deformations between points above and between the loops for the pavement with different HDPE and aluminum loop spacing are summarized in Table 6 and Table 7, respectively. The displacements of the pavement surface versus the loop spacing when the tire is above the loop and between the loop are shown in Fig. 34(a) for HDPE loops and in Fig. 34(b) for the aluminum loops.

Table 6 Surface deformation of pavement with HDPE loops at different loop spacing

Loop spacing (mm)	Deformation (mm)		
	Tire above loop	Tire between loops	Differential (mm)
300	2.66691	2.6624	0.00451
400	2.66911	2.66249	0.00662
500	2.67303	2.66334	0.00969
600	2.67703	2.66241	0.01462
700	2.68247	2.66398	0.01849
800	2.68857	2.66404	0.02453
900	2.69662	2.6648	0.03182

As shown in Fig. 34(a) for HDPE loops, the pavement surface deformation when the tire is above the HDPE is larger than that when the tire is between the HDPE loops indicating that the effective modulus of HDPE loops is less than the modulus of the base. Furthermore, the pavement surface deformations when the tire is between the HDPE loops are independent of the loop spacing. On the other hand, Fig. 34(b) shows that using aluminum loops causes less pavement surface

deformations when the tire is above the loops compared to those occurring when the tire is between the loops. This is believed to be due to the higher effective modulus of the aluminum loops in comparison with the modulus of base layer. Moreover, the pavement surface deformations considering aluminum loops increase continuously as the loop spacing increase for the two considered tire locations.

Table 7 Surface deformation of pavement with HDPE loops at different loop spacing.

Loop spacing (mm)	Deformation (mm)		Difference (mm)
	Tire above loop	Tire between loops	
300	2.59739	2.62612	0.02873
400	2.60386	2.64431	0.04045
500	2.60896	2.6538	0.04484
600	2.61294	2.65675	0.04381
700	2.61811	2.66024	0.04213
800	2.62568	2.66131	0.03563
900	2.6336	2.66265	0.02905

As presented in Table 6 and Table 7, it should be noticed that the maximum approximated differential surface settlement between the two considered tire locations is about 0.045 mm (~0.00177 inch) occurring when the tire is applied on a pavement with aluminum loops at a spacing of 500 mm. This maximum surface differential settlement is less than the selected limit, i.e. 1.275 mm (~ 0.05 inch). Therefore, all of loop geometries considered in this parametric analysis satisfy the design requirement. Overall, the loop spacing has a small effect on the pavement surface deformation as the variation of the pavement surface deformation is less than 2% for loop spacing ranging between 300 mm and 900 mm.

Fig. 35 presents the effect of loop material on the pavement surface deformations versus loop spacing. As shown in Fig. 35(a) for the tire above the loop, the surface displacement of the pavement with aluminum loops are slightly less than that for a pavement with HDPE loops for all loop spacing. This is because of the higher stiffness of the aluminum loops compared to the HDPE loops, when helps the aluminum loops to provided higher deformation resistance. Similarly, Fig. 35(b) shows that when the tire is applied between loops, the difference in the surface deformations

between a pavement with HDPE loops and an identical pavement with aluminum loops reduces as the loop spacing increases. This is attributed to the fact that as the tire is applied between loops, the effect of loop on the surface deformation would be weakened with the increase of the loop spacing. It should be noticed that the pavement surface displacements for the two loop types converge to the displacement approximated for a pavement without loops (~2.665 mm), mimicking the case of infinite loop spacing, shown in Fig. 35(b).

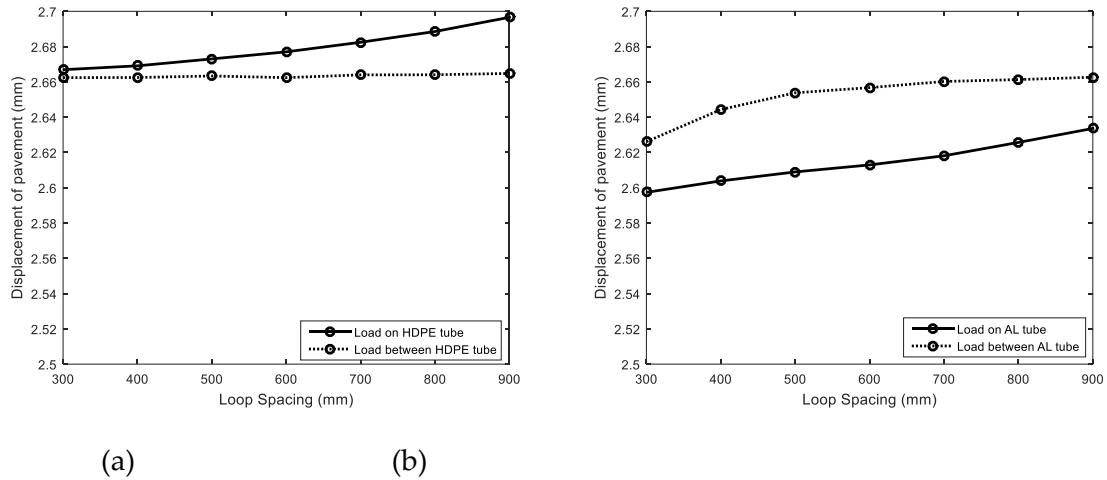


Fig. 34 (a) Change of surface deformation with different HDPE loop spacing; (b) Change of surface deformation with different aluminum loop spacing.

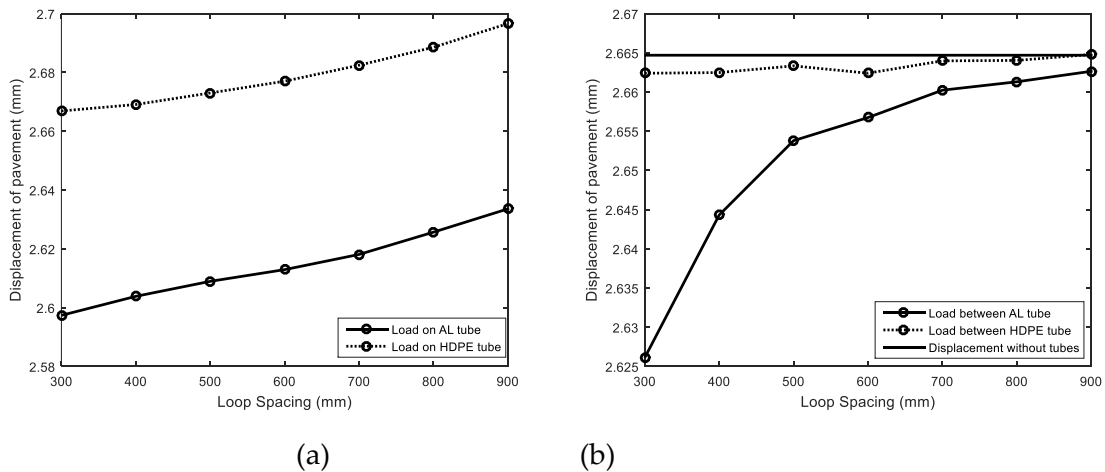


Fig. 35 Effect of tube material on surface deformation when the load is applied (a) on tube; and (b) between tubes.

5.3.2 Effect of loop depth

By following the same approach followed in Section 5.3.1, the effect of loop depth below the bottom of the HMA layer is considered in this section. For simplicity, the loop depth is measured to the top of loops with the two considered loop materials, i.e. aluminum and HDPE. The loop spacing is set to be 500 mm and the loop depth is varied between 25 mm and 275 mm with an increment of 25 mm. The geometry and material properties are similar to those presented earlier in Table 3 and Table 4.

Table 8 and Table 9 summarize pavement surface displacements at the center of the tire for pavements with different loop depths, loading locations, and loop materials. As shown in these tables, the maximum surface differential settlement is about 0.043 mm (~ 0.0017 inch), which occurs for a pavement section with aluminum loops at 25 mm spacing. This maximum surface differential settlement is acceptable per the selected design limit of 1.275 mm (0.05 inch).

Table 8 Surface deformation of pavement with HDPE loops at different loop depths.

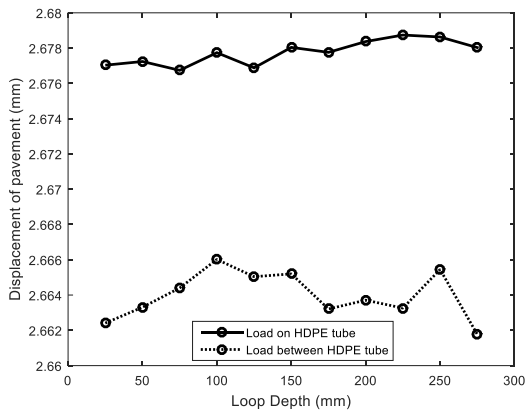
Loop depth (mm)	Deformation (mm)		Difference (mm)
	Tire above loop	Tire between Loop	
25	2.67703	2.66241	0.01462
50	2.67724	2.66331	0.01393
75	2.67674	2.6644	0.01234
100	2.67774	2.66602	0.01172
125	2.67688	2.66504	0.01184
150	2.67804	2.6652	0.01284
175	2.67776	2.66321	0.01455
200	2.67837	2.66371	0.01466
225	2.67874	2.66326	0.01548
250	2.67863	2.66545	0.01318
275	2.67803	2.66177	0.01626

Table 9 Surface deformation of pavement with aluminum loops at different loop depths.

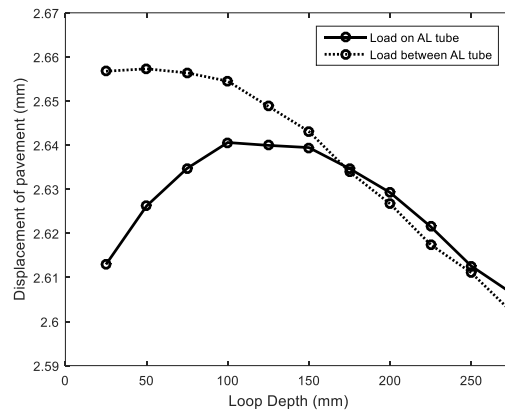
Loop depth (mm)	Deformation (mm)		Difference (mm)
	Tire above loop	Tire between loop	
25	2.61294	2.65675	0.04381
50	2.6262	2.6573	0.0311
75	2.63473	2.65638	0.02165
100	2.64059	2.65451	0.01392
125	2.63994	2.6488	0.00886
150	2.63944	2.64309	0.00365
175	2.63468	2.63394	0.00074
200	2.62924	2.62669	0.00255
225	2.62152	2.61744	0.00408
250	2.61259	2.61108	0.00151
275	2.6064	2.60213	0.00427

Fig. 36 shows the relationship between the pavement surface deformation and the loop depth. As shown in Fig. 36(a) for HDPE loops, the pavement surface deformation at the center of the tire when the tire is above the loop is more than the deformation occurring when tire is between the loops. This is attributed to the fact that the assumed stiffness of the HDPE is less than the stiffness of the base layer as discussed in Section 5.3.1. However, for pavement with aluminum loops shown in Fig. 36(b), the surface pavement deformations at the center of the tire when the tire is applied above the loops is smaller than that when the tire is between the loops because the aluminum loops are stiffer than the base layer.

Based on Fig. 36(a), there is no explicit relationship between the surface deformations of pavement with HDPE loops and the loop depth. For the pavement with aluminum loops, it is noticed that when the tire is between the loops, the surface deformation decreases with an increase of the loop depth. However, when the tire is above the loops, the surface deformation initially increases as the loop depth increases then it decreases with further increase in the loop depth, as shown in Fig. 36(b). Also, Fig. 36(b) shows that the differential surface settlements above and between the loops decreases and converges to zero as the loop depth increases indicating that the effect of tire location can be ignored as the loop depth reaches the tire diameter (i.e. 150 mm).



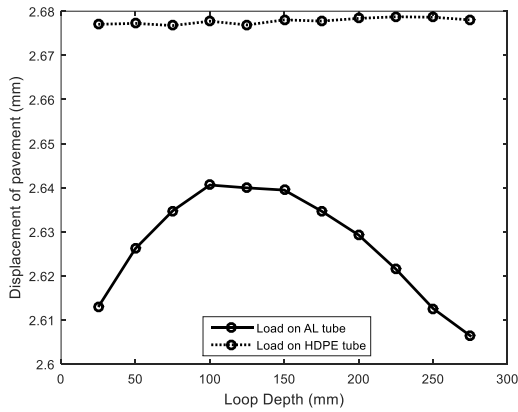
(a)



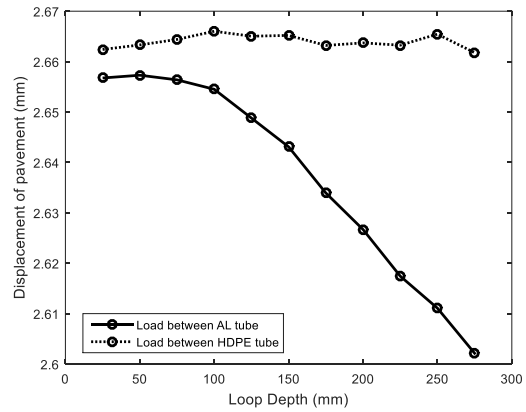
(b)

Fig. 36 (a) Change of surface deformation with different HDPE loop depth; (b) Change of surface deformation with different aluminum loop depth.

Fig. 37 compares the response of pavements with different types of loops. Both Fig. 37(a) and Fig. 37(b) show that the surface deformations of pavements with aluminum loops are less than that for the pavements with HDPE loops. This result is consistent with Fig. 35, as the modulus of the aluminum loops is higher than the modulus of the HDPE loops.



(a)



(b)

Fig. 37 Effect of tube material on surface deformation when the load is applied (a) on tube; and (b) between tubes.

5.4 Simplified 1-D analytical approximation

Based on the previous discussions, the proposed self-heated pavements technology is proven to be feasible from the thermal performance perspective and has acceptable mechanical effect on the pavement structure. The aim of this section is to adopt currently available analytical techniques used in the design of pavements to perform preliminary designs of the proposed self-heated pavements. For this purpose, a series of possible designs were considered for analysis using

mechanistic methods in addition to a more constructible pavement design with a 25-year life. Furthermore, the possible effect of construction errors on the expected life of the newer pavement design was investigated.

The finite element method (FEM) to analyze the expected mechanical and thermal performances of the proposed self-heated pavements technique and created a series of acceptable pavement designs that meets the thermal and mechanical demands of the project. Pavement loops would be placed into the base of the three-layer pavement as shown in Fig. 38. This would ease construction and also provide thermal protection to the plastic pipes during construction; hot mix asphalt is typically placed at well above 121 °C and could damage the pipes. (NYSDOT 2002)

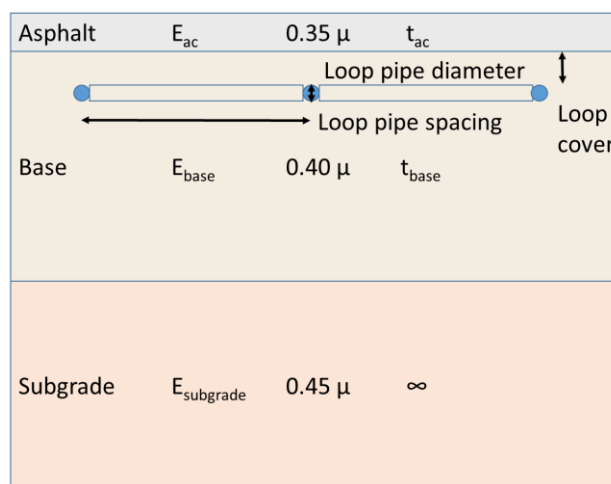


Fig. 38. Generic Pavement Cross Section

For each pavement alternative, finite element models were developed to determine two critical strains in the pavement: the tensile strain at the bottom of the AC layer and the vertical strain on the top of the subgrade. These values are the most common used in mechanistic pavement design. (Irwin 2002, NCHRP 2002) The relationship to pavement lifespan used in this research is based upon an average of several strain-fatigue curves from the Asphalt Institute, Danish Road Institute, the ME-PDG and others. (Irwin 2002)

Each pavement section was modeled using CHEVLAY (Irwin 1994), a computer program to determine the same critical strains using mathematical closed form solutions. CHEVLAY computes stresses, strains, and displacements in a system of elastic layers based upon a multi-layered analysis of a half space. The layers are assumed to be of a constant thickness and infinite in all horizontal

directions. The load must be a single, static, vertical load applied uniformly over a circular area at the surface. Note that CHEVLAY uses US Customary units. Metric data are converted to US Customary prior to calling CHEVLAY and converted back when reading the data.

5.4.1 Mechanistic-Empirical Review of Base Pavement Section

A base pavement model was set up with 50 mm of asphalt concrete over a 300 mm granular base as shown in Fig. 39. The wheel load for the FEM and mathematical analysis comparison was 550 kPa on a tire-pavement contact radius of 150 mm.

AC	700 Mpa	0.35 μ	50 mm
Base	100 Mpa	0.40 μ	300 mm
Subgrade	20 Mpa	0.45 μ	∞

Fig. 39. Base Pavement Section.

The analytical models performed using the CHEVLAY (Irwin 1994) computer program considered a 5-layer system with the loops as a separate layer. These layers are, listed from top to bottom:

- Asphalt concrete (HMA)
- Base above loops
- Loop layer
- Base below loops
- Subgrade

It should be noticed that CHEVLAY assumes the following about the pavement model.

- Layers are linearly elastic with constant modulus at every point in the layer.
- The load is applied uniformly over a single, flexible circular area
- Layers extend infinitely in all horizontal directions.
- There is 100 percent horizontal strain and vertical stress continuity across layer interfaces.
- The bottom layer is semi-infinite in depth.

This allows to account for the loop layer in the mathematical analysis even for the base model (i.e. no loops). To check the results, the stresses and strains at the same locations should be the same if the extra layer has the same inputs (moduli, Poisson's ratio) as if modeled as a single layer and the overall thickness are still the same. To confirm the assumptions above, an analysis was performed considering only three layers and the results compared to the five-layer analysis with the loop layer assigned the same properties as the base layer. The inputs to these two analyses are shown in Table 10, which shows that the properties of the loop layer were the same properties of the granular base layer. As expected, the critical strains are the same in both the three- and five-layer models.

Table 10. Base model with pipe layer setup.

Layer	Modulus(MPa)	Poisson's ratio	Thickness(m)
HMA	700.0	0.35	0.050
Base (above)	100.0	0.40	0.025 ^a
Base (pipe)	100.0 ^b	0.40 ^b	0.021 ^c
Base (below)	100.0	0.40	0.254 ^d
Subgrade	20.0	0.45	infinite

- a. The thickness of the Base above the loop is the cover from the parameter table.
- b. The modulus and Poisson's ratio of the loop layer are the average of the moduli and Poisson's ratio based upon percentage of the material in the layer with various parameters. For the initial design section, the modulus and Poisson's ratio are the same as the rest of the base layer.
- c. The thickness of the Base (loop) layer is the outer diameter of the loop.
- d. The thickness of the Base (below) is the total base thickness minus the thickness of the other base layers.

Then, eight acceptable configurations of the pavement loops were developed based on the thermal performance: one reference pavement section and seven alternatives. The reference pavement section has 21.4 mm diameter loops at 300 mm spacing between the loops with 25 mm cover of base material above the loops. The properties for the HMA, base, and subbase for the reference pavement section are as shown in Table 10. The loop material is assumed to have a modulus of 800 MPa and a Poisson's ratio of 0.45. The loops are assumed to be solid matching Stony Brook FEM model assumptions. Each of the seven alternatives differ from the above reference pavement in only one parameter, as listed below:

1. Loop spacing decreased to 100 mm
2. Loop diameter increased to 48.4 mm

3. Loop cover increased to 250 mm
4. Young's modulus for HMA layer increased to 3100 MPa
5. Young's modulus for base layer increased to 300 MPa
6. Young's modulus for subgrade layer increased to 100 MPa
7. Thickness of the HMA layer increased to 150 mm

To utilize the mathematical methods in CHEVLAY, loops' moduli and Poisson's ratios must be converted to a layer with a single material rather than a mixture of loops and granular base. The conversion was performed using an arithmetical average based on the percentage of the area covered by the loop layer with respect to the total area, as shown in Fig. 40.

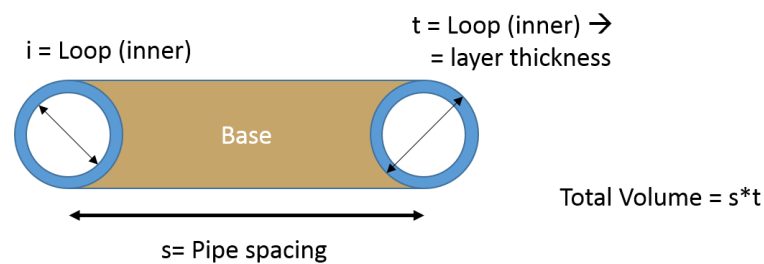


Fig. 40. Loop spacing and distance nomenclature.

Table 11 summarizes the results of the mathematical analysis performed using CHEVLAY, and compares these results to the results estimated by Stony Brook using FE models. The FEM analysis without loops has a lower vertical strain than any of the analyses with pipe, which is the opposite of what would be expected. The addition of stiffer loops should reduce the vertical strain by spreading the load. Other than the preliminary model without loops, the vertical strains at the top of the subgrade are in good agreement. On the other hand, the tensile strain at the bottom of the HMA are not as close as might be expected. However, the critical strain for the lifespan in every case was found to be the vertical strain at the top of the subgrade. Thus, the differences in the surface strains may not be as concerning as appears.

5.4.2 Updated Design

Cornell reviewed the base design from a constructability and maintenance perspective and determined the pavement was too prone to rutting and would not have enough life to be cost effective (NYSDOT 1993, NYSDOT 2000, NYSDOT 2002, Orr 2006). The reference design would only be able to handle approximately 5,000 tuck passes before rutting would too severe. A new

design was developed using mechanistic-empirical design methods, but also took into account typical pavement thicknesses used by NYSDOT and local agencies in New York State.

Rather than the use of the new AASHTO Mechanistic-Empirical Design procedure, a series of average tensile strain criteria developed by Irwin were employed to design a simple pavement for comparison (Irwin 2002, NCHRP 2002). Also, for this initial analysis, a simple 40 kN load was used. This is the Equivalent Single Axle Load used in the older AASHTO pavement design methods (AASHTO 1993). If phase II of the project is moved forward, it is recommended to do a complete check of the test pavement design using the AASHTO ME-PDG and site conditions.

The concept in the design is to use fatigue strain criteria for the surface (Fig. 41) and subgrade (Fig. 42) with Minor's hypo study of cumulative fatigue. The equation for fatigue used is an average of several pavement designs from the United States and Europe and includes the ME-PDG for the surface strain. The number of cycles to failure are show below in Eqs. 26 and 27.

Table 11. Comparison of CHEVLAY and FEM analysis.

Model	CHEVLAY Analysis		Finite element results		Differences between models	
	Tensile Strain Bottom HMA	Vertical Strain Top Subgrade	Tensile Strain Bottom HMA	Vertical Strain Top Subgrade	Surface Strain (HMA)	Subgrade Strain (Subgrade)
	($\mu\%$)	($\mu\%$)	($\mu\%$)	($\mu\%$)	%	
Preliminary model <i>without</i> loops	699.1	-2627	764.2	-1680	9.3%	-36.0%
Reference model <i>with</i> loops	645.6	-2597	764.5	-2590	18.4%	-0.3%
Loop spacing = 100 mm	580.8	-2572	770.0	-2611	32.6%	1.5%
Loop diameter = 48.4 mm	512.1	-2511	786.8	-2596	53.6%	3.4%
Loop cover = 250 mm	697.3	-2606	752.1	-2647	7.9%	1.6%
HMA Young's modulus = 3100 MPa	607.8	-2207	646.4	-2194	6.3%	-0.6%
Base Young's modulus = 300 MPa	64.3	-1407	114.3	-1377	77.8%	-2.2%
Subgrade Young's modulus = 100 MPa	711.2	-1063	793.6	-1066	11.6%	0.3%
HMA thickness = 150 mm	645.7	-1335	673.4	-1295	4.3%	-3.0%

Asphalt Horizontal Tensile Strain Criteria

$$N_{f \text{ surface}} (10^6) = \left(K \left(\frac{E}{E'} \right)^b \frac{1}{\varepsilon_t} \right)^a \tag{26}$$

where the average of the coefficients are 223.2 for K , 4.165 for a , -0.835 for b , and 435,000 psi for E' .

$$N_{f \text{ subgrade}} (10^6) = \left(K \frac{1}{\varepsilon_v} \right)^a \tag{27}$$

where the average of the coefficients are 618.6 and 3.903 for K and a , respectively.

The pavement needed to be as thin as possible to ensure adequate thermal performance, but traffic could not be too low so the pavement would be applicable as broadly as possible. Using a moderate to low level of traffic average of 800 vehicles per day and a design life or 25 years, a pavement design was developed. Growth rates and truck percentages were the defaults used by the New York State Department of Transportation. (Chen et al. 1995) The estimated count of ESALs for the pavement was estimated to be 473,000.

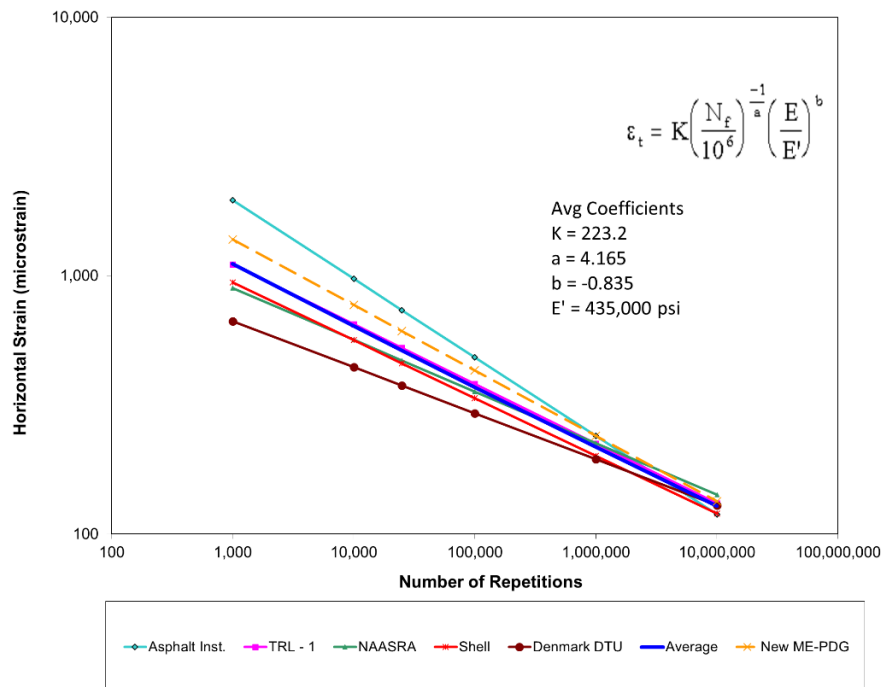


Fig. 41. Asphalt Horizontal Tensile Strain Criteria (Irwin 2002)

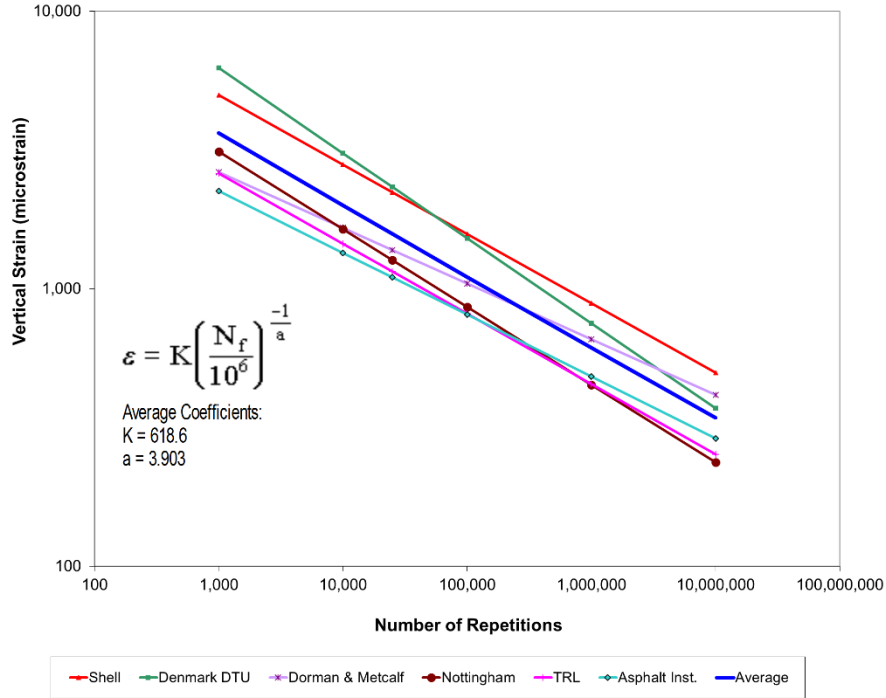


Fig. 42. Subgrade Vertical Compressive Strain Criteria (Irwin 2002).

Subgrade Vertical Compressive Strain Criteria

The developed design is shown in Fig. 43. The loop geometry (spacing and depth) is the same as the reference pavement section used in the parametric study in the previous section. For a final design of a test pavement the final configuration will need to be used in the actual design. A granular subbase was added to the final design as this will allow better control of the thermal characteristics and kept the asphalt surface relatively thin at 150 mm.

AC	2,000 Mpa ± 20%	0.35 μ	150 mm	± 10
Base	275 Mpa	0.35 μ	25 mm	
Pipe Layer			21.4 mm	
Base	275 Mpa ± 20%	0.35 μ	203.6 mm ± 25 mm	(Same error used on upper base & pipe layer)
Subbase	200 Mpa ± 30%	0.40 μ	300 mm ± 50 mm	
Subgrade	135 Mpa ± 40%	0.45 μ	∞	

Fig. 43. Design with 25-year expected lifespan.

5.4.3 Probabilistic Analysis of Updated Pavement Design

A final check of the design was performed to illustrate the expected variations in the life of the pavement that may be expected due to real world stochastic variations. For the moduli and thicknesses, the moduli were allowed to change randomly around the design value by either percentage of average (moduli) or a given thickness error. The amount used are shown in Fig. 43 and were taken from several sources. (Johnson and Sallberg 1960, Isada 1965, Carmichael-RF-III 1987, Briggs et al. 1992, Djakfar and Roberts 1999, Briggs and Lukanen 2000, Hossain et al. 2000)

The pavement design was then randomly changed and checked using a probabilistic analysis tool that works with Microsoft *Excel*, *Decision Tools* by Palisades Software. (Microsoft 2000) *Decision Tools* allows stochastic analysis of a variety of data. In this case, the variation was assumed to be Normal with a truncated minimum and maximum as illustrated in Fig. 44. The theory is that if the thickness or modulus is too low, this will be caught by quality control at the low end. The contractor will not want to place too much material and is not likely to do the additional compaction to increase the modulus. The maximum variation allowed was plus or minus twice the expected variation (standard deviation).

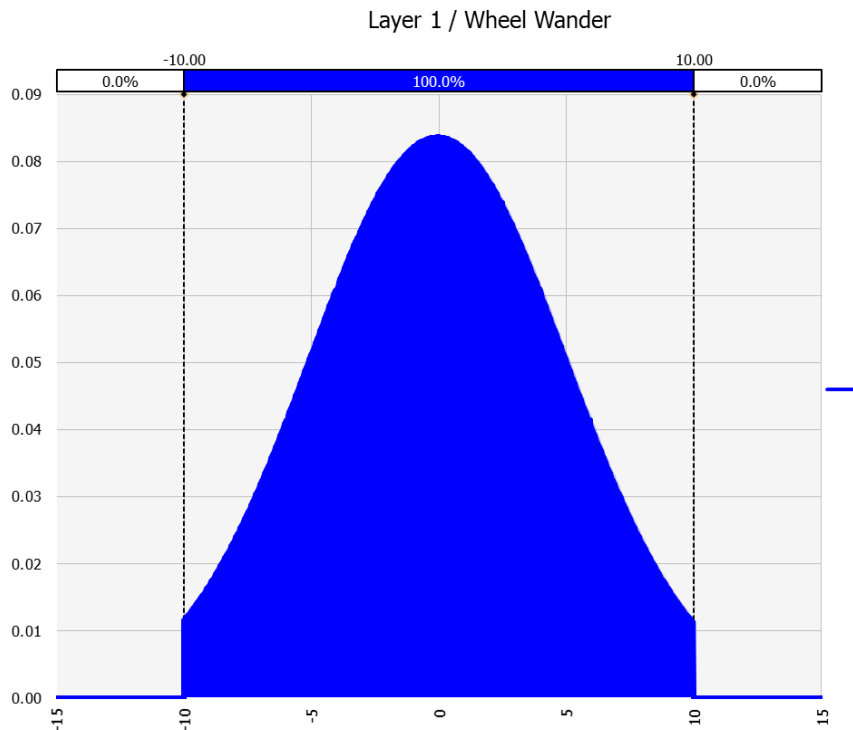


Fig. 44. Typical variation curve for moduli and thickness.

A total of 1,000 runs were complete using *Decision Tools*. The results were then analyzed using Minitab statistical software. (Minitab 2013) Fig. 45 shows the histogram of the data. The median value is 502,000 ESALs which is close to the original design value of 473,000. The 85th percentile lifespan is only 254,000. As expected, the shape of the distribution is skewed since the life cannot be negative.

In terms of the pavement, this means that at the design life, there will be many places that have begun to crack. Maintenance is critical. If it was desired to have the entire pavement survive the full 25 years with an 85th percentile reliability, the asphalt would need to be increased in thickness by 35 mm. Surprisingly, changing the thickness of the lower layers does not affect the overall design using probabilistic methods. This is part due to the asphalt surface cracking being the controlling factor in the design.

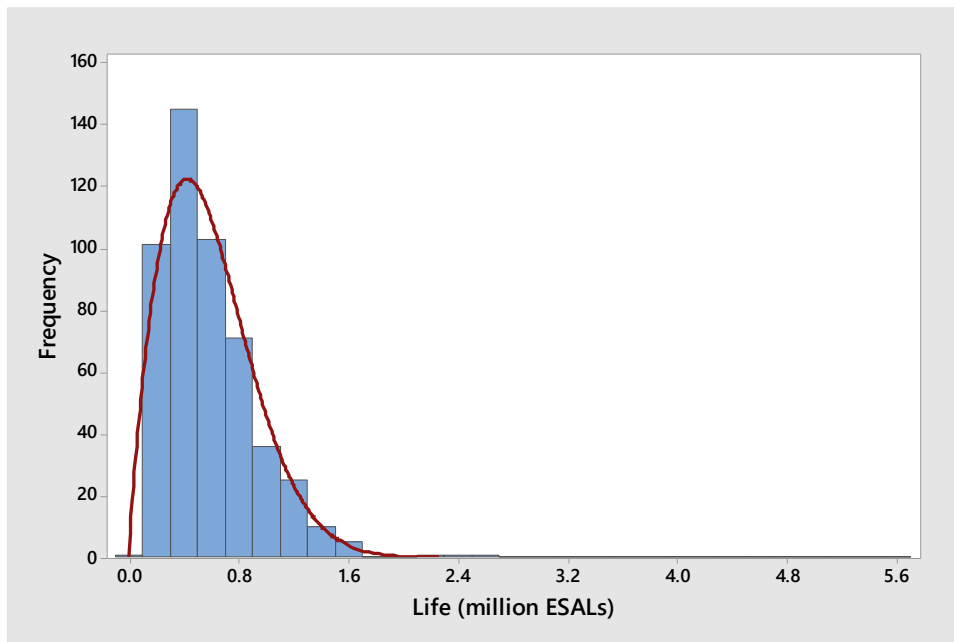


Fig. 45. Histogram of Design Life for Updated Pavement in Probabilistic Study.

6 Conclusions

A new self-heated pavement technology is proposed in this study. Compared with the current technologies to de-ice pavement surfaces, the innovation in the approach proposed in this study is that pavement loops are to be buried in the base layer, beneath the pavement surface layer, rather than embedding the loops directly inside the pavement surface layer. Further, a solar system will be used to power pumps to circulate a geothermal fluid between the pavement and ground loops.

To optimize the pavement loop geometry and material for acceptable pavement mechanical several FEM simulations were conducted. Firstly, the displacement and stress fields in the pavement with an elastic HMA layer subjected to a static tire load was considered. Then, viscoelasticity was introduced to the HMA layer and the displacements and stress fields were analyzed. Compared with the elastic HMA layer, the pavement with viscoelastic HMA layer developed less stresses and displacements indicating that the design of self-heated pavements (e.g. loop geometry and material) can be accurately performed considering an elastic HMA layer. After that, the response of pavement under moving load was modeled. For simplicity, the contact between the tire and the pavement was simulated using a uniformly distributed stress over a circular loaded area mimicking the tire on the pavement surface.

Moreover, the thermal performance of the proposed self-heated pavement technique was investigated using a 2-D heat transfer FEM models. Different types of pavement loops, loop spacing, and depths were considered. These models indicate that the pavement surface temperature is above freezing for the two considered loop materials, i.e. HDPE and aluminum, after introducing warm water to the loops for 48 hours. The heat transfer process approaches to the steady state after about 24 hours as temperature distribution does not change after 24 hours of the system operation. Based on the fact that the temperature at the surface of pavement with aluminum tube is about 1.5°C higher than that with HDPE tube after introducing the warm water into the loop for 48 hours, aluminum tube is recommended to be used in the proposed self-heated pavement for faster deicing.

Finally, the results of the parametric study considering various loop depths and spacing show that the effective modulus of HDPE tube is smaller than that of the base layer. This is supported by the observation that differential surface deformations above and between the loops increase as the loop spacing increases. As for the effect of loop depth, no explicit relationship was found between the surface deformations and the loop depth for pavements with HDPE tubes, while for pavements with aluminum loops the differential surface deformations above and between the loops decrease and converge to zero with increasing the loop depth.

In summary, the proposed self-heated pavement is feasible with acceptable mechanical and thermal performance. However, it is highly recommended to perform a pilot test for an actual pavement section. The results of the pilot test will be used to validate the expected performance of the system as approximated from the numerical models performed as part of this study.

Overall there are several conclusions which need to be incorporated in any future analysis.

- 1) **Larger error between FEM and layered model for points closer to the pipes.** There is an error between the FEM and the layered analysis which was expected as the pipe are stress concentrators. The FEM is probably a better final check of the actual design.
- 2) **For an initial design, the layered model is adequate.** To create any initial designs, the layered elastic approach is acceptable to determine a feasible design. This large difference between the FEM and layered elastic approach need in the base model without pipes needs to be reviewed.
- 3) **The asphalt in the originally designed base pavement is too thin for most applications.** A thicker surface is needed for most pavements actually built. Also, due to expected maintenance issues, any design should be for at least 25 year life.
- 4) **A thicker pavement is feasible, but may need to be thicker to account for real world errors.** The thickness of the asphalt layer either needs to be increased to deal with real world variations or tighter tolerances and more intensive quality control during construction need to be employed to reduce the variability.

References

- AASHTO (1993). AASHTO Guide for Design of Pavement Structures. Washington, D.C., American Association of State Highway and Transportation Officials.
- Abdelaziz, S.L., Olgun, C.G., and Martin, J.R. (2015). “Counterbalancing ambient interference on thermal conductivity tests for energy piles”. *Geothermics*, 56(1): 45-59.
- Abdelaziz, S., Ozudogru, T., Olgun, C., and Martin, J. (2014). “Multilayer finite line source model for vertical heat exchangers”. *Geothermic*, 51(1): 406-416.
- Alabi B. (1992). “A parametric study on some aspects of ground-borne vibrations due to rail traffic”. *Journal of Sound and Vibration*, 153(1): 77–87.
- Al-Qadi, I., Wang, H., Yoo, P., and Dessouky, S. (2008). “Dynamic analysis and in situ validation of perpetual pavement response to vehicular loading”. *Journal of the Transportation Research Board*, 2087(1): 29–39.
- Balbay, A., Esen, M. (2010). “Experimental investigation of using ground source heat pump system for now melting on pavements and bridge decks”. *Scientific Research and Essays*, 5(24):3955-3966.
- Bagher, A.M., Vahid, M., and Mohsen, M. (2014). “Geothermal Energy”. *Engineering and Technology Research*, 6(8): 146-150.
- Bentz, D.P. (2000). “A computer model to predict the surface temperature and time of wetness of concrete pavements and bridge decks”. National Institute of standards and technology, NISTIR. 6551.
- Bernard, A. C. L., Hunt, W. A., Timlake, W. P., and Varley, E., (1966). “A theory of fluid flow in compliant tubes”. *Biphysical Journal*, 6(6): 717-724.
- Brubaker, Alan P.E., <http://www.summitengineer.net/resources/learning/52-potholes>
- Briggs, R. C. and E. O. Lukanen (2000). “Variations in backcalculated pavement layer moduli in LTPP seasonal monitoring sites.” *Nondestructive Testing of Pavement and Backcalculation of Moduli: Third Volume*. S. D. Tayabji and E. O. Lukanen. Philadelphia, PA, American Society for Testing and Materials.

- Briggs, R. C., Scullion, T., and Maser, K. R. (1992). "Asphalt Thickness Variation on Texas Strategic Highway Research Program Sections and Effect on Backcalculated Moduli". Washington, DC, 20418, USA, Transportation Research Board: 115-127 (116 Fig., 120 Tab., 113 Ref.).
- Carmichael, H.S. (1987). Surface design and rehabilitation guidelines for low-volume roads. Washington, DC, Federal Highway Administration: 228.
- Calwell C. (2003), California State Fuel-Efficient Tire Report, Volume II, California Energy Commission. January
- Churchill, S. W. (1997). "Friction factor equations spans all fluid-flow regimes". Chemical Engineering, 84, 91-92.
- Chen, H. J., Bendana, L. J., and McAuliffe, D. E. (1995). Adapting the AASHTO Pavement Design Guide to New York State Conditions. Albany, N.Y., Transportation Research and Development Bureau, New York State Dept. of Transportation.
- COMSOL (2014). COMSOL Multiphysics™ Version 5.0: User's Guide and Reference Manual. COMSOL Inc., Burlington, MA.
- Cole J. D., and Huth J. H. (1956). Elastic stresses produced in a half plane by steadily moving loads.
- de Bondt, A.H. (2003). "Generation of energy via asphalt pavement surfaces.", Asphaltica Padova 2003
- de Bondt, A.H. and Jansen, R. (2006). "Generation and saving of energy via asphalt pavement surfaces", OIB aktuell, Nov 13, 2006.
- De Beer M, Fisher C, and Jooste F (2002). Evaluation of non-uniform tire contact stresses on thin asphalt pavements. In: Ninth international conference on asphalt pavements. pp 19–22
- Djakfar, L. and Roberts, F. L. (1999). Performance Comparison of Base Materials under Accelerated Loading. Washington, DC, 20418, USA, Transportation Research Board: 211-218.
- Evans L.R., MacIsaac J.D., and Harris J.R. (2009). NHTSA tire fuel efficiency consumer information program development: phase 2—effects of tire rolling resistance levels on traction, treadwear, and vehicle fuel economy. East Liberty, OH: National Highway Traffic Safety Administration
- Friedrich A. (2002), Fuel saving potential from low rolling-resistance tires. Presentation for the

Umweltbundesamt at the September.

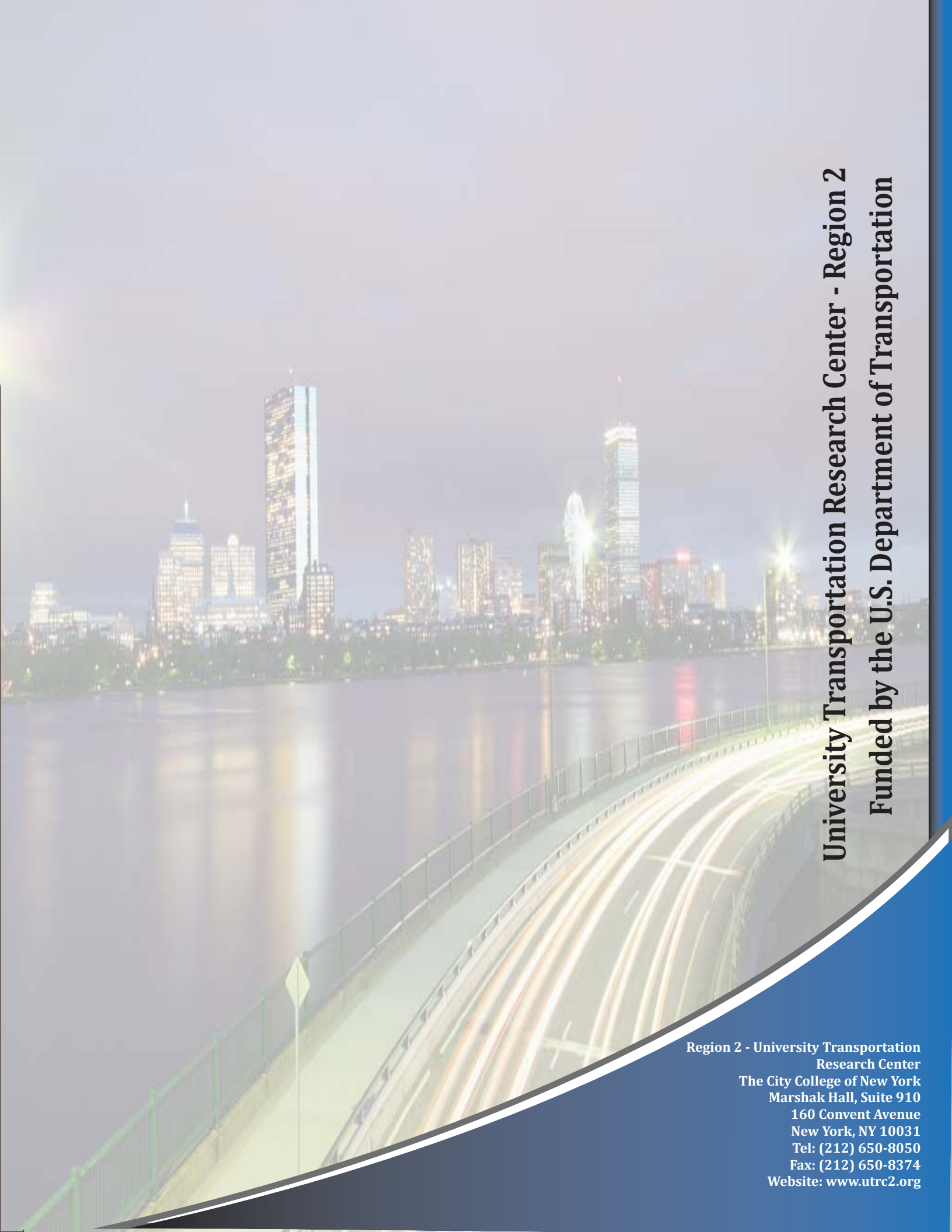
- Gnielinski, V. (1976). "New equations for heat and mass transfer in turbulent pipe and channel flow". *International Journal of Chemical Engineering*, 16(1): 359-368.
- Hao H., and Ang T. C. (1998). "Analytical modeling of traffic-induced ground vibrations". *Journal of Engineering Mechanics*, 124(8):921–928.
- Hamada, Y., Nakamura, M., Kubota, H. (2007). Field measurements and analyses for a hybrid system for snow storage/melting and air conditioning by using renewable energy. *Applied Energy*, 84 (2):117-134.
- Hanazato T., Ugai K., Mori M., and Sakaguchi R. (1991). "Three-dimensional analysis of traffic-induced ground vibrations". *Journal of Geotechnical Engineering*, 117(8):1133–1151.
- Havens, J., Azevedo, W., and Rahal, A. (1978). "Heating bridge decks by electrical resistance", *Proceedings of the 2nd International Symposium on Snow Removal and Ice Control Research*, Special Report 185, Hanover, 159-168, 15-19 May 1978.
- Henry, J.J. (1991). Highway deicing: Comparing salt and calcium magnesium acetate. *Transportation Research Board Special Report 235*:
- Hoppe, E.J. (2001). "Evaluation of Virginia's first heated bridge". *Transportation Research Record*, 1741(1): 199-206.
- Huang, B., Mohammad, L., and Rasoulia, M. (2001). "Three-dimensional numerical simulation of asphalt pavement at Louisiana accelerated loading facility". *Transportation Research Record*, 1794(1): 44–58.
- Hossain, M., Romanoschi, S., and Gisi, A. J. (2000). Seasonal and spatial variation of subgrade response. *Geo-Denver 2000*, Denver, CO, American Society of Civil Engineers.
- Ivanovskii , M.N., Sorokin, V.P., and Yagodkin, I.V. (1982). "The physical principles of heat pipes". Translated by R. Berman. New York: Oxford University Press.
- Irwin, L. H. (1994). CHEVLAY2. Ithaca, NY, Cornell Local Roads Program.
- Irwin, L. H. (2002). Backcalculation: An Overview and Perspective. 6th International Conference on the Bearing Capacity of Roads, Railways, and Airfields: FWD / Backcalculation Workshop, Lisbon, Portugal, Instituto Superior Tecnico.

- Isada, N. M. (1965). Detecting variations in the load-carrying capacity of flexible pavements; final report. Buffalo,, Cornell Aeronautical Laboratory Inc.
- Jackson, R.B. and Jobbagy, E.G. (2005). “From Icy roads to salty streams”. Proceedings of the National Academy of Sciences of the United States of America. 102(41): 14487-14488.
- Jones, D., Le Houedec, D., and Petyt, M. (1998). “Ground vibrations due to a rectangular harmonic load”. Journal of Sound and Vibration, 212(1): 61–74.
- Johnson, A. W. and Sallberg, J. R. (1960). Factors that influence field compaction of soils; compaction characteristics of field equipment. Washington, D.C.
- Kaushal, S.S., Groffman, P.M., Likens, G.E., Belt, K.T., Stack, W.P., Kelly, V.R., Band, L.E., and Fisher, G.T. (2005). “Increased salinization of fresh water in the northeastern United States.” Proceedings of the National Academy of Sciences of the United States of America. 102(38): 13517-20.
- Kenney, J. (1954). “Steady-state vibrations of beam on elastic foundation for moving load”. Journal of Applied Mechanics, 21(1): 359–364.
- Kumagai, M. and Nohara, I. (1988). “Studies on a practical use of snow melting system by using the heat of ground water through pipes.” National Research Center for Disaster Prevention, Japan, Report No. 41: 285-309.
- Krylov, V. V. (1996). “Vibrational impact of high-speed trains. I. Effect of track dynamics”. The Journal of the Acoustical Society of America, 100(1): 3121–3134.
- Lazzari, S., Priarone, A., and Zanchini, E. (2010). “Long-term performance of BHE (borehole heat exchanger) fields with negligible groundwater movement”. Energy, 35(12): 4966–4974.
- Li, G., and Zheng, X. (2016). “Thermal Energy storage system integration forms for a sustainable future”. Renewable and Sustainable Energy, 62: 736-757.
- Liao, Y. (2007). Viscoelastic FE modeling of asphalt pavements and its application to US 30 perpetual pavement. ProQuest
- Liu, X., Rees, S., and Spitler, J. (2006a). “Modelling snow melting on heated pavement surfaces. Part I: Model Development”. Applied Thermal Engineering, 27(5-6): 1115-1124

- Liu, X., Rees, S., and Spitler, J. (2006b). "Modelling snow melting on heated pavement surfaces. Part II: Experimental Validation". *Applied Thermal Engineering*, 27(5-6): 1125-1131.
- Loomans, M., Oversloot, H., and de Bondt, A. (2003). Design tool for the thermal energy potential of asphalt pavements. Eighth International IBPSA Conference, Eindhoven, Netherlands
- Lund, J.W. (1999). Reconstruction of a pavement geothermal deicing system. *Geo-Heat Center Quarterly Bulletin*. 20(1): 14-17.
- Lu, S., and Xuejun, D. (1998). Dynamic analysis to infinite beam under a moving line load with uniform velocity. *Applied Mathematics and Mechanics*, 19(4): 367–373.
- Minsk, L.D. (1999). "Heated bridge technology: Report on ISTE A Sec. 6005 program". Publication FHWA-RD-99-158, FHWA, US Department of Transportation.
- Microsoft (2000). Microsoft Excel 2000. Redmond, WA, Microsoft Corporation.
- Minitab (2013). Minitab Statistical Software. State College, PA, Minitab, Inc.
- NCHRP. (2002, May 2). "2002 Pavement Design Guide Home - Using Mechanistic Principles to Improve Pavement Design." 2003, from www.2002designguide.com/.
- Novotny, E.V., Murphy, D., and Stefan, H.G. (2008). Increase of urban lake salinity by road deicing salt. *Science of The Total Environment*. 406(1-2): 131–144. doi:10.1016/j.scitotenv.2008.07.037
- NYSDOT (1993). The New York State Thickness Design Manual for New and Reconstructed Pavements. Albany, NY, New York State Department of Transportation.
- NYSDOT (2000). Comprehensive Pavement Design Manual. Albany, NY, New York State Department of Transportation.
- NYSDOT, (2002). Standard Specifications Construction and Materials. Albany, NY, New York State Department of Transportation.
- NYSDOT Standard Specifications, 2008.
- Orr, D. P. (2006). Pavement Maintenance. Ithaca, NY, Cornell Local Roads Program.
- Olgun, C.G., Abdelaziz, S.L., and Martin, J.R. (2012). Long-Term Performance and Sustainable Operation of Energy Piles. In International Conference on Sustainable Design, Engineering, and Construction.

2012. Fort Worth, TX, USA: ASCE.
- Ozudogru, T.Y., Olgun, C.G., and Senol, A. (2014). "3D numerical modelling of vertical geothermal heat exchangers". *Geothermics*, 51(1): 312-324.
- Pimentel et al., *Renewable Energy: Current and Potential Issues*, 2002
- Phillippe M., Bernier M., and Marchio D. (2009). "Validity ranges of three analytical solutions to heat transfer in the vicinity of single boreholes". *Geothermics*, 38(4): 407-413.
- Qin, Y. and Heller, J.E. (2014). "Understanding pavement-surface energy balance and its implications on cool pavement development." *Energy and Building*, 85(1): 389-399.
- Ramsey, J. W., Hewett, M. J., Kuehn, T. H., and Petersen, S. D. (1999). "Updated design guidelines for snow melting systems." *ASHRAE Transactions*, 105(1): 1055.
- Rees, S.J., Spitler, J.D., and Xiao, X. (2002). "Transient analysis of snow-melting system performance." *ASHRAE Transactions*, 108(2): 406-423.
- Roque, R., Myers, L., and Birgisson, B. (2000). "Evaluating measured tire contact stresses to predict pavement response and performance". *Transportation Research Record*, 1716(1): 73–81.
- Spitler, J.D. and Ramamoorthy, M. (2000). "Bridge deck deicing using geothermal heat pumps". *Proceedings of the 4th International Heat Pumps in Cold Climates Conference*. 2000. Aylmer, Quebec.
- Shi, X. (2018). Impact of airport pavement deicing products on aircraft and airfield infrastructure. A Synthesis of Airport Practice. [online] WASHINGTON, D.C: TRANSPORTATION RESEARCH BOARD. Available at: https://westerntransportationinstitute.org/wp-content/uploads/2016/08/4W1527_Final_Synthesis.pdf [Accessed 1 Nov. 2018].
- Shoop, S.A. (2001). *Finite Element Modeling of Tire-Terrain Interaction*.
- Stefano, L., Antonella, P., and Enzo, Z., (2010). "Long term performance of BHE (borehole heat exchanger) fields with negligible groundwater movement". *Energy*, 35(12): 4966-4974.
- Surface Energy Balance Gerratt 5.1-5.2, Lecture 10, Atm S Boundary Layer Meteorology, University of Washington.
- Sullivan, C., de Bondt, A.H., Jansen, R., and Verweijmeren, H. (2007). *Innovation in the production and*

- commercial use of energy extracted from asphalt pavements. 6th Annual International Conference on Sustainable Aggregates, International Journal of Pavement Engineering and Asphalt Technology 8:
- Tielking, J.T., and Roberts, F.L. (1987). "Tire contact pressure and its effect on pavement strain". Journal of Transportation Engineering, 113(1): 56–71.
- U.S. Department of Transportation - Federal Highway Administration (2018, September 17). How Do Weather Events Impact Roads?. Retrieved November 1, 2018, from https://ops.fhwa.dot.gov/weather/q1_roadimpact.htm
- Van Bijsterveld, W.T., and de Bondt A.H. (2002). Structural aspects of asphalt pavement heating and cooling systems. Third International Symposium on 3D Finite Element Modeling, Design and Research, Amsterdam, Netherland
- Wang, H., and Al-Qadi, I. (2010). "Evaluation of surface-related pavement damage due to tire braking. Road Materials and Pavement Design, 11(1): 101–121.
- Wang, H., Al-Qadi, I., and Stanciulescu, I. (2012). "Simulation of tyre–pavement interaction for predicting contact stresses at static and various rolling conditions. International Journal of Pavement Engineering, 13(4): 310–321.
- Wilcox, S. and Marion, W. (2008). "Users Manual for TMY3 Data Sets, N.R.E.L". NREL/TP-581-431556. National Renewable Energy Laboratory: Golden, Colorado 50 p.
- Yavuzturk, C., and Spitler, J. D. (1999). "A short time step response factor model for vertical ground loop heat pump system in China." In: Proceedings of IEA 7th Heat Pump Conference, Beijing, China, May 19-22, pp. 356-364.
- Zaghoul, S.M., and White, T. (1993). Use of a three-dimensional, dynamic finite element program for analysis of flexible pavement.

A long-exposure photograph of a city skyline at night, reflected in a body of water. In the foreground, a bridge or highway is visible with light trails from moving vehicles. The sky is dark, and the city lights are bright and colorful.

University Transportation Research Center - Region 2
Funded by the U.S. Department of Transportation

**Region 2 - University Transportation
Research Center**
The City College of New York
Marshak Hall, Suite 910
160 Convent Avenue
New York, NY 10031
Tel: (212) 650-8050
Fax: (212) 650-8374
Website: www.utrc2.org